The Institute of Paper Science and Technology

Atlanta, Georgia

Doctor's Dissertation

Inorganic Aerosol Formation During Black Liquor Drop Combustion

Christopher Lee Verrill

September, 1992

INORGANIC AEROSOL FORMATION DURING BLACK LIQUOR DROP COMBUSTION

A thesis submitted by

Christopher Lee Verrill

B.S. 1985, University of Maine

M.S. 1987, Lawrence University

in partial fulfillment of the requirements
of the Institute of Paper Science and Technology
for the degree of Doctor of Philosophy,
Atlanta, Georgia

September, 1992

TABLE OF CONTENTS

ABSTRACT

The submicron-sized inorganic aerosol generated during kraft black liquor combustion is known as fume. Sodium carbonate fume removes sulfur compounds from the flue gas, but it also contributes to plugging of recovery furnace gas passages. Research has focused on fume formation during the char burning and smelt oxidation stages of black liquor combustion; however, experimental data indicate that sodium loss is continuous throughout combustion. It has recently been proposed that sodium release prior to char burning may be a major contribution to overall fume formation.

The main objective of this thesis was to propose a valid mechanism of sodium release prior to char burning and to predict its impact on overall fume formation. Individual 2 mm drops of black liquor were exposed to non-combustive atmospheres over a range of temperature, gas composition, and flow rate. This experimental technique allowed sodium loss during the drying and devolatilization stages to be isolated from that occurring during char burning and smelt oxidation. During these pyrolysis experiments, change in char sodium content was measured as a function of exposure time. Additional experiments were conducted in which films of black liquor were pyrolyzed at 750°C.

It was found that approximately 5-30% of the sodium present in black liquor was released during drying and devolatilization of the individual drops. The extent of this initial loss increased with increasing furnace temperature (600-900°C). Increasing relative gas velocity (0.61-1.83 m/s) resulted in a significant reduction in sodium release. After liquor swelling was complete, additional sodium release during pyrolysis was only measured at 900°C; this resulted from Na_2CO_3 decomposition and produced a substantial amount of fume.

There was no sodium loss during pyrolysis of the liquor films, yet there was a 30% volatile yield during this experiment. This result and the fact that increasing gas velocity did not increase sodium loss during the single drop experiments suggest that initial sodium loss was not due to evaporation.

Sodium loss during drop pyrolysis may have resulted from physical ejection of alkali-containing material. Gas eruptions were observed during all stages of black liquor pyrolysis and combustion. While the lost material was not conclusively identified, some 1-100 μm diameter inorganic aerosol was collected during the single drop experiments. The significance of ejected material on the physical and chemical processes occurring within the kraft recovery furnace remains to be evaluated by furnace aerosol sampling and computational modeling.

Aerosol generation during drop combustion was coordinated with combustion stages. A moving collection system was used to continuously capture the aerosol while a video camera recorded drop combustion events. These experiments demonstrated that a maximum in fume formation occurred during the char burning and smelt oxidation stages of combustion. SEM photomicrographs showed that more fume was produced during the combustion of a single drop of black liquor than during the pyrolysis of five drops at similar furnace conditions. While the sodium loss prior to char burning may contribute to fume formation, analysis of collected aerosol samples indicated that it is not the most important source of submicron-sized fume in the recovery furnace.

LIST OF FIGURES

LIST OF TABLES

INTRODUCTION

PERSPECTIVE

Cost effective operation of the kraft pulping process requires recovery of the chemicals used to liberate cellulosic fibers from wood. A solution of sodium hydroxide (NaOH) and sodium sulfide (Na_2S), applied to wood chips at elevated temperature and pressure, degrades the lignin that binds the fibers together. After digestion the mixture of dissolved organic compounds and inorganic salts, know as black liquor, is washed from the wood pulp fibers. Black liquor is commonly concentrated to 65-75% solids content by a series of evaporators, then it is burned in a Tomlinson recovery furnace. The energy released during combustion of the organic compounds is used to generate process steam and electricity for the mill; the inorganic residue is removed from the furnace as molten smelt. Pulping chemicals are reformed by dissolving the smelt in process water and causticizing the resulting green liquor.

Black liquor undergoes three distinct stages of combustion when it is sprayed into the recovery furnace: drying, devolatilization, and char burning.[1] A significant portion of drying and devolatilization occurs as the 0.5-5 mm drops fall to the char bed at the bottom of the furnace; much of the char burning takes place on the char bed. Under certain conditions drops can be entrained in the gas flow and burn in flight. Airborne drops exhibit a fourth combustion stage: oxidation of the residual smelt.[1] The extent to which the combustion processes occur on the char bed and in flight depends on furnace design, liquor properties, and operating strategy.[2]

Combustion air is introduced at three levels in the kraft recovery furnace. By only introducing a fraction of the stoichiometric requirement for complete combustion in the lower furnace, reducing conditions can be maintained in the char bed. A reducing environment is necessary to recover the sulfur as Na_2S in the smelt. The remainder of the combustion air enters the furnace above the liquor spray level. In this region the combustible gases, produced by liquor pyrolysis and gasification in the lower furnace, are completely burned.

The submicron-sized inorganic aerosol generated during kraft black liquor combustion is known as dust or fume. Fume particles are composed primarily of sodium carbonate (Na_2CO_3), sodium sulfate (Na_2SO_4), sodium chloride (NaCl), and the analogous potassium salts. Fume composition varies with location in the recovery furnace and is dependent on the conditions of combustion.[3,4] Furnace material balances indicate that approximately 10% of the sodium entering with the black liquor becomes fume.[5] The principal benefit of fume formation is that the alkali aerosol reacts with environmentally undesirable sulfur compounds in the flue gas; the resulting Na_2SO_4 dust is removed by the electrostatic precipitator and returned to the system by mixing with the black liquor. Fume has detrimental effects on recovery furnace operation because it deposits on the heat transfer surfaces which reduces thermal efficiency, requires process steam to remove the deposits, and contributes to blockage of gas passages. Control of fume formation has recently become an issue of concern. Higher combustion temperatures, resulting from burning higher solids content liquor, have increased fume formation by 15-100%.[6,7,8] If electrostatic precipitators are not designed to handle the increased dust loading, then particulate emissions may exceeded regulated limits.

Fume generation has historically been attributed to sodium vaporization from the high temperature and strongly reducing environment of the char bed.[9] Laboratory data from molten salt studies showed that the rate of fume formation is an order of magnitude higher during sodium sulfide oxidation than the rate under reducing conditions.[10] Entrained char particles and smelt droplets are exposed to an oxidizing atmosphere; therefore, they may be a significant source of fume. Most researchers have studied fume formation only during char burning and smelt reactions. Experimental data indicate that sodium loss occurs during all stages of black liquor combustion.[11,12,13] Furthermore, recent work has suggested that sodium release during devolatilization may be a major contribution to overall fume formation.[13,14]

The general goal of this thesis was to contribute to the understanding of fume formation during black liquor combustion by determining the type and amount of aerosols generated during each combustion stage. An experimental system was developed that coordinated timed observation of drop combustion with a continuous record of collected aerosol. Equipment difficulties limited the extent of this work. However, limited results indicate that the majority of submicron-sized fume is formed during the char burning and smelt oxidation stages of drop combustion.

A study of sodium release prior to char burning and its impact on overall fume formation was conducted, as this was the least understood potential source of inorganic aerosol. Results of this study demonstrate that sodium release during black liquor drying and devolatilization does not significantly contribute to fume formation. A previously ignored class of aerosol, resulting from physical ejection of sodium containing material during black

liquor combustion, contributes to the observed sodium loss. This 1-100 μm diameter fraction of inorganic particulate may play an important role in the physical and chemical processes occurring within the kraft recovery furnace.

BACKGROUND

The following literature review is intended to provide general information regarding black liquor and coal combustion that pertains to sodium release and aerosol formation. Observations from laboratory drop combustion studies are presented and characteristics of black liquor combustion stages are discussed in the first two sections. After a brief overview of coal combustion and fly ash formation, the results of particulate sampling studies from kraft recovery furnaces are summarized. Theories of aerosol formation during combustion of black liquor are then presented. Following a discussion of sodium loss during black liquor devolatilization, the review concludes with a summary of the types of aerosol expected to be produced during black liquor combustion.

Appendix I contains a glossary of terms associated with the processes of combustion and aerosol formation. As there are several clear distinctions made from popular usage, familiarization with this vocabulary is suggested to prepare the reader for the following discussion.

Black Liquor Drop Combustion Studies

The understanding of combustion obtained from single drop studies can be utilized to predict the performance of industrial combustion systems.[15] A single drop experimental system has the advantage of allowing combustion events to be monitored

without interference caused by simultaneous processes occurring within a furnace environment. A major advance in the understanding of spent liquor combustion was made when cinematographic imaging was first utilized in 1962.[16]

Observation of Drop Combustion

Monaghan and Siddall[16] recorded on film the combustion of calcium sulfite liquor drops at a rate of 8 frames per second. Drops of 53% solids content liquor, 2 mm in diameter, were formed on silica fibers and inserted into a furnace where they were burned in air at 550-810°C. The authors noted four distinct stages of combustion. An initial "boiling period" exhibited rapid, violent expansions and partial contractions of the drop. During the "carbonization" or devolatilization stage no significant change in drop size or shape was noted. After a brief delay, there was a sudden ignition of volatiles surrounding the blackened particle. The final stage was characterized by glowing combustion; a hollow white ash remained at the end of this stage. Huldén[17] presented an important observation from this study not reported by Monaghan and Siddall: the drying and devolatilization behavior of the sulfite liquor drops was no different in an inert nitrogen atmosphere than it was in air.

Björkman[18] reported the results from a sodium-based sulfite liquor pyrolysis study. Single drops, 0.25 mm in diameter, were formed on tungsten wires and placed in the fuel rich region of a diffusion flame. A cinematographic framing rate of 1500-2500 frames/s allowed excellent time resolution of drop pyrolysis "history." During heating at 1000°C, the drops expanded slowly for about one third of a second. There followed a brief (0.03 s) period of bursting; bubble sizes nearly three times the diameter of the initial liquor drop were observed. After a period of "surface boiling," the drop appeared to "solidify" into a porous

mass. The diameter decreased for about 0.3 seconds during gasification of the liquor char. Occasional bubbling and the ejection of tiny particles were noted during this gasification stage. The reported trajectory of the ejected matter indicates that it was released with substantial initial velocity. There was a sudden "melting" or coalescence of the inorganic residue at the end of the gasification stage. At 1000°C the liquid residue completely evaporated within 0.15 seconds. Liquor drops were completely consumed at temperatures above 900°C. Below 800°C no physical changes were observed after solidification of the char. Björkman[18] noted that the bursting seemed to be less violent and the surface boiling more pronounced at 800°C than at 1000°C.

Volkov et al.[11] reported incidental observations of drop behavior from their investigation of sodium loss during kraft black liquor combustion. They formed 2-5 mm drops of 75% solids content liquor on platinum wires and inserted them into a reactor for a specific amount of time. Reactor temperature was varied from 900 to 1100°C. Gas composition was controlled by mixing air with unspecified combustion products; the stoichiometric ratio ranged from 0.88 to 1.4. At stoichiometric ratios greater than one, high-speed films of drop combustion revealed "fine glowing particles" or sparks escaping from the main particle "surrounded by a visible corona of flames."[11] Neither the corona nor the sparks were observed if the stoichiometric ratio was at or below unity.

At Åbo Akademi University Hupa et al.[1] studied the combustion of single drops of sodium-based liquors in a muffle furnace with no forced convection. Drops of liquor (0.5-2.5 mm) were formed on platinum wires or thermocouples; combustion was conducted in air over a temperature range of 600-900°C. Cinematographic films, taken at a rate of 36

frames/s, revealed four distinct and sequential stages of drop combustion: drying, combustion of volatiles, char burning, and inorganic reactions (smelt oxidation). Large drops had a tendency to exhibit partial overlap of the second and third stages under some conditions. Sodium-based sulfite liquors did not swell during the devolatilization stage; however, the kraft liquors swelled 20-30 times their initial volume. During the smelt oxidation stage, large incandescent sparks were ejected from the molten residue. There followed a momentarily visible cloud of fine particulate that originated close to the smelt bead surface.

IPST Single Particle Reactor Studies

At the Institute of Paper Science and Technology (IPST), a convective single particle reactor was utilized to study aspects of black liquor combustion.[19,20,21] Black liquor drops or pellets of dried liquor solids were formed on nichrome wires and hung from a microbalance. The lower portion of the furnace was raised to surround the drop, then preheated gases were directed to the reaction chamber. Drop behavior was observed through a view port and either recorded on videotape[19,21] or photographed with a 35 mm camera.[20] The hot gas stream was the only source of heat in most of these experiments; Kulas[21] created a more realistic recovery furnace environment by installing a radiant heating element that surrounded the drop combustion zone. A greater overlap of combustion stages was seen in the video images from the IPST single particle reactor than those from the Åbo Akademi muffle furnace due to unsymmetrical heating.[22]

Characterization of Black Liquor Combustion

The high inorganic content of black liquor and the extensive swelling associated with devolatilization make its combustion behavior unique among fuels. Aspects

of each stage of black liquor combustion, important to the discussion of inorganic aerosol formation, are considered in this section. The following discussion treats drying, devolatilization, char burning, and smelt oxidation as distinct and sequential stages of combustion; note, however, that there is always some overlapping of the physical processes occurring during drop combustion.[23] The extent of stage overlap depends on liquor properties and combustion conditions.

Drying

The drying stage of black liquor drop combustion is characterized by violent bursting as the water is vaporized. Drops increase in size approximately 1-2 times their initial diameter during drying.[24,25] The end of the drying stage is identified by the first sign of a visible flame.[1] Depending on liquor properties and heating rate, drops may ignite before they are completely dry. For a large fixed drop in a hot flowing gas, the average solids content at ignition may be as low as 75%.[23]

Devolatilization

Black liquor devolatilization is characterized by rapid particle volume expansion and continuously increasing particle temperature. Organic components of the black liquor solids begin to decompose as particle temperatures reach 200°C.[26] Volatile gases are released as particle temperature increases from 250°C to 500°C; the period of rapid swelling occurs between 400 and 500°C.[20] If the temperature of the gaseous environment is above 550°C and the oxygen content is greater than 10%, the escaping volatiles ignite and form a visible flame around the swelling particle.[23]

Extinction of the visible flame is commonly used to mark the end of the

devolatilization stage.[22] Normally this event corresponds with the point of maximum particle size, but the flame may persist a few tenths of a second after maximum swollen volume is reached. Devolatilization is a complex process; however, the duration of the stage has been shown to depend primarily on heating rate and the volatiles yield of the black liquor.[26]

Swelling During Devolatilization

The extent of swelling during devolatilization is primarily a function of temperature, liquor properties, and gas composition. Over a studied range of 300-900°C, maximum swelling occurred at 500°C.[20] Miller[20] found that a number of black liquor components affected swelling behavior, e.g., increasing extractives content greatly reduced the extent of swelling. Frederick et al.[25] investigated the swelling of single drops of softwood kraft liquor at 800°C. They reported the specific swollen volume -- volume of swollen char divided by initial mass of liquor solids -- for various gas compositions. In atmospheres of nitrogen containing 21% O_2 (air), 20% CO_2, or 20% H_2O, the specific swollen volume was 43-66 cm^3/g. They reported an average swollen volume of 133 ± 33 cm^3/g for exposure to pure N_2 and 234 ± 121 cm^3/g for exposure to N_2 with 4-12% O_2.

Char Burning

Char burning is the longest stage of black liquor combustion; it extends from extinction of the volatiles flame to the sudden collapse of the residue into a molten smelt bead.[1] The process has been treated as oxygen mass transfer-limited heterogeneous combustion. It has been proposed that molten inorganic salts enhance the rate of char carbon consumption by a regenerative sulfate-sulfide cycle.[19] Gasification of the char carbon by CO_2 and H_2O contributes to char burning in regions of the recovery furnace having high

concentrations of these reactants.[2] The high gasification rate of kraft black liquor has been attributed to the catalytic effect of finely dispersed sodium salts in the char.[27,28]

Char burning rate depends strongly on particle surface area, which is a function of initial drop size and the extent of swelling. The duration of char burning depends on the gasification and/or combustion reaction rates and the amount of carbon remaining in the char at the end of devolatilization.[23] Residual carbon content is determined by the volatiles yield of the liquor.

Smelt Oxidation

Approximately 35% of the initial black liquor solids remain at the end of char burning as inorganic smelt. The elapsed time from collapse of the char particle to visible cooling of the smelt bead has been termed the inorganic reactions or smelt oxidation stage.[1] Sodium sulfide in the smelt is oxidized to Na_2SO_4 after all the char carbon has all been consumed. This exothermic process increases smelt temperature about 100°C above furnace temperature.[1] The incandescent sparks ejected during this stage are presumably a result of rapid gas evolution caused by gasification of carbon particles trapped during smelt coalescence.

Overview of Coal Combustion

This section serves as a general introduction to coal combustion and identifies important analogies to black liquor combustion. Several mechanisms that have been proposed to explain aerosol formation during coal combustion are also outlined. Review articles and textbooks have been referenced which encompass portions of the vast coal literature. Individual articles are cited when they contain data or discussions which are of particular

relevance to this thesis. Some citations have been included because they were not considered in the reviews of associated topics.

Coal Origin, Combustion, and Conversion

Coal originated from the accumulation of dead vegetation in primordial bogs. A combination of biochemical action, temperature, pressure, and time changed this material, known as peat, into a combustible rock.[29] There are four general classifications of coal; listed in order of increasing rank, they are lignite, subbituminous, bituminous, and anthracite. Increasing rank implies a greater extent of metamorphosis.[30] In general, a coal of higher rank has a lower moisture and volatiles content and a higher amount of fixed carbon.

The combustion of coal to produce steam for electrical power generation is generally conducted in large pulverized fuel furnaces. These are similar in design to kraft recovery units, but they are operated very differently.[31] Finely ground coal is entrained in a stream of combustion air entering the furnace. The suspended coal particles follow a sequence of combustion stages that are similar to those of airborne black liquor drops: drying, ignition, devolatilization, and heterogeneous char burning.[32,33] While coal combustion does produce a silica aerosol (fly ash) that must be removed from the flue gas, the behavior of most of the inorganic compounds in coal is not of particular interest to a study of black liquor combustion. However, physical and chemical transformations of the alkali compounds in coal parallel some of those occurring during black liquor devolatilization and char burning. These processes are discussed in following sections.

Coal is not only used as a fuel in its native state, but it is also converted into cleaner-burning fuels and valuable chemical feedstocks. Destructive distillation or pyrolysis

is used to produce coke, a solid metallurgical fuel, and liquid and gaseous by-products.[31] Coal gasification involves reaction with substoichiometric air, CO_2, and/or water vapor to produce a gas containing CO and H_2 which can be used as a fuel or chemical feedstock.[32] For environmental and economic reasons, coal conversion processes have been extensively studied. Results of this research is of interest because the devolatilization and char burning processes for certain types of coal are similar to those for black liquor.

Coal Devolatilization Behavior

Coals that soften and become deformable upon heating are known as plastic coals; they are typically of bituminous rank and exhibit swelling during devolatilization.[34] Several investigators have observed the formation of bubbles and eruption of gas jets through the surface of plastic coals during devolatilization.[34] Ragland and Weiss[35] studied single particle combustion of various coals suspended in a gas stream (10.5 and 21% O_2 in N_2) at 705 to 816°C. Bituminous coal exhibited swelling and pronounced bubble bursting during its devolatilization stage. For the range of conditions studied, swelling of this coal was greater at the lower temperature and oxygen content. It is interesting to compare devolatilization behavior between plastic coals and black liquor; evidence of bubble bursting[18,20] and the effects of furnace conditions on swelling[20,25] are similar for both materials.

Ragland and Weiss[35] did not observe swelling during the devolatilization of lignite and subbituminous coals; however, they noted that small pieces of burning material were occasionally ejected during devolatilization. Pyrolysis of these nonplastic coals leaves a residue of friable char instead of a hard coke.[29] In this regard, low grade coals are similar to black liquor.

Coal Mineral Matter and Fly Ash

Coal is a heterogenous substance containing discrete regions of organic plant remains, known as macerals, and mineral matter. The mineral content of coal ranges from 5 to 20%, on a dry mass basis.[32,36] More than 75% of coal inorganic matter is present as inclusions of quartz, clays, limestone, and other minerals (sulfides, sulfates, phosphates, chlorides).[36] Irrespective of rank, the mean size of this adventitious mineral matter is 1-2 μm.[37] The remainder of the coal inorganic content is organically bound within the macerals; this is known as inherent mineral matter.[29] By comparison, all the inorganic material in black liquor could be considered to be inherent because it is either dispersed throughout the medium in the form of dissociated salts, or is ionically associated with certain functional groups of the organic compounds.[38]

The amount, composition, and distribution of mineral matter varies greatly with both coal rank and geographic location. Huffman and Huggins[39] illustrate how this variation pertains to alkali compounds. Most of the potassium in bituminous coals is found in the clay mineral illite. Only small amounts of adventitious illite are present in low rank coals; however, significant amounts of potassium are organically bound to the humic and carboxylic acid groups of lignite.[39] Sodium follows a similar mode of occurrence with coal rank.[40] Although alkali species are not major coal components, the combined alkali content (Na and K) may account for more than 5% of the total mineral matter present in coal.[30,36] For comparison, the alkali content of black liquor solids ranges from 17 to 22%.[38]

The majority of the mineral matter in coal produces fly ash during combustion. During exposure to the high temperature furnace environment (1400 to 1700°C) some of the

minerals in coal ash melt, chemical reactions take place (such as calcining), and some species volatilize.[41] The resulting fly ash is a complex heterogenous mixture of particulates. Size distribution, morphology, and chemical composition of coal combustion aerosols have been reported from both field studies of utility boilers[42,43,44] and laboratory studies of specially-designed combustors.[45,46,47] Mass size distributions of coal combustion aerosols were found to be distinctly bimodal in both types of experiments. The particle size of the larger fraction ranges from 0.5 to 20 μm. Reported mass mean (or median) diameters of this coarse fraction range from 1.6 μm[42] to 10 μm.[46] It is generally agreed that the submicron-sized fraction is narrowly distributed around 0.05 μm.[44,45] While the coarse fraction comprises more than 90% of the total aerosol mass, the number of submicron-sized particles far exceeds that of the larger aerosol.[47] Particles greater than 0.3 μm are similar in composition to the mineral matter in the parent coal.[45] However, the composition of the submicron-sized fraction depends strongly on coal rank and combustion conditions.[44,46,48]

Aerosol Formation During Coal Combustion

There are two general categories of aerosol, dispersion and condensation.[49] Dispersion aerosols are formed by grinding or spraying, e.g., dust and atomized mists. Condensation aerosols result when supersaturated vapors condense or when gaseous reactions produce non-volatile products; this category includes mists, smokes, and fumes. A combination of these mechanisms of aerosol formation explain the bimodal size distribution of fly ash produced from coal combustion.[37] During pulverized coal combustion the mineral inclusions adhere to the receding char surface, where they fuse and coalesce to form large ash particles. Fragmentation of the char during combustion results in 3-5 ash particles being produced per original coal particle. The resulting 1-20 μm ash particles account for the

majority of the fly ash produced during combustion.[37] Certain organically-bound salts, as well as a small portion of the adventitious mineral compounds vaporize during combustion and subsequently condense in the gas phase to form submicron-sized fume.[46]

Organically-bound alkaline earth metals are primarily responsible for the submicron-sized aerosols produced during combustion of Western lignites.[46] Enhanced vaporization of alkaline earth metals has been explained by a two-step process. First the stable refractory oxide (e.g., MgO) is reduced to the more volatile metal (Mg) species within localized environments of the burning coal particle. Oxidation of the vaporized metal in the gas phase results in supersaturation and homogenous condensation of the refractory oxide in the atmosphere surrounding the coal particle.[46]

Neville and Sarofim[40] found that sodium fume formation during lignite combustion depends on both the rate of sodium vaporization and the extent of its capture by molten silica ash. For combustion temperatures below 1600°C, all the inherent sodium was expected to be released. As combustion temperature was increased -- by increasing oxygen partial pressure in their laminar entrained flow particle reactor -- the extent of sodium loss unexpectedly decreased from 100% in 5% O_2 to 22% in 50% O_2. Neville and Sarofim[40] proposed that the solubility of sodium in molten silica increased as the combustion temperature increased above the silica melting point. That which was not captured by the silica slag as it was diffusing out through the pores would condense homogeneously in the cooler zone of the furnace.

Volatile alkali species may also condense heterogeneously on the surface of refractory oxide particulate.[36,40] Raask[36] proposed a mechanism of "captive" sodium and

potassium sulfate fume formation to explain the nodules observed in scanning electron microscope (SEM) photomicrographs of silica ash particles.[37,43] It was suggested that alkali vaporizes from the chloride minerals in bituminous coal. The sodium vapor is subsequently captured on the surface of vitrified silicate ash particles. When the silica aerosol cools to approximately 1000°C, sulfation of the alkali creates Na_2SO_4 fume nodules.[36]

The submicron-sized silica aerosol fraction has been attributed to a vaporization-condensation process, similar to that which was proposed for alkaline earth fume formation.[40,46] Smith et al.[50] proposed an entirely different mechanism of silica fume generation. They suggested that bursting ash particles are responsible for a large fraction of the submicron-sized aerosol formed during pulverized coal combustion. During rapid heating, gas jets were observed erupting through the slag film surrounding fly ash particles. It was proposed that these eruptions liberate volatile substances that subsequently condense as fume.[50] Raask[36] observed that some larger particles were ejected during slag film rupture but contended that very few submicron-sized particles were formed as a result of the gas explosions. Faist et al.[51] suggested that an intermediate size of aerosol could be formed by slag film rupture.

Aerosol Formation During Black Liquor Combustion

There are surprisingly few published studies of recovery furnace particulate analysis. The limited information available is reviewed in this section; clearly there is a need for a comprehensive analysis of recovery furnace aerosol. This section discusses major theories of fume formation in the kraft recovery furnace, considers the role of potassium, and presents recent results which suggest that a significant amount of sodium is released during

black liquor devolatilization.

Analysis of Recovery Furnace Aerosols

Bosch et al.[52] measured the particle size distribution of aerosol collected from a kraft recovery furnace. They inserted a cascade impactor into the flue gas stream at both the inlet and outlet of the electrostatic precipitator. Two distinct types of particles were collected: black carbonaceous ash and white sodium salt fume. Ash particles were between 7 and 20 μm in diameter. The size of the white fume fraction ranged from less than 0.6 to about 2 μm. Half of the material by weight entering the precipitator was under 1.0 μm.

Nguyen and Rowbottom[53] investigated the morphology of the particulate in two recovery furnaces using a cascade impactor. The mass mean diameter of particles entering the precipitator was 0.5-1.9 μm. Below 0.3 μm the fraction of dust decreased sharply with decreasing diameter. About 20% of the particulate was larger than 10 μm. The predominant fraction of their samples was submicron-sized, smooth, spherical fume. They described three other distinct fractions: 2-4 μm spherical particles with regular pebbled surfaces; 11-83 μm hollow spheres with a somewhat porous crystallized surface partially covered with fine fume; and carryover char, consisting of 10 μm fragments and 2-3 mm spherical shells.

During their experiments, Nguyen and Rowbottom[53] recorded an unexpected drop in combustion air temperature from 138 to 25°C which resulted in a 20% lower dust loading in the flue gas. As they did not report the corresponding furnace temperatures, it is not certain if the reduction in fume formation was due to decreased bed temperature or a change in air flow rate. A regression analysis of various firing conditions versus particulate

loading indicated fume generation increased with increased firing rate and salt cake (makeup Na_2SO_4) addition. These regression equations only accounted for 40% of the variability, indicating a high degree of experimental uncertainty.

Reeve et al.[54] conducted superheater deposit studies using an insulated air-cooled probe to collect entrained particulate. Analysis of the upstream deposits on the probe, inserted near the bottom of the superheater, revealed predominantly partially-burned black liquor residue. These deposits were rich in carbonate and hydroxide ions, and lean in chloride and potassium. The material that deposited on the downstream side was almost entirely a fine white powder of submicron-sized particles. This fume fraction was composed primarily of Na_2SO_4 with only small amounts of carbonate and hydroxide; the downstream deposits were significantly enriched in chloride and potassium. Higher in the superheater (5.2 m below the roof), both sides of the probe were covered with the fine white powder. SEM photomicrographs showed a number of 30-100 μm spheres among the upstream deposits.[55] These spheres were thought to be the inorganic residue from complete combustion of entrained liquor drops. The authors noted that the ratio of Na_2SO_4 to Na_2CO_3 increased with furnace sampling elevation. Sodium chloride content increased while NaOH disappeared entirely at the higher elevation in the superheater. Analysis of precipitator dust revealed it to be mostly Na_2SO_4 with less than 10% Na_2CO_3.[54]

Rizhinshvili and Kaplun[4] used a two stage impactor to extract dust samples from various locations in a recovery furnace. The coarse fraction of their samples contained 2-20 mm black carbonaceous particles. These were numerous at the liquor spray level, but amounted to only 3-5% of the material leaving the furnace cavity. The fine fraction,

collected on glass fiber filters, was submicron-sized fume. As long as auxiliary fuel was being burned, the fume was observed to persist in the furnace after liquor firing stopped. At the tertiary air level the fine fraction was 64% Na_2SO_4, 6% Na_2CO_3, 11% Na_2S, and 18% Na_2SO_3 + $Na_2S_2O_3$; at the furnace outlet the Na_2SO_4 composition had increased to 96%. In a similar study, Zhuchkov et al.[56] reported the composition of the fine fraction to be 66-72% Na_2SO_4, 23-26% Na_2CO_3, 0-7% Na_2S, and 0-4% carbon.

The effect of process conditions on the particulate sampled at the exit of the economizer was investigated by Rizhinshvili and Kaplun.[4] Total particulate loading was found to be directly proportional to char bed temperature at the primary air level; they reported a doubling of dust concentration for a temperature increase of 1090 to 1200°C. The temperature of other zones of the furnace had no apparent effect on the dust load. It was also noted that increasing bed temperature and decreasing excess air decreased the Na_2SO_4 content of the fume fraction.

The effects of liquor solids content on furnace dust loading and fume composition have been reported by Hyöty et al.[7,57] One advantage of burning higher solids content liquor is reduced heat loss to water evaporation. The mill test results showed that increasing liquor solids from 65 to 80% increased lower furnace temperatures by 100°C[57] and approximately doubled dust loading.[7] At higher temperature, the increased generation rate of sodium fume relative to sulfur release also results in more effective removal of SO_x in the flue gas. This explains the decreased Na_2SO_4 content of the fume, observed by Rizhinshvili and Kaplun.[4]

In summary, discounting char carryover, recovery furnace aerosol sampling

indicates there is a single submicron-sized mode of particulate produced during black liquor combustion. Unfortunately, the impactor samples were all taken at the entrance to the electrostatic precipitator. Deposition on heat transfer surfaces within the recovery furnace could have significantly biased the size distribution. It is therefore not certain that there is only one size of inorganic aerosol formed during black liquor combustion.

Fume Formation During Black Liquor Combustion

Although the final composition of fume is primarily Na_2SO_4 with approximately 10% Na_2CO_3, it is unlikely that fume originates from direct vaporization of these species. The vapor pressure of pure Na_2SO_4 is 2.7 x 10^{-2} Pa at 980°C.[58] At the same temperature the vapor pressure of Na_2CO_3 is approximately 11 Pa.[59] Advanced equilibrium calculations indicate that elemental sodium vapor, NaOH, and NaCl are the primary sodium species in the gas phase above the char bed.[60] The vapor pressures of these compounds at 980°C are at least four orders of magnitude higher than Na_2SO_4.[26] Fume must therefore originate from gas phase reactions of volatile alkali species, e.g., Na and NaOH, to form condensed products. An excellent review of all the reactions proposed to explain fume formation and subsequent capture of oxidized sulfur gases in the kraft recovery furnace has been provided by Blackwell and King.[61]

Fume formation in the kraft recovery furnace was first attributed to sodium vaporization from the reducing environment of the char bed.[9] A condensed fume species (Na_2O) was thought to form just above the bed, where the reactive metal vapor first encountered oxygen. Lang et al.[9] suggested the actual fume formation rate would be higher than that indicated by their equilibrium calculations because the gaseous products would be

swept out of the reaction zone by convection. Equilibrium models of complex combustion systems are often utilized because they do not require a detailed understanding of reaction mechanisms and they provide a valid first approximation of furnace chemistry.[62] In general, equilibrium model predictions agree with limited furnace gas composition data.[5] A Gibbs free energy minimization model predicted an eight to ten-fold increase in Na and NaOH vaporization for each 100°C increase in char bed temperature (over the range of 900 to 1200°C).[60] This calculation does not agree with mill data that suggests fume formation approximately doubles for a 100°C increase in bed temperature.[4,7] Another shortcoming of equilibrium calculations is overestimation of potassium and chloride enrichment in the fume.[63]

Researchers at IPST found that when oxygen-containing gas was contacted with molten Na_2S-Na_2CO_3 systems an order of magnitude more fume was produced than what had been measured under reducing conditions.[10] The measured rate of "oxidative" fume formation was much greater than that estimated by assuming that equilibrium sodium vapor pressure had been established. Extensive molten salt reactor studies were conducted to evaluate the effects of temperature, gas and melt composition, gas flow rate, and gas-melt contact geometry on fume formation rate.[64] Cameron[65] proposed a reaction-enhanced mechanism of fume formation, wherein rapid oxidation of sodium vapor near the smelt surface reduces the partial pressure of sodium in the boundary layer. The resulting increase in driving force enhances the rate of sodium vaporization. Similar mechanisms have been used to explain enhanced vaporization and metal oxide fume formation during high temperature metallurgical processing[66] and formation of refractory oxide fume during coal combustion.[46]

Cameron's model predicted that, at a smelt temperature of 927°C, fume formation rate would double for a 108°C increase in temperature.[64] This dependance agrees well with available mill data.[4,7,53] The model more accurately predicted the potassium and chloride composition of fume than had the equilibrium models.[63] Reaction-enhanced sodium vaporization has been generally accepted as the main source of fume in the recovery furnace. As described below, this model can explain fume formation during both the char burning and inorganic reaction stages of black liquor combustion.[26]

Grace et al.[19] proposed a sulfate-sulfide cycle to explain the high degree of sulfate reduction achieved during char burning. Theoretically, this sulfate-sulfide cycle establishes an equilibrium concentration of elemental sodium in the char.[26] Sodium has a high vapor pressure at char burning temperatures; thus, it is present in the boundary layer above the char bed or surrounding entrained char particles. Condensed fume species will be produced by reactions among sodium vapor, oxygen, water vapor, and carbon dioxide.[61] Once the char carbon has been consumed, the reduction of Na_2CO_3 by Na_2S maintains a sodium vapor pressure above the molten smelt. Thus, the residual inorganics, in the form of entrained droplets or flowing smelt, will produce fume in the presence of oxygen. Fume formation continues until all the molten Na_2S is oxidized to Na_2SO_4.[65]

Potassium and Fume Formation

The potassium equivalents of sodium compounds form a small, but significant, portion of recovery furnace fume. Wood generally contains more potassium ions than sodium ions, which readily accumulate in a mill liquor cycle with low effluent discharge.[67] Because KOH, K_2S, K_2SO_4, and K_2CO_3 are more soluble than their sodium counterparts, potassium is

difficult to purge from the kraft liquor system.[68] Reeve et al.[69] predicted that increasing mill closure and hardwood usage will cause potassium concentrations to reach levels of 10-20% K/(K+Na) in the liquor cycle.

Although the presence of potassium species is not necessarily detrimental to the pulping and recovery process,[68] the effect of potassium on fume formation is not clearly understood. However, the mechanisms responsible for sodium fume generation should also be applicable to potassium species. The vapor pressure of KCl and KOH are higher than NaCl and NaOH, which results in an enrichment of potassium in the aerosol deposits.[69]

Potassium was not considered during this investigation of aerosol formation during drop combustion largely because the potassium content of a single liquor drop or collected aerosol sample were very close to the analytical detection limit for this compound.

Sodium Loss During Devolatilization

Sodium release prior to char burning has only recently been considered as a possible source of fume in the recovery furnace. Frederick and Hupa[13] proposed that sodium loss during devolatilization could be the most significant source of fume because it can account for the total amount of sodium collected in the electrostatic precipitator. The focus of this thesis was to evaluate the significance of this sodium loss on overall fume formation. This section reviews the literature most closely related to the thesis topic; specifically, the measurement of sodium loss during black liquor drop studies and thermogravimetric analysis (TGA) of black liquor solids.

Volkov et al.[11] exposed drops of kraft black liquor to oxidizing conditions over

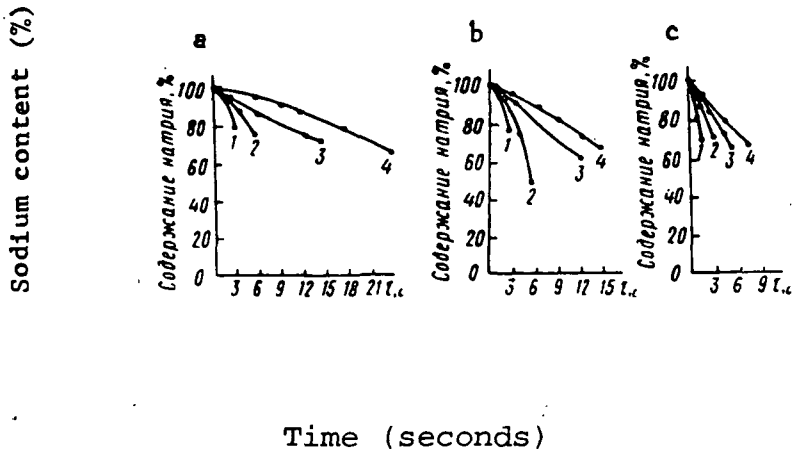

Figure 1. Sodium loss vs. exposure time for combustion in air at temperatures: a) 900°C, b) 1000°C, c) 1100°C. Drop diameter: 1) 2 mm, 2) 3 mm, 3) 4 mm, 4) 5 mm. Reprinted from Volkov et al.[11]

a temperature range of 900-1100°C. Char residue was extracted through a nitrogen quench stream after fixed exposure times. The total sodium released during combustion ranged from 20-50% of the sodium present in the liquor. Figure 1 shows that sodium loss (i.e., relative decrease from initial sodium content) increased sharply with exposure time for higher temperatures and smaller drop sizes. At the minimum exposure time of three seconds, Volkov et al.[11] reported a 20% sodium loss for 2 mm diameter drops burned in air at 900°C. Model predictions indicate that drying and devolatilization of similar sized drops in air at 800°C would be complete in about three seconds;[26] therefore, it is likely that part or all of the initial sodium loss reported by Volkov occurred during devolatilization.

Frederick et al.[14] measured the change in sodium content during pyrolysis of 8-20 mg drops of black liquor. The drops were exposed for 5-60 seconds to an environment of 95% N_2 with 5% CO within a muffle furnace. A nitrogen stream was used to quench the residue as it was extracted from the furnace. Sodium content was measured by atomic

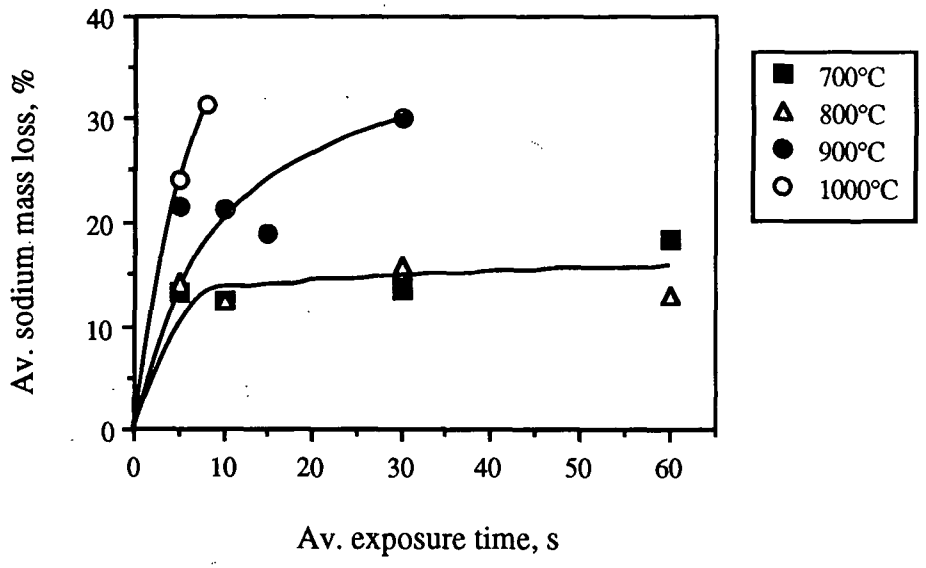

Figure 2. Sodium loss from softwood liquor drops as a function of exposure time and furnace temperature. Stagnant environment of 95% N_2/5% CO. Data replotted from Frederick et al.[14]

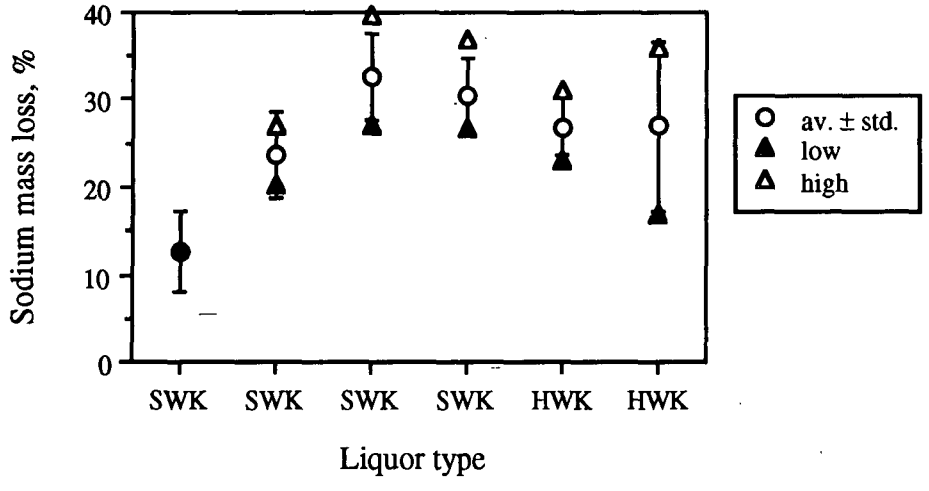

Figure 3. Sodium loss after 10 s drop pyrolysis at 800°C in 95% N_2/5% CO. SWK = softwood kraft, HWK = hardwood kraft, filled circle from Fig. 2. Data replotted from Frederick and Hupa.[13]

absorption spectroscopy for each acid-digested char particle.[70] The effect of furnace temperature on sodium loss is shown in Figure 2. Each of the data points is an average of several sodium loss determinations for individual char particles. The lines are shown in Fig. 2 to group the data; these lines are not based on statistical regression. These results indicate there was a rapid sodium mass loss of 14-18% prior to the end of the devolatilization stage.[14] For temperatures above 800°C, sodium loss did not subside, but continued to increase with exposure time. The continued sodium loss was at a much lower rate than the initial release.

Char sodium content data for five kraft liquors, reported by Frederick and Hupa,[13] are replotted as sodium loss in Fig. 3. Average sodium mass losses of 23 to 33% occurred during pyrolysis for 10 seconds at 800°C. Frederick and Hupa[13] concluded that sodium loss was not dependent on liquor type because the average results were not statistically different. The average sodium loss value for 10 seconds exposure at 800°C from Fig. 2 is included for comparison in Fig. 3. Presumably one of the three softwood kraft liquors shown in Fig. 3 was also used for the experiment reported in Fig. 2. Therefore, the smaller sodium loss observed at otherwise identical conditions was likely the result of different average drop sizes between the two experiments.

In a thermogravimetric study of organic alkali compounds, Stewart et al.[71] found that sodium and potassium benzoate samples exhibited two distinct weight loss regions at 450-550°C and 750-900°C (heating rate 25°C/min in argon). Considerable evidence was presented to suggest that no alkali losses occurred over the lower temperature range, and that substantial amounts of alkali were vaporized as a result of Na_2CO_3 reduction by carbon at the

higher temperatures. This result is supported by the findings of Srinivasachar et al.,[72] who studied sodium release from coal char with atomic absorption spectroscopy. During pyrolysis in argon at high heating rates (250°C/s), sodium release began at 800°C and reached a maximum at 1000°C. Two possible reaction for Na_2CO_3 reduction are given in Eqs. 1 and 2:

$$Na_2CO_3 + 2\,C \rightleftharpoons 2\,Na_g + 3\,CO \quad (1)$$

$$Na_2CO_3 + C \rightleftharpoons 2\,Na_g + CO + CO_2 \quad (2)$$

Li and van Heiningen[12] reported the TGA results of black liquor exposed to various atmospheres. In their experiments, 10 mg samples of dried liquor solids were heated at a rate of 20°C/min under flowing helium; the final temperature of each run was maintained for a fixed amount of time. Table 1 summarizes the conditions and relative changes in sodium content during selected experiments. The values of sodium loss in Table 1 were calculated from their reported liquor and char analyses.

The values in Table 1 indicate that a substantial amount of sodium was released in pyrolysis experiment A. Total sodium loss was reported to increase from 64 to 75% as final temperature was increased from 750 to 800°C.[12] In inert environments, the sodium carbonate remaining in the char is expected to decompose by reaction with carbon to form atomic alkali and CO (Eq. 1).[71] For temperatures up to 750°C, Li and van Heiningen[12] reported that sodium release was suppressed after CO was added to the He gas stream in experiment B. It can therefore be inferred that the 9.7% sodium loss given in Table 1 occurred *before* the sample reached 550°C.

Table 1. Sodium loss during slow pyrolysis of black liquor solids. Calculated from data of Li and van Heiningen.[12]

Experiment (see text)	Temperature program,[a] °C	Elapsed time,[a] min	Gas comp., %[b]	Na mass loss, %
A	25-750	35	100% He	-[c]
	750	60	100% He	63.6
B	25-550	25	100% He	-[c]
	550-750	10	12% CO	-[c]
	750	30	12% CO	9.7
C	25-750	35	100% He	17.9
	750	30	20% CO_2/10% CO	0.3

[a] Temperature ranges and elapsed times are approximate values, taken from reported thermogravimetric analyses.
[b] Gas composition; volume percent of given components, He balance.
[c] Char analyses not available for these calculations.

The addition of CO is expected to suppress sodium vaporization by shifting the equilibrium of the Na_2CO_3 reduction reactions (Eqs. 1-2). Sodium loss was however measured in an atmosphere of 88% He with 12% CO when the final temperature was 800°C; the rate of this loss was less than 5% than that observed in a pure He atmosphere.[12] In experiment C of Table 1, the sample was gasified with CO_2 after the final temperature was reached. Although there was a significant sodium loss during the heating period (in pure He), the amount of sodium in the char remained relatively constant after the CO and CO_2 were added. The stoichiometry of Eq. 2 explains the stability of Na_2CO_3 in the gasification mixture.[27]

Expected Types of Aerosol From Black Liquor Combustion

Approximately two-thirds of the total sodium initially present in black liquor is

associated with ionized organic liquor components.[38] This "organically-bound" sodium typically accounts for 12% of the mass of dry liquor solids.[38,73] Material balances on samples taken from TGA studies indicate that these organic alkali compounds largely decompose to form Na_2CO_3, organics, and CO_2 during pyrolysis.[12,71] As long as the local environment of a char particle contains CO or CO_2 and is kept below 800°C, then Na_2CO_3 reduction by char carbon will be minimal.[12,27,71] Initial sodium loss measured in CO-containing atmospheres must therefore occur before all the organically-bound sodium is stabilized as Na_2CO_3 in the char. One goal of this thesis was to determine the form of the fugitive sodium and assess its significance to overall aerosol formation in the kraft recovery furnace.

Review of literature information suggests that, after the completion of devolatilization, reaction-enhanced vaporization of sodium is expected to produce submicron-sized fume from burning drops of black liquor until the Na_2S in the smelt is fully oxidized to Na_2SO_4. The high temperature and reducing conditions which are maintained in the lower region of a recovery furnace will establish a vapor pressure of sodium above the char bed and flowing smelt. As the sodium vapor diffuses away from the char and smelt it will react with oxygen and condense as submicron-sized fume particles.

Another source of particulate matter in the recovery furnace may result from the physical ejection of material during the violent drying and devolatilization periods of black liquor combustion. Fragmentation of char particles and sparking during smelt coalescence may also produce aerosols. The size range of this ejected material would presumably be 1-100 μm and its chemical composition would depend on the combustion stage

of its origin and the extent of carbon depletion from the black liquor particle.

According to the definitions in Appendix I, the particulate expected to be produced during kraft black liquor combustion is a mixture of fume, dust, and mist. The term fume specifically applies to submicron-sized material originating from condensation of vaporized species. The dust would arise from the ejection of bits of char during devolatilization and char burning. A mist fraction would result from the ejection of tiny droplets during both drying and smelt coalescence. The popular usage of the terms dust and mist may confuse their interpretation in the context of this dissertation; therefore, use of the term *ejecta* is suggested. In the following discussion the term *fume* refers only to material that results from condensation of metallic vapors or evaporated alkali-containing compounds. The term *inorganic aerosol* implies the fume fraction as well as inorganic ejecta.

THESIS OBJECTIVES

There is experimental evidence of sodium release during all stages of black liquor drop combustion. Variations in measured sodium loss rates and observed combustion behavior at different conditions suggest that several aerosol formation mechanisms are associated with the various combustion stages. With the exception of fume formation during smelt oxidation, the relations between sodium loss and inorganic aerosol formation have not been adequately explained.

The goal of this study was to contribute to the understanding of aerosol formation during each stage of black liquor combustion by determining the history of aerosol formation throughout the stages of drop combustion. Aerosol formation was to be quantified by measuring the amount of material collected as a function of combustion progress. Identification of changes in aerosol morphology with combustion conditions would qualitatively indicate the different types of aerosol formed.

Sodium release measured during the pyrolysis of individual liquor drops can account for all the fume collected in a recovery furnace precipitator. It has been suggested that sodium loss during devolatilization is therefore the most significant source of fume; however, important information to support such a hypothesis is lacking. A possible mechanism to explain this sodium release has not been proposed. The form of the lost sodium has not been identified, nor has its impact on overall fume formation in the recovery furnace been verified.

The main objectives of this thesis were to propose a tenable mechanism of

sodium release prior to the char burning stage of drop combustion and to predict the importance of this sodium release on overall fume formation. Conducting single drop experiments in non-combustive atmospheres would allow sodium loss during drying and devolatilization to be isolated from other combustion stages. Evaluating the effects of changing process variables (temperature, exposure time, gas composition, gas flow rate, and drop size) and liquor properties on sodium release from black liquor drops would indicate which factors were controlling the process. The results of this evaluation would suggest the mechanism responsible for sodium loss, e.g., evaporation or physical ejection. Microscopic investigation of aerosol samples, collected during pyrolysis experiments, would identify the form of the released sodium. Comparison of these aerosol samples with those obtained under combustive conditions would indicate the relative amount of fume formed prior to char burning.

Results of these experiments and consideration of literature information should suggest the fate of alkali released prior to char burning in a recovery furnace. Due to the simultaneous processes occurring during black liquor combustion, the impact of sodium loss measured during laboratory experiments on overall fume formation in an operating recovery furnace would best be evaluated by a complex recovery furnace model. Such a computational study and requisite validation by industrial particulate sampling was beyond the scope of this work.

EXPERIMENTAL

A unique experimental apparatus was developed to achieve the thesis goals. It was necessary to simulate recovery furnace combustion conditions, and to minimize material losses within the system. Coordination of measured sodium loss or collected aerosol mass with observed combustion progress was essential for producing meaningful results.

This chapter contains descriptions of the apparatus, procedures, and materials used in the experimental work. Specific equipment configurations are presented on a case-by-case basis as they apply to analysis of the results. A detailed list of major equipment components is included in Appendix II.

APPARATUS AND PROCEDURE

Two principal kinds of experiments were conducted during this thesis: sodium mass loss determinations and dynamic aerosol collections. The sodium mass loss determinations were part of a focused investigation to assess the extent of sodium release prior to char burning. A drop furnace and a muffle furnace apparatus were employed to study sodium loss. In the drop furnace experiments, the relative change in sodium content during pyrolysis was determined as a function of temperature, gas composition, and exposure time. The muffle furnace experiment was conducted to differentiate the sodium loss during drying from that occurring during devolatilization.

During the dynamic aerosol collection experiments, drop combustion events were recorded on videotape while a moving collection medium simultaneously captured the generated particulate. Knowing the speed of the moving medium and the reactor residence

time, it was possible to coordinate the timed-observation of drop combustion with the analysis of collected material, thereby creating a history of aerosol formation throughout the respective stages of drop combustion. Details of the experimental procedures are presented following a description of the drop furnace.

Drop Furnace

The IPST drop furnace was designed to study the combustion and pyrolysis of individual black liquor drops in a simulated recovery furnace environment. The following sections describe the components of the drop furnace system and evaluate its performance.

Drop Furnace Construction

The major components of the drop furnace are shown in Fig. 4. The gas heater was constructed from a 64-mm (2.5-in.) ID mullite tube packed with ceramic Berl saddles and surrounded by ceramic fiber heating elements. A 152-mm (6-in.) preheater section, controlled by a variable autotransformer, reduced the heating load on the main elements. A time-proportioning PID electronic controller maintained the gas temperature at the exit of the packed tube. Gas temperature was measured by a bare-junction thermocouple that was oriented away from the open end of the reactor tube.

The drop reactor was custom-fabricated from a 65-mm ID quartz tube, surrounded by custom-fabricated ceramic fiber heating elements. A second PID controller maintained the wall temperature of the drop reactor. The wall temperature control thermocouple was situated in the annulus between the quartz tube and the heating elements. In this configuration accurate wall temperature control was possible, as described in the next section. The drop insertion rod placed liquor drops rapidly and precisely into the center of

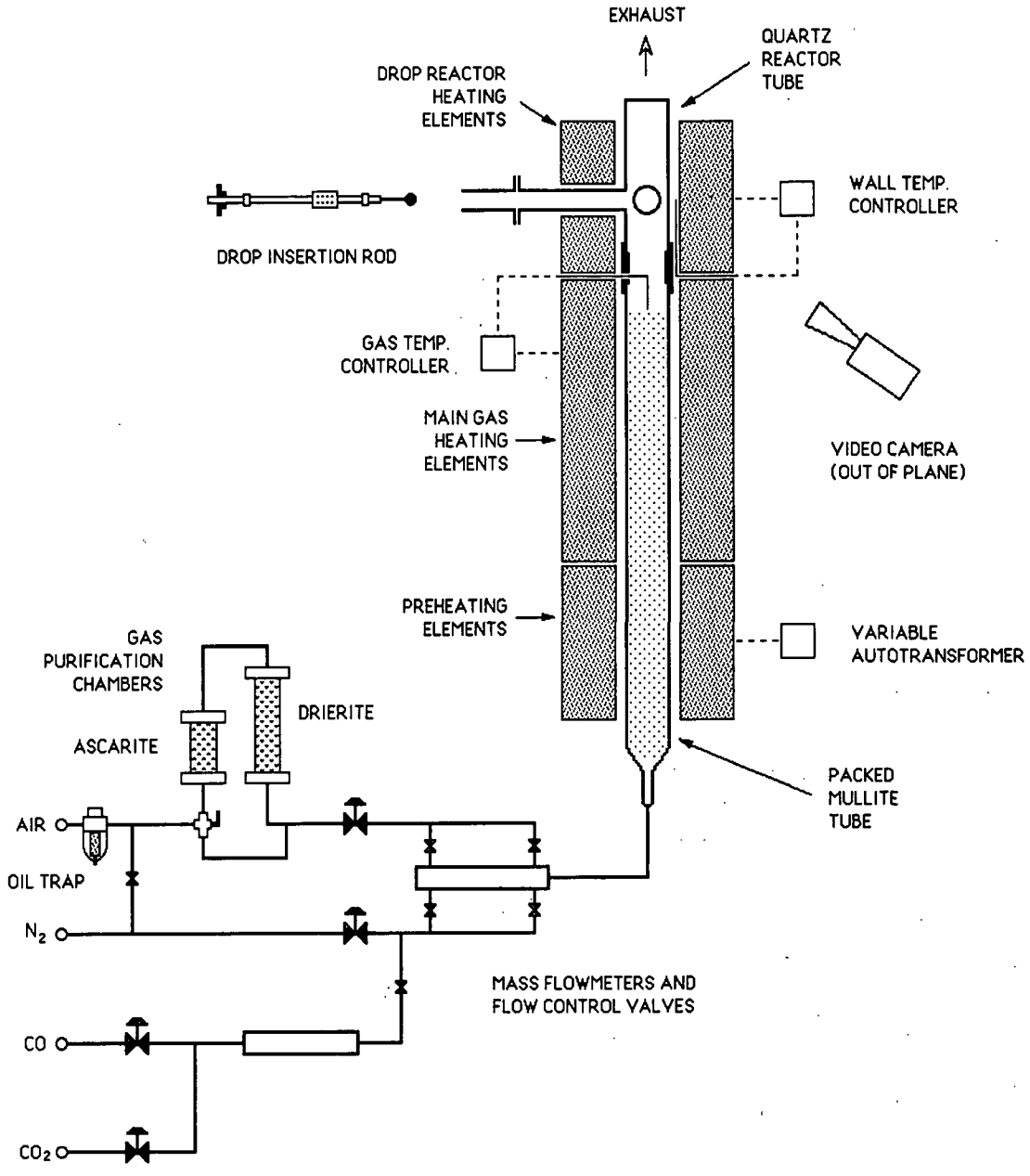

Figure 4. Schematic of drop furnace showing main components and temperature control system.

the reaction chamber.

Gas purification chambers, packed with Ascarite II™ (NaOH on granular silica) and indicating Drierite® (anhydrous $CaSO_4$), removed CO_2 and water vapor from the

house air supply. The chambers were bypassed during heat up, cool down, and furnace condition changes to increase the life of the absorbents. Air and nitrogen flows were regulated by globe valves and monitored by a Hastings digital mass flowmeter. This device measured mass flow independently of gas temperature and pressure. The instrument was calibrated for air; thus, the reading for mixtures of gases had to be corrected by appropriate heat capacity factors. An additional Hastings mass flowmeter was used to monitor the addition of auxiliary gases (CO and CO_2) to the carrier gas flow.

Drop Furnace Evaluation

For evaluation of drop furnace performance, the following values were taken from an analysis of typical recovery furnace operation.[26] Gas temperature increases from 900-1100°C in the lower furnace to about 1200°C at the tertiary air level, then decreases to 900-1000°C at the bullnose (water wall arch), and further to 650°C at the steam generating bank inlet. Radiation accounts for a significant fraction of the heat transfer between any given droplet and its surroundings. The primary radiating regions are the furnace walls at about 500°C, the fireball at 1500-1750°C (for 73% solids content liquor), and the char bed surface at 900-1100°C.

The mean gas velocity in a furnace ranges from 3 to 6 m/s (10-20 ft/s); the settling velocity of a liquor drop, 2 mm in initial diameter, would be 1-11 m/s (3-35 ft/s) depending on the extent of combustion. Relative velocity between the drop and furnace gases could therefore vary from 0 m/s for an entrained particle to 8 m/s (25 ft/s) for a falling smelt bead. Gas composition varies extensively within the furnace. Oxygen content ranges from 21% by volume at the air ports to 2% (wet basis) in the exhaust stack. Partial pressures of

both water vapor and CO_2 can reach 10% by volume in certain regions of the furnace.

A stable temperature of 500-900°C could be maintained in the IPST drop furnace over a gas flow rate range producing an average gas velocity of 0.15-1.83 m/s (0.5-6 ft/s) in the reaction zone of the furnace. The gas environment was controlled by mixing compressed gases; thus, virtually any gas composition was possible. Based on the above analysis, the IPST drop furnace could produce an environment similar to the upper region of a recovery furnace. While limited in maximum achievable temperature, this system offered the advantage of combined radiative and convective heating. Previous studies of black liquor drop combustion processes relied primarily on forced convection of hot gases[19,20,21] or radiant heating in a stagnant controlled atmosphere;[1,13] some of the data obtained in these studies may therefore be limited in application to recovery furnace environments. It has been argued that the convective environment best simulates that of the recovery furnace, and that the uniform heat transfer within a muffle furnace with no forced convection is best for comparative analysis of liquor burning behavior.[22] The actual environment of a liquor drop in a recovery furnace lies somewhere between these two cases. Although the "real" drop moves through a flow field with some relative velocity, it may also freely rotate which would tend to reduce heating non-uniformities.

Independent control of wall and gas temperatures was possible with the IPST drop furnace; however, all of the experiments were conducted with these temperatures being equal. Figure 5 presents a comparison of drop reactor wall temperature measurements by the control thermocouple and a two color pyrometer. Over the range of operating conditions, temperatures determined by the pyrometer are within 20°C of the thermocouple

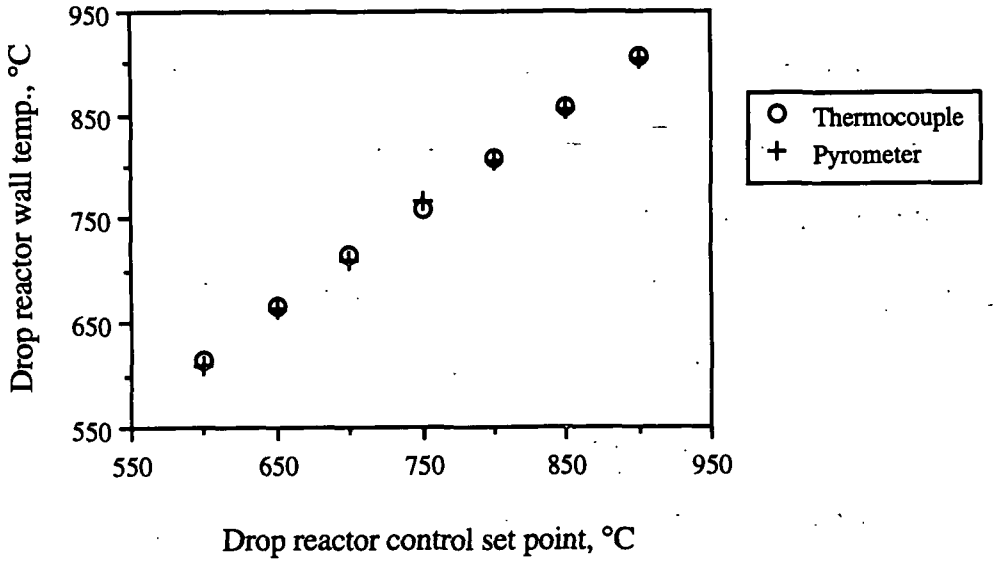

Figure 5. Comparison of thermocouple and pyrometer measurements of drop reactor wall temperature. Av. gas velocity: 0.91 m/s.

measurements. This result demonstrates that radiation errors were not significantly affecting the measurement of wall temperature by the control thermocouple. Details of the design and operation of the two color pyrometer are given by Kulas.[21]

Drop Observation

Observations of drop combustion and pyrolysis in the furnace were made by a color video camera and recorded on VHS videotape. The video system produced 30 images per second. Times for each stage of drop combustion were calculated from the elapsed time indicated on the video images. The first appearance of the drop in the field of view was used to denote the start of drying. The first sign of swelling or ignition indicated the onset of devolatilization. The maximum swollen volume of the char particle was taken as the start of char burning. Coalescence of a smelt bead denoted the start of smelt oxidation. Visible cooling of the smelt was taken as the end of drop combustion. These definitions imply that

drying, devolatilization, char burning, and smelt oxidation are distinct and sequential stages of combustion; note, however, that there is always some overlapping of the processes occurring during drop combustion.[23]

Sodium Mass Loss Determination

Drop Furnace Experiments

For the investigation of sodium loss during drop pyrolysis, the insertion port to the quartz reaction chamber was modified to prevent air infiltration and to allow char residue from individual drops to be extracted though a quench stream of nitrogen. A wide range of pyrolytic conditions were chosen to extend the temperature range that had been investigated in previous sodium loss studies: 500-900°C in atmospheres of 95% N_2 with 5% CO, 95% N_2 with 5% O_2, and 75% N_2 with 20% CO_2 and 5% CO. For the non-oxygen-containing atmospheres, 5% CO was added to scavenge O_2 from the carrier gas and to suppress Na_2CO_3 decomposition during liquor pyrolysis.[12] During these experiments the nitrogen stream was diverted through the gas purification chambers. House air was metered into the nitrogen carrier gas to create the environment containing 5% O_2. A constant average gas velocity of 0.61 m/s (2 ft/s) was maintained in the quartz reaction chamber in all but one experiment, where the total gas flow was increased to produce 1.83 m/s (6 ft/s) average velocity.

Individual drops of an industrial kraft black liquor, weighing 2 to 10 mg, were formed on nichrome wires and inserted into the reaction chamber of the furnace. After 3 to 30 seconds exposure to the pyrolytic environment, the char was withdrawn into the quench stream and allowed to cool. A constant quench flow of 2-5 std. L/min N_2 was maintained in the 14-mm diameter insertion port. Exposure time was controlled manually with reference to

a hand held stopwatch. As discussed in the Results chapter, control of exposure time was very precise.

Each experiment consisted of 4-9 determinations of sodium mass loss; a typical experiment included 2-3 replicates of three exposure times at a given set of furnace conditions. Composite samples of 4-20 fully-intact char particles were accumulated for each determination. Inductively coupled plasma emission spectrometry (ICP) was used to measure the amount of sodium in acid-digested composite char samples. The initial mass of sodium was calculated from the sum of the drop solids and the sodium content of the liquor, which was determined during each experiment from acid-digested liquor samples. The acid digestion procedure and calculations of sodium mass loss are described in following sections.

Muffle Furnace Experiment

The muffle furnace apparatus, shown in Fig. 6, was used to investigate the sodium loss occurring during the drying stage independently of that occurring during the devolatilization stage of black liquor pyrolysis. The 18-mm ID quartz U-tube was partially packed with ceramic Berl saddles to increase heat transfer to the gas. The pyrolysis environment was 750°C in 95% N_2 with 5% CO flowing at an average open-tube gas velocity of 0.61 m/s. These conditions were chosen for comparison to the drop furnace experiment with the most reproducible sodium mass loss results.

Approximately 100 mg of liquor was applied with a spatula to form a 2 mm by 50-mm line along the bottom of six alumina combustion boats. The 71% solids content liquor was warmed to about 50°C to facilitate application. The six liquor samples were dried overnight at 105°C; liquor was applied to six additional boats at the time of the experiment.

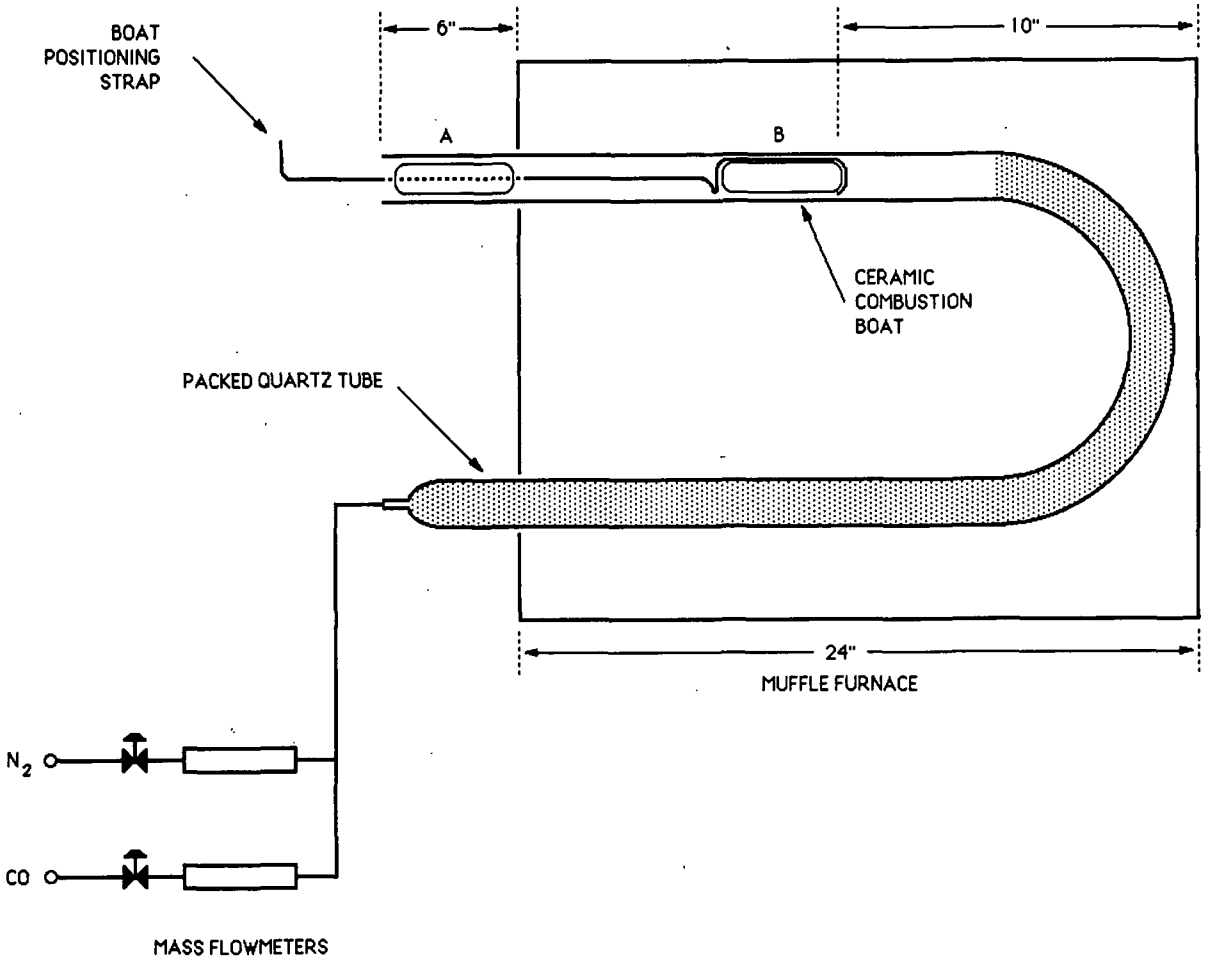

Figure 6. Schematic of muffle furnace apparatus used for sodium loss experiments.

Three boats each of dried solids and wet liquor were pyrolyzed for 60 seconds in the quartz tube. The boats were first placed in the cool end of the quartz tube and then moved into position with a nichrome guide strap. After exposure to the pyrolytic environment, the samples were withdrawn to the end of the tube and allowed to cool for one minute under the nitrogen purge.

After acid digestion each sample and boat was transferred to a 50-ml centrifuge

tube and covered with Type I water.* The mass of the dilution water was determined by difference between the tare weight (centrifuge tube and ceramic boat) and the total sample weight. The char residue was broken up by shaking and ultrasonic agitation. Sodium concentration in all samples was measured by ICP. Three clean alumina boats were also refluxed in the acid solution to determine the background sodium level. The average of these blanks was subtracted from the sample sodium concentration measurements. Three replicate calculations of the relative change in sodium content (sodium loss) during drying and devolatilization were made.

Aerosol Collection

Two equipment configurations were utilized for capturing aerosols generated during drop combustion: static and dynamic collection. Static collection accumulated the aerosol on a small area of a stationary collection medium. Dynamic collection distributed the material over a relatively large area of moving collection medium. Equipment configurations used during the preliminary static aerosol collection trials are described in Appendix V.

Aerosol Collection Media

The aerosol collection system design was based on the use of Whatman EPM-2000 borosilicate glass fiber (BGF) filters as the collection medium. This material was chosen for its high operating temperature limit, high filtration flow capacity, and relatively low cost. Silver membrane filters, manufactured by Poretics Corp., were found to be a more suitable aerosol collection medium. This material combines the desirable characteristics --

* Produced by reverse osmosis filtration of distilled, deionized feed water (specific resistance = 18.3 MΩ·cm).

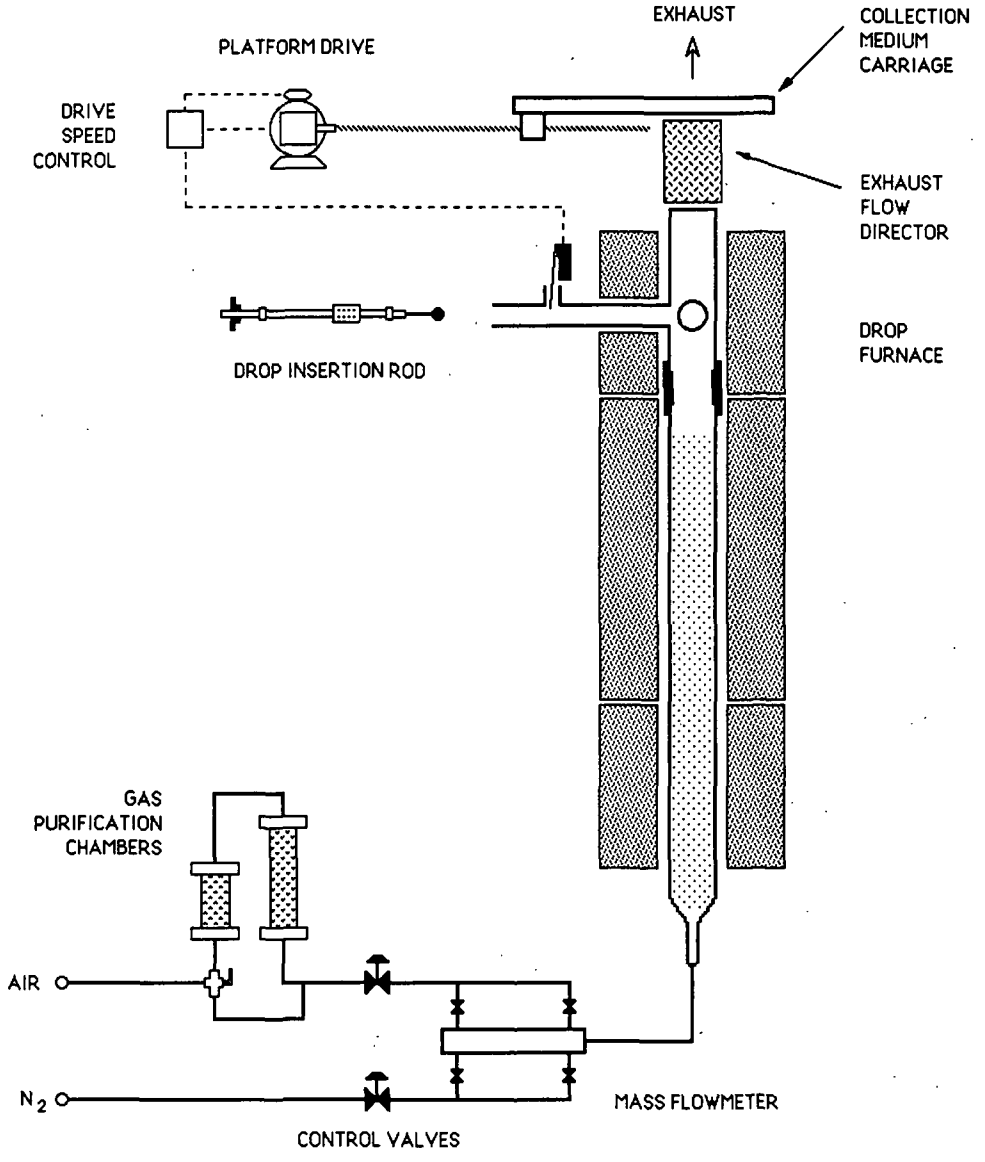

Figure 7. Schematic of experimental system used for dynamic aerosol collection.

high purity and surface capture -- of polymeric screen membranes with the superior strength and thermal stability of BGF filters. High cost and low flow capacity are substantial disadvantages of silver membranes.

Dynamic Aerosol Collection

A schematic of the dynamic aerosol collection system is shown in Fig. 7. For each dynamic aerosol collection, an individual drop of industrial kraft black liquor was formed on a nichrome wire and inserted into the reaction chamber of the furnace. At the moment the drop entered the reaction chamber, a remote switch activated the fume capturing apparatus. The aerosol collection medium was mounted on a carriage that moved over the furnace exit. A constant carriage linear speed of 254.0 ± 0.2 mm/min (10.00 ± 0.01 in./min) was maintained by a dc adjustable-speed reversing drive with a tachometer feedback loop and PID speed control.

The nominal combustion environment in the quartz reaction chamber was 750°C in 92.5% N_2 with 7.5% O_2 flowing at an average gas velocity of 0.61 m/s. This condition was the midpoint of the desired range of gas temperature and composition; the flow rate had to be reduced from the targeted level of 0.91 m/s (3 ft/s) to prevent damage to the aerosol collection medium. House air was mixed with compressed technical grade nitrogen to produce the desired gas composition.

Figure 8 is an overall view of the dynamic aerosol collection system; details of the collection zone are shown in Fig. 9. An "exhaust flow director" was mounted above the quartz reactor tube to cool the exhaust gases and direct their flow to a 25 by 152-mm (1 by 6-in.) rectangular cross section of the 203 by 254-mm (8 by 10-in.) BGF filter. The narrow opening in the direction of filter motion reduced overlap of aerosols formed at different times during drop combustion. The "vacuum flow director" induced flow of the exhaust gases through a continuously moving 25 by 152-mm area of the filter. A backup 50-mm square

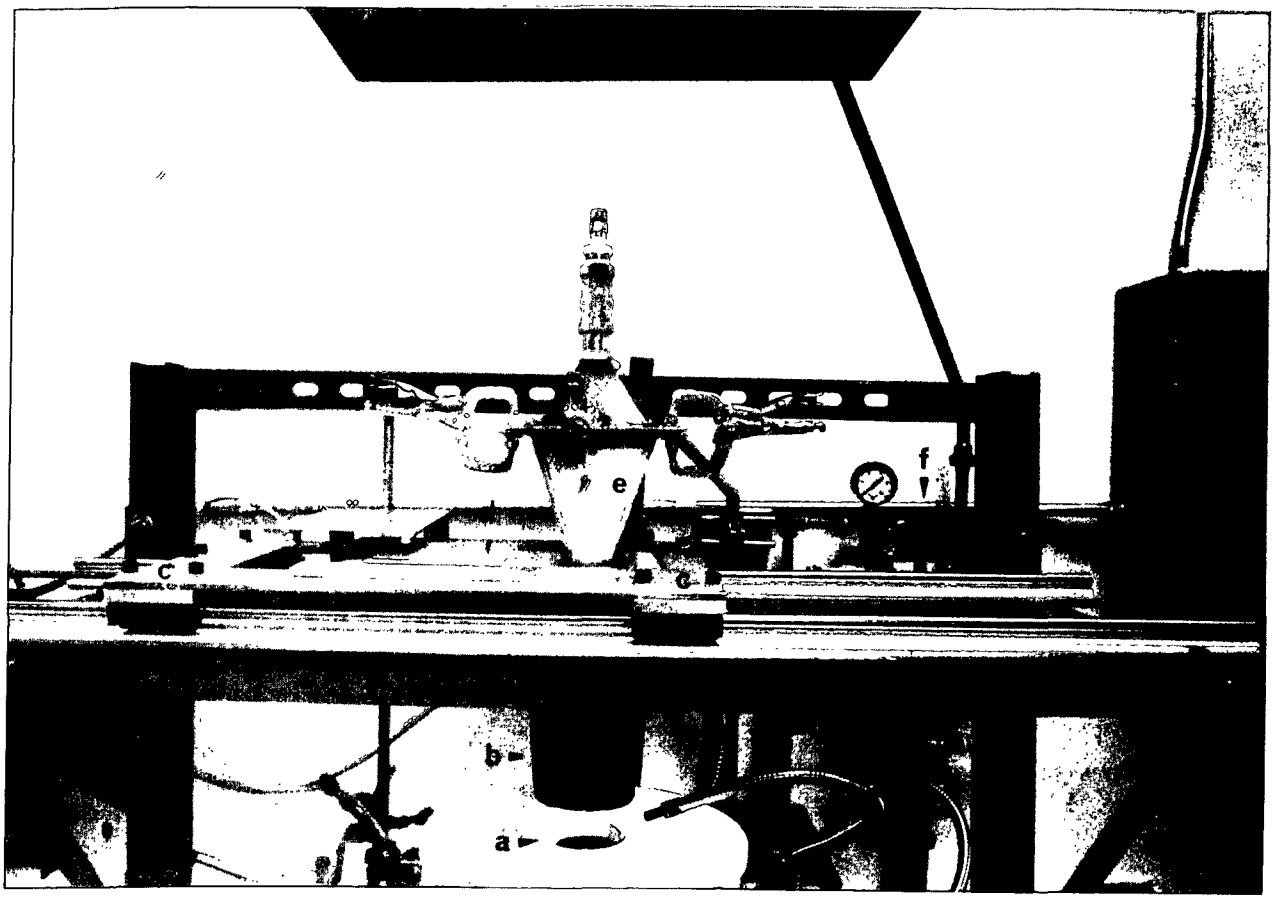

a - quartz reactor tube exit
b - exhaust flow director
c - collection medium carriage
d - Whatman EPM-2000 BGF filter
e - vacuum flow director
f - Piab pneumatic vacuum pump

Figure 8. Front view of the dynamic aerosol collection system.

filter was clamped inside the vacuum flow director chamber to capture material passing through the moving filter. Vacuum induced flow was controlled to maintain air infiltration between the exhaust flow director exit and the BGF filter in order to cool exhaust gases and prevent fume escape.

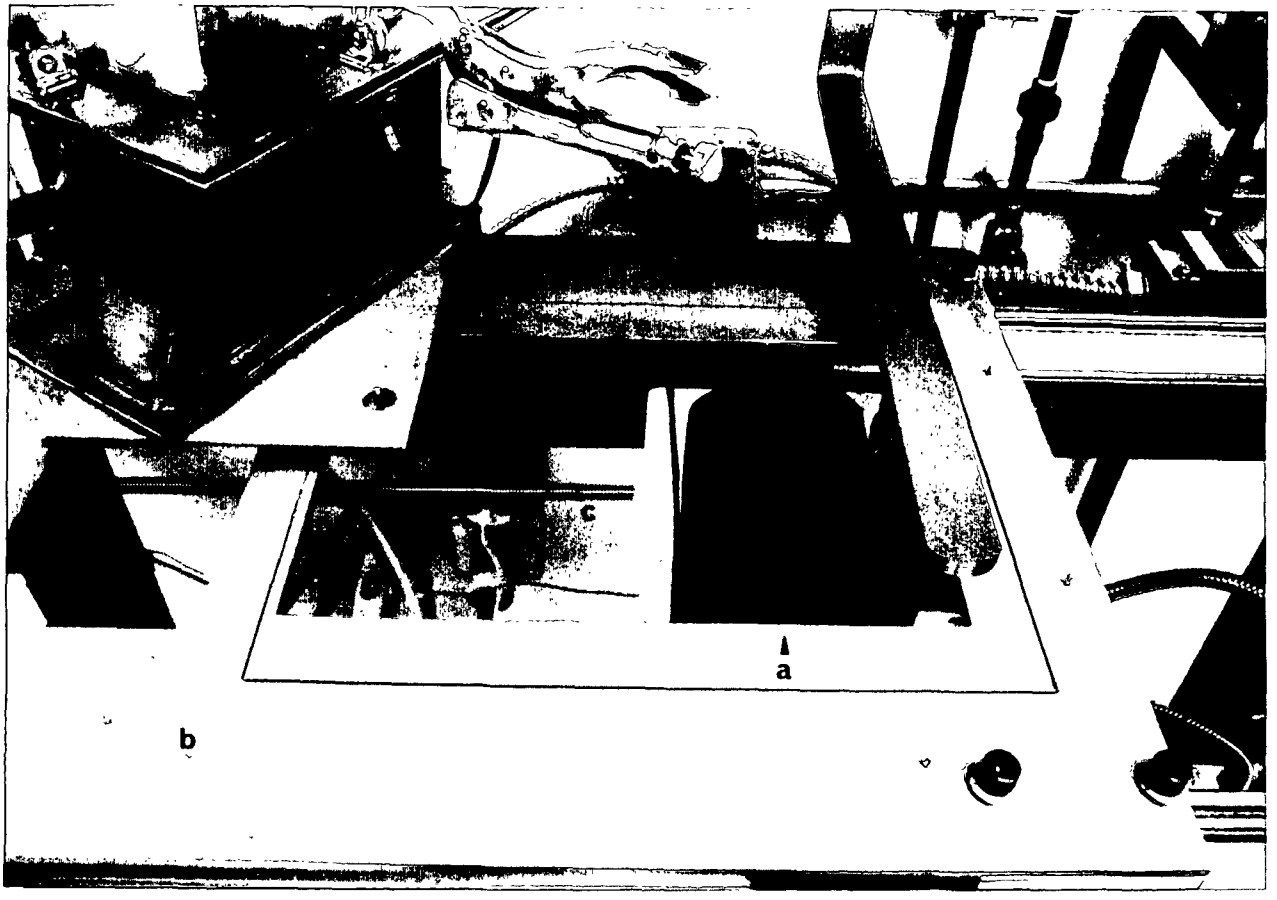

a - rectangular opening of exhaust flow director
b - collection medium carriage
c - carriage drive lead screw
d - vacuum flow director

Figure 9. Top view of dynamic aerosol collection system.

In a typical determination, 150-250 mm (5-10 in.) of the aerosol collection medium was exposed to combustion products. Fume component assays and scanning electron microscopy (SEM) were utilized for locating aerosol deposits on the collection media. Small samples were cut from precise locations on some media and investigated by SEM. This visual observation provided qualitative information about the morphology, size distribution,

and density of collected aerosols. Two microscopes were used at IPST to investigate collected aerosol samples. The newer JEOL JSM-6400 instrument was able to resolve images at much higher magnification than the JEOL JSM-35C microscope. Both microscopes were equipped with a Link Analytical LZ-4 EDS unit. Energy dispersive X-ray spectrometry (EDS) was used for qualitative determination of aerosol composition. Details of SEM analyses are described as they apply to results.

For fume component measurement on BGF filters, the media were carefully divided into nine 25.4-mm (1-in.) sections. All filter sections, the entire backup filters, and drop residues were placed in individual 50-ml centrifuge tubes and agitated in Type I water to lixiviate the captured inorganic compounds. The dispersed filter fibers were settled by centrifugation. A 25-ml aliquot was taken from each sample and ion chromatography (IC) was used to measure the concentrations of $CO_3^=$ and $SO_4^=$. Analysis was conducted at IPST on a Dionex ion chromatograph, following TAPPI recommended procedure.[74] The remaining sample was diluted to 40 ml and acidified with HNO_3 to a 2% acid strength; ICP was used to measure sodium concentration. The silver membranes were treated in a similar fashion, except that the section size was 12.7 mm (0.5 in.), and the samples were not acidified for ICP analysis.

BLACK LIQUOR SAMPLES AND ANALYSIS

Three industrial black liquors were obtained specifically for this thesis, they were designated liquor numbers 1, 2B, and 3. Liquor no. 1 was not used after the preliminary experiments because of its tendency to fall off the nichrome wire during char burning. An old sample from the same mill site as liquor no. 2B was used before the fresh

Table 2. Black liquor characteristics and elemental analyses.[a]

Liquor no.	2A	2B	3
Source	Central US	Central US	Southeastern US
Wood Species	Softwood	Softwood	Soft/hardwood
Date Sampled	1986	October 1990	March 1991
Solids (%)[b]	~ 62	71.3	70.9
Carbon (%)	35.6	35.3	37.8
Hydrogen (%)	3.7	3.4	3.6
Oxygen (%)	33.7	32.5	35.4
Sulfur (%)	4.2	4.1	5.4
Chlorine (%)	0.9	1.6	0.4
Sodium (%)	20.1	19.2	19.3[c]
Potassium (%)	1.8	1.7	1.0

[a] Standard black liquor analyses by Huffman Laboratories, Golden, Colorado unless noted; elemental composition reported as percent of black liquor solids.

[b] Initial solids content of liquor from large samples; determined by CLV.

[c] Average of 20 ICP determinations of acid-digested samples.

samples arrived; it is referred to herein as liquor no. 2A.

Liquor Analysis

Characteristics of the liquors used for the aerosol collection and sodium mass loss experiments are given in Table 2. The samples were obtained "as fired," i.e., taken after the addition points for precipitator dust, ash hopper catch, and make-up chemicals. Initial liquor solids content was determined at the time of transferring each heated one liter liquor sample into several 50 ml bottles. The use of small sample bottles facilitated the process of forming individual drops. Head space in all bottles was purged with nitrogen before returning the samples to cold storage.

The black liquor samples were heated to 50-70°C to reach an optimum viscosity for forming individual drops on nichrome wires; liquor solids content of each small sample was periodically determined to account for water evaporation. The method used was based on TAPPI recommended procedures[75] with the exception that the black liquor was not diluted prior to recording initial mass. After the mass of each sample (concentrated liquor, sand, and weighing dish) was recorded, a sufficient quantity of distilled water was added to dissolve and uniformly distribute the liquor before placing the samples in a drying oven.

Acid Digestion Procedure

It was necessary to determine the sodium content of numerous black liquor and char samples. All samples were identically prepared for analysis using an EPA standard procedure for determining total recoverable sodium.[76] The samples were refluxed for three to four hours in a mixture of 1 ml concd. HNO_3, 6 ml concd. HCl, and 9-10 ml Type I water. Digested samples were transferred to 50 ml centrifuge tubes and diluted to 50 ml with Type I

water. Any insoluble residue was dispersed by ultrasonic agitation and allowed to settle.

ICP was used to measure Na concentration in all samples. A majority of the analyses were conducted by Huffman Laboratories; several samples were analyzed using the IPST Thermo Jarrell Ash PLASMA-300™ ICP Emission Spectrometer. Once the sodium concentration was known, the mass of sodium in each sample could be determined from the total liquid sample volume or the liquid mass and density. Calculations of the amount of sodium in each sample from the ICP analyses are presented in Appendix IV.

Digestion blanks and quality control samples were run periodically during the ICP measurements to insure that the instrument calibration was being maintained. The accuracy of determination was ± 25 mg/L for sodium concentrations of approximately 500 mg/L. Potassium content was not determined for most samples because the expected level of concentration was too near the ICP detection limit.

RESULTS AND DISCUSSION

This chapter presents the results of sodium mass loss determinations and aerosol collection experiments. The first set of results contains characterization of drop pyrolysis behavior, determination of volatiles yield and sodium mass loss, and a discussion of possible mechanisms responsible for sodium release prior to char burning. A description of aerosol morphology, characterization of drop combustion behavior, and estimation of the rate of fume formation during drop combustion are included in the second part. The discussion following these results considers the significance of sodium loss during the various stages of combustion on overall fume formation within a recovery furnace.

SODIUM MASS LOSS DETERMINATION

Relative change in sodium content was measured in a series of experiments in which individual drops were exposed to pyrolytic or reducing environments over a wide range of temperatures. In order to isolate the processes occurring during the drying and devolatilization stages from those of char burning, experiments were conducted in non-combustive atmospheres. Some experiments were carried out under gasification conditions with either oxygen or carbon dioxide as the oxidant. After a brief description of drop pyrolysis behavior, the measurement of volatiles yield is presented. Sodium mass loss results from each group of experiments are then considered and compared with results from related studies. The complete set of individual drop data from the pyrolysis experiments is included in Appendix III. Appendix IV contains liquor and char sodium analysis data as well as calculations of volatiles yield and sodium mass loss for each determination.

Drop Pyrolysis Behavior

A summary of the furnace conditions, average drop size, and pyrolysis stage times of the 409 char particles selected for sodium mass loss determinations is presented in Table 3. There were two phases of experimentation in the sodium mass loss determinations. The initial group of experiments included the first three trials at 600°C as well those at 900 and 500°C. Reduced drop mass variability (standard deviation of drop o.d. mass in Table 3) indicates progressive technique improvement within the first group of experiments; the control of drop exposure time was also greatly improved with experience. Of the 66 drop data sets presented in Appendix III, the variation (± 95% confidence limit) in exposure time was less than 5% of the mean for all but 13 of the early determinations.

Several minor changes were made during the first group of experiments to establish a reliable experimental procedure. These changes are described below as they affect interpretation of the results. The second experimental group contained gasification in CO_2 (600°C [5]), two trials at 750°C, and a final replication of the base case (600°C [4]) for comparison to previous experiments. No procedural changes were made during this group of experiments.

Observation of Drop Pyrolysis

Video images revealed that all drops exhibited some bubble bursting during drying. There were substantial differences in devolatilization observed at the different conditions. Particles produced in 95% N_2 with 5% CO were porous and brittle. Swelling of these particles was uniform and spherical. Char formed during all experiments at 600°C shrank substantially after reaching maximum swollen volume; much less collapse was noted

Table 3. Summary of sodium mass loss experiments: furnace conditions, average drop size, and stage times. Drop data reported as mean value ± one standard deviation.

Furnace temp., °C	Rep. at temp.	Gas comp.,[a] %	Av. gas velocity,[c] m/s	No. of drops[d]	Drop o.d. mass,[e] mg	Drying time,[f] s	Devol. time,[g] s
600	1	5% CO	0.61	30	3.7 ± 1.9	3.0 ± 0.5	2.8 ± 0.9
600	2	5% CO	0.61	120	4.2 ± 0.5	4.0 ± 0.6	2.7 ± 0.6
600	3	5% CO	0.61	30	4.4 ± 0.5	3.4 ± 0.4	1.8 ± 0.4
600	4	5% CO	0.61	36	3.5 ± 0.2	3.0 ± 0.3	2.2 ± 0.4
750	1	5% CO	0.61	44	3.4 ± 0.3	1.9 ± 0.2	1.3 ± 0.3
750	2	5% CO	1.83	42	3.5 ± 0.3	1.9 ± 0.2	1.3 ± 0.3
900	1	5% CO	0.61	30	2.8 ± 1.3	0.8 ± 0.2	1.2 ± 0.3
900	2	5% CO	0.61	20	3.9 ± 1.0	1.2 ± 0.2	1.2 ± 0.3
500	1	5% O_2	0.61	30	3.5 ± 1.3	5.8 ± 0.7	2.8 ± 0.7
600	5	5% CO_2[b]	0.61	27	3.4 ± 0.2	3.4 ± 0.3	1.8 ± 0.4

[a] Gas composition; volume percent of given component, 95% nitrogen balance, unless noted.
[b] Also contains 5% CO by volume, 75% nitrogen balance.
[c] Average gas velocity at drop location; calculated from gas temperature and mass flow rate.
[d] Total number of drops exposed for all determinations in each experiment (5 or 20 particles per determination).
[e] Average drop solids mass; calculated from individual drop masses and liquor solids content.
[f] Drying stage elapsed time; taken from drop insertion until visible onset of swelling.
[g] Devolatilization stage elapsed time; taken from onset of swelling until point of maximum swollen volume.

at 750 and 900°C. The average specific volume (reciprocal density) of char particles exposed for 30 seconds to oxygen-free atmospheres was found to increase over the range of temperature studied.[77] There was no visible or quantifiable effect of gas velocity on the chars produced at 750°C.

The swelling behavior of drops exposed to the oxygen-containing atmosphere at 500°C was like that observed during combustion at higher temperatures and oxygen concentrations. These drops underwent random serpentine expansion and formed hollow char particles with a delicate but resilient surface. Enhanced swelling in atmospheres containing low (2-5%) oxygen has been reported by others.[25,35] The other gas atmosphere investigated in the sodium mass loss experiments, 75% N_2 with 20% CO_2 and 5% CO at 600°C, produced chars that were identical in appearance to the samples obtained from pyrolysis at 600°C.

Stage Times During Pyrolysis

The effect of furnace conditions on drying time is shown in Fig. 10. Each plotted point represents the average drying time measured from all videos of drop pyrolysis at each condition, e.g., the point at 600°C for 95% N_2 with 5% CO is an average of approximately 200 individual time measurements. Error bars indicate ± one standard deviation of the mean for each set of furnace conditions. The values in Fig. 10 demonstrate a decrease in average drying time with increasing temperature; this was a result of the corresponding change in heat transfer mechanisms from primarily convection to radiation.[26] It is apparent that gas composition and velocity had no effect on drying time for the conditions studied.

Figure 11 presents the mean swelling or devolatilization time as a function of

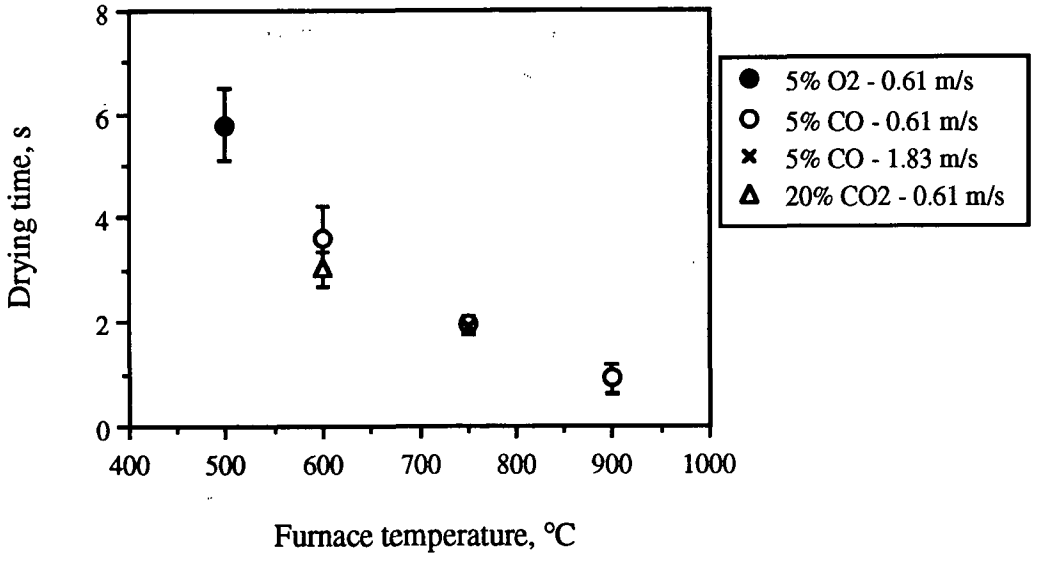

Figure 10. Drop drying time as a function of furnace conditions for all experiments given in Table 3. Plotted points are mean time for each condition ± one standard deviation.

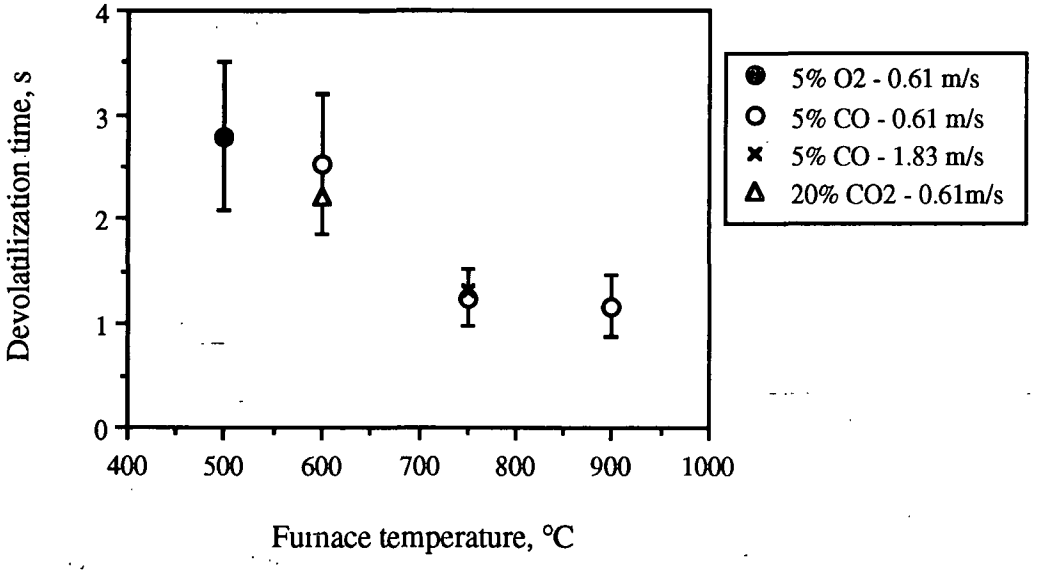

Figure 11. Drop devolatilization time as a function of furnace conditions for all experiments given in Table 3.

furnace conditions. Because there was no luminous flame surrounding the particles, the effect of furnace temperature on swelling time in the pyrolytic environments of this study was greater than that reported for devolatilization in a combustive environment.[1] These data agree with other indications that devolatilization time is a weak function of temperature over a wide range of conditions.[26] The temperature of the char particles in the oxygen-containing atmosphere at 500°C may have been higher than that of the surroundings due to exothermic oxidation of the char. This explains the somewhat lower than expected devolatilization time at 500°C.

Average Drop Size

Liquor mass was used as the measure of drop size throughout the thesis experiments. In order to extract char from the drop reactor its swollen size had to be less than the insertion port diameter (14 mm). An average drop mass of 5 mg was targeted because drops larger than 6 mg tended to fall off the nichrome wire while being extracted. Known variations in liquor solids content were compensated for by forming correspondingly larger or smaller drops. Much of the literature reports drop size as effective diameter; therefore, the average diameter of a representative sample of drops was measured to facilitate comparison of results.

Image analysis was utilized to determine the diameter for a group of 28 liquor drops with an average drop mass of 5.0 ± 0.5 mg. The mean size for all 409 drops reported in Appendix III was 5.2 ± 1.3 mg as liquor. Video images corresponding to the first clear frame of the inserted drop were acquired, digitized, and filtered by a Tracor-Northern TN-8502 image analyzer. Images of a spherical ball of known diameter were also acquired to

calibrate the instrument. The area of the two dimensional binary image (silhouette) of each selected frame was then calculated. Average projected area diameter (D_{PA}) of the particle was defined as diameter of a circle with area equal to the binary image. For the 28 chosen drops, D_{PA} was 2.1 ± 0.3 mm.

Particle volume (V_d) can be estimated from its projected area diameter as

$$V_d = \alpha_V \times D_{PA}^3 \quad , \tag{3}$$

where α_V is a volume shape factor to account for irregular particle shapes.[78] For a sphere α_V is $\pi/6$. Knowing the average drop mass (m_d), black liquor density (ρ) can be estimated from Eq. 3:

$$\rho = \frac{m_d}{\alpha_V \times D_{PA}^3} \quad . \tag{4}$$

A volume shape factor of 0.43 (averaged value for sphere and prolate ellipsoid of axial ratio equal to 5) reasonably describes the somewhat flattened shape of liquor drops. Using this shape factor, the mean density calculated by Eq. 4 for the 28 drops was 1.34 ± 0.51 g/cm^3; this agrees very well with the accepted value of 1.38 g/cm^3.[26]

Total Mass Loss During Pyrolysis

Calculated black liquor mass losses for all conditions are plotted against exposure time in Figs. 12 and 13. Significant volatiles yield was not expected to occur until the particles began to swell; accordingly, average drying times from Table 3 were used as origins of the curves in Figs. 12 and 13. Lines are shown in the figures to group the data;

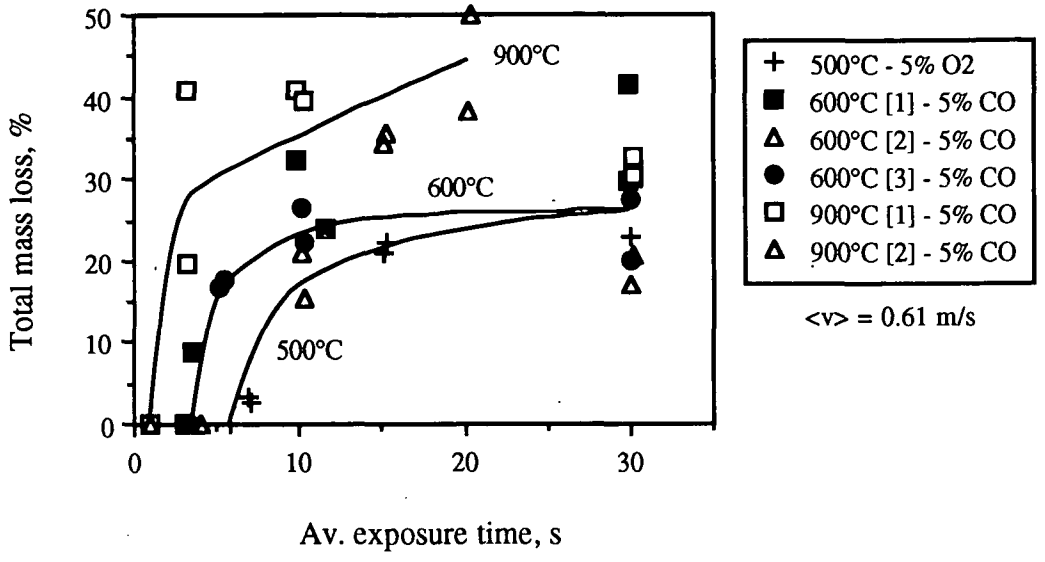

Figure 12. Total mass loss as a function of exposure time and furnace conditions for the first group of experiments. Quench flow: 2 L/min N_2 for 500°C, 5 L/min N_2 for 600 and 900°C.

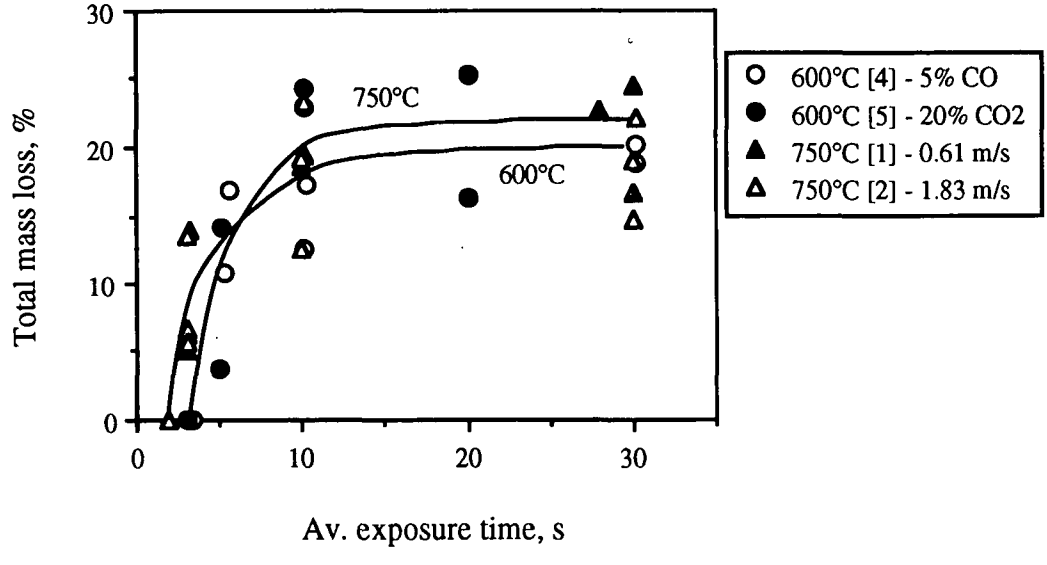

Figure 13. Total mass loss as a function of exposure time and furnace conditions for the second group of experiments. Quench flow: 5 L/min N_2.

these lines are not based on statistical regression. In this section results from each set of experiments are considered separately.

Volatiles yield or total mass loss (ML) was defined as the percent difference between the initial liquor solids mass and the char sample mass for each determination:

$$ML = 100\left[1 - \frac{m_c}{\sum_{i=1}^{n}(x_s \times m_d)_i}\right] . \qquad (5)$$

In Eq. 5 m_c is the mass of accumulated char, x_s is solids content of the liquor, m_d is mass of the individual drops, and n is the number of accumulated char particles (typically 5 or 20). As the liquor samples were heated to facilitate drop formation, solids content was periodically determined during each experiment to account for water evaporation.

First Set of Drop Experiments

During three of the first minimum exposure time determinations at 600°C, char was withdrawn from the furnace before drying was complete. The resulting negative values of calculated mass loss are not shown in Fig. 12, but are reported in Table 9 of Appendix IV. This error was prevented in subsequent experiments by choosing a minimum exposure of 1.25 times the average drying time, which was determined from several video sequences of drop pyrolysis. Improvement in experimental technique is evident in the reduced scatter of volatiles yield from the third experiment at 600°C (as compared to 600°C [1] and 600°C [2]).

The measurement of liquor solids content for the first two experiments, 600°C [1] and 900°C [1], was in error because the samples were not dried to constant weight,

as specified in TAPPI procedures.[75] After the solids content of several liquor samples had been carefully measured, it was concluded that the first solids measurement was approximately 5% high. The values of total mass loss corresponding to these experiments in Fig. 12 are therefore expected to be 10-30% high.

The results of the experiment at 500°C indicate that, after the rapid initial volatiles loss, char mass continued to decrease slowly with time. This was due to slow combustion or gasification of the char in 95% N_2 with 5% O_2 at 500°C. Given sufficient exposure time, the char carbon would have been completely consumed. As a result of particle heating at these conditions, the average initial mass loss may have been somewhat higher than would have occurred in an oxygen-free atmosphere.

During the first pyrolysis experiment at 900°C, there was a smaller volatiles yield after 30 seconds exposure time than after 10 seconds. This may be a result of partial oxidation of highly reduced char immediately upon removal from the quench stream. Spontaneous combustion was observed when many of these char particles were removed from the nitrogen quench and exposed to ambient laboratory air. Photomicrographs of several intact particles, pyrolyzed at 900°C for 30 seconds, revealed holes in the surface surrounded by regions of feathery gray ash. Evidently, the mass gained by oxidation of the highly reduced char exceeded the mass lost during extended thermal decomposition. The anomalous points at 30 s were disregarded when drawing the line through the 900°C data in Fig. 12.

Second Set of Drop Experiments

Figure 13 shows the results from the second set of pyrolysis experiments. Considering the scatter in the data, there is no significant difference between the volatiles

yield at 10 and 30 seconds. This result suggests that the total mass loss during pyrolysis was not affected by temperature or gas velocity over the range of conditions used in the second set of experiments. The 20-25% ultimate volatiles yield at 750°C is somewhat lower than what has been reported in other studies of black liquor pyrolysis and combustion. During the TGA study of black liquor solids, 34-41% of the original material was lost during heating to a final temperature of 750-800°C.[12] The volatiles yield of seven samples of char produced in a large drop tube furnace was 34.3 ± 3.1%.[79] Direct comparison of these results with the single drop experiments is difficult because volatiles yield is as much a function of thermal history as it is of the parent material composition.[34]

Conditions that support thermal decomposition of inorganics or gasification of carbon would be expected to result in additional mass loss, as discussed for Fig. 12. Total mass loss during gasification in 75% N_2 with 20% CO_2 and 5% CO at 600°C was not statistically different than that from the fourth experiment in 95% N_2 with 5% CO at 600°C. The gasification rate was very slow at these conditions;[27] therefore, no measurable amount of carbon would have been consumed in the short duration of the drop exposure.

Comparison of Char Removal Procedures

Total mass loss at 600°C is somewhat higher in Fig. 12 than in Fig. 13. The following analysis indicates that, on average, a small amount of material was lost during handling in the first set of experiments. In the early experiments friable char particles were accumulated for each determination by scraping the residue from the nichrome wires into a clean dry beaker. The weight change of the individual wires is reported in Appendix III as "loss on wires." The average loss on wires from 22 determinations in which the char was

removed by scraping was 0.4 ± 3.0 mg.

Particles quenched at the minimum exposure time were tar-like. After the accumulated mass of these particles and wires was recorded, a small amount of water was added to the beaker to dissolve the residue. The group of wires was then removed from the beaker, rinsed with a few drops of water, and dried before weighing. A similar procedure was utilized in order to minimize material loss in the second group of experiments. In this case, char residue from all exposure times was removed from the wires by adding 8-9 ml of Type I water to the beakers and agitating the samples in an ultrasonic bath for several minutes.

Total material "loss" for each determination was estimated from the mass of the rinsed group of wires minus the sum of the initial wire masses. These values are reported as the sum of "loss on wires" in Appendix III. The average value from 32 determinations in which the char was removed by washing was 0.0 ± 0.5 mg. This variation is identical with the expected accuracy of the Sartorius analytical microbalance in the IPST laboratory environment. Comparison of the averaged loss on wires values from the two procedures suggests a systematic loss of 0.4 mg in the first set of experiments. This explains the somewhat higher volatile yields measured during the first experiments at 600°C.

Adventitious Moisture in Char

Another procedural difference between the experimental groups was the method of char mass measurement. During the early experiments the char mass was recorded after accumulating a sample. The time required to complete a determination (accumulate the char from 5-20 drop exposures) varied from 20 minutes to over one hour. Char extracted at

the minimum exposure time should have contained 1-5% residual moisture.[24] After 10-20 s exposure time the char should have reached absolute dryness, but would have quickly absorbed moisture from the air. The scatter in the results in Fig. 12 can be attributed to variation in adventitious moisture gained by the char.

In the second set of experiments, accumulated char was weighed, dried at 105°C for 60-90 minutes, cooled in a desiccator for one hour, and reweighed. This process was repeated until constant weight was achieved. It was necessary to shield the char from the air currents in the drying oven by inverting a large beaker over the 150 ml beaker containing the char sample. Mass losses of greater than 10% were measured during drying of some char samples. However, when volatiles yield was recalculated using the dried char mass, there was no significant change in the trends of the results presented in Fig. 13. No systematic effect of drop furnace temperature or exposure time on char moisture content could be determined. This discussion suggests that the char drying procedure was unnecessary. Additional handling increased the probability of unwanted material loss; moreover, char drying did not reduce the variability of the total mass loss results. The char drying procedure is not recommended for future sodium mass loss determinations.

Sodium Mass Loss During Pyrolysis

The primary objective of the experimental work was measurement of sodium mass loss prior to the char burning stage of black liquor combustion. The single drop pyrolysis technique was utilized for most of the experiments because it allowed the drying and devolatilization processes to be isolated from those of char burning and smelt oxidation. This section contains the results of the single drop experiments, followed by consideration of

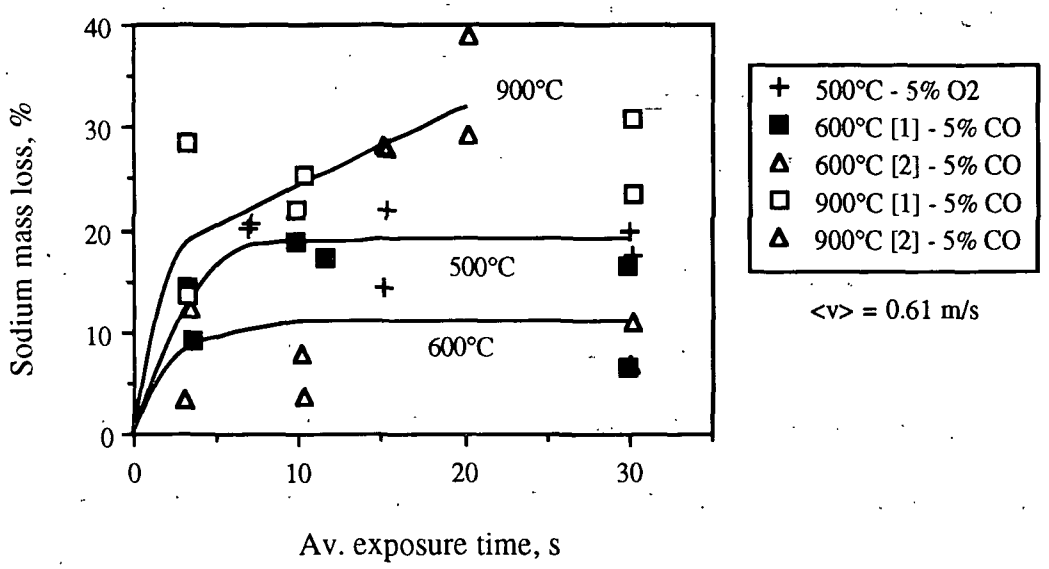

Figure 14. Sodium mass loss as a function of exposure time and furnace conditions for the first group of experiments. Lines are not based on statistical regression.

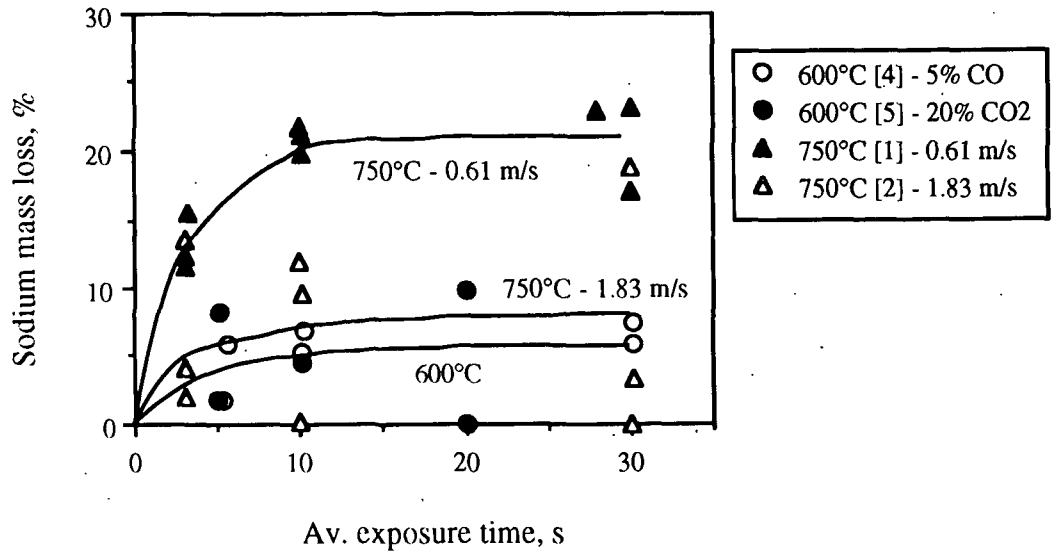

Figure 15. Sodium mass loss as a function of exposure time and furnace conditions for the second group of experiments.

the thermal history of liquor drops. Results of the muffle furnace experiment are also presented and compared with those of the single drop experiments. Two mechanisms which have been proposed to explain the initial sodium release during the pyrolysis experiments are discussed in light of the results.

Sodium Loss in Single Drop Experiments

The amounts of sodium lost from the char as functions of exposure time and furnace conditions are plotted in Figs. 14 and 15. There were significant sodium losses at the shortest exposure times in all experiments; thus, the curves in Figs. 14 and 15 were drawn assuming zero sodium loss occurred at zero exposure time. The single lines drawn through the 600 and 900°C data represent the average behavior exhibited by both data sets at each temperature. These lines were not determined by statistical regression. For reasons discussed in the previous section, the 30 second data were disregarded when drawing the line for the experiment at 900°C in Fig. 14.

Sodium mass loss was defined as the percent difference between the amount of sodium in the liquor solids and the mass of sodium in the acid-digested char samples:

$$NaL = 100\left[1 - \frac{m_{Na,c}}{x_{Na,l}\sum_{i=1}^{n}(x_s \times m_d)_i}\right] . \qquad (6)$$

The mass of sodium in the char ($m_{Na,c}$) was calculated from the sodium concentration in digested char samples and the sample volume. Sodium content of the liquor ($x_{Na,l}$) was determined during each experiment from acid-digested liquor samples:

$$x_{Na,l} = \frac{m_{Na,l}}{x_s \times m_l} \quad , \tag{7}$$

where $m_{Na,l}$ is the mass of liquor sodium and m_l is the mass of digested liquor.

Unlike the total mass loss results, char moisture content would not affect the accuracy of the sodium mass loss values because the amount of sodium was determined from the concentration of a dissolved sample. A liquor doping experiment was conducted to determine if there was a systematic error in the acid digestion procedure caused by changes in the form of the sodium during devolatilization. The results of this experiment (presented in Appendix IV) indicate that the form of the sodium -- organically bound or inorganic salt -- does not affect its determination.

Figures 14 and 15 indicate there was a sudden sodium mass loss that occurred prior to the end of the devolatilization or swelling period; this is referred to as the initial sodium loss. Comparison of the results from pyrolysis (in 95% N_2 with 5% CO at 0.61 m/s) at 600, 750, and 900°C in Figs. 14 and 15 shows that this initial loss increased with increasing furnace temperature. The results from pyrolysis at 600 to 750°C exhibit the same trends as the 700 and 800°C data presented by Frederick and Hupa.[13] In all cases, except for pyrolysis at 900°C, there was no further sodium release after the initial loss of 5-20% of the sodium contained in the black liquor.

The fourth replication of the pyrolysis experiment at 600°C, shown in Fig. 15, was not statistically different than the second, given in Fig. 14. Results from these two experiments indicate that only 5% of the sodium was lost after 10 seconds pyrolysis. The higher loss values from the first experiment (600°C [1]) may be due to incomplete removal of

the char residue by scraping from the nichrome wires. As described in the previous section, material loss was minimized during the second set of experiments by removing the char from the wires with a small amount of water.

Sodium loss during pyrolysis at 900°C, shown in Fig. 14, did not subside after swelling was complete but continued to increase with exposure time. Frederick et al.[14] reported similar behavior for liquor drops pyrolyzed at 900 and 1000°C. In gas atmospheres containing CO at temperatures above 800°C, Na_2CO_3 decomposes by reaction with char carbon (see Eqs. 1-2).[12] Clearly this is the cause of the second phase of sodium loss occurring during pyrolysis at temperatures of 900°C and greater, shown in Figs. 2 and 14.

Although more scattered, the sodium loss during gasification in 75% N_2 with 20% CO_2 and 5% CO at 600°C was not statistically different than that from the second and fourth experiments in 95% N_2 with 5% CO at 600°C. A single line was drawn through all the 600°C data in Fig. 15 to indicate similar behavior. Other work has shown that, during CO_2 gasification, Na_2CO_3 remains fixed in the char.[12,71] One proposed char gasification mechanism suggests that the alkali carbonate is cyclically reduced by reaction with carbon and subsequently oxidized by CO_2.[27] According to this type of mechanism, elemental sodium should not be released during CO_2 gasification unless the temperature is high enough for Na_2CO_3 decomposition to occur.[12]

In the other experiment investigating the effect of gas composition, greater sodium loss was measured at 500°C in an oxygen-containing atmosphere than at 600°C in an oxygen-free atmosphere. Twenty percent of the sodium was released from the partially-swollen char during 7 seconds exposure to 95% N_2 with 5% O_2 at 500°C. Char particles

withdrawn from 95% N_2 with 5% CO at 600°C after 3 seconds had swollen to approximately the same extent, but the sodium mass had decreased by only 5%. Although no glowing combustion was observed during this experiment, it is likely that oxidation of the char increased the particle temperature above that of the furnace environment. The higher particle temperature would result in a higher heating rate and correspondingly greater sodium loss than would be expected in a non-oxidizing environment at 500°C. Interestingly enough Volkov et al.[11] reported a 20% sodium loss for 2 mm drops exposed to air at 900°C for 3 seconds. This agreement with the initial sodium loss in 95% N_2 with 5% O_2 at 500°C suggests that there is little temperature effect on sodium release during drying and devolatilization in oxygen-containing environments.

Average gas velocity was tripled in the second experiment at 750°C to isolate the effect of flow rate from that of heating rate. As seen in Fig. 15, this resulted in a large decrease in initial sodium loss. A t-test of the mean mass losses for each experiment indicated that the decrease in sodium release (i.e., greater sodium retention) caused by increased gas velocity was significant at the 99.9% confidence limit. The following paragraphs consider possible explanations for the effect of gas velocity.

At 750°C the convective contribution to total heat transfer is much smaller than the radiative component. The coefficient for convective heat transfer (h_c) to a 2-mm spherical liquor drop is given by:[80]

$$h_c = \frac{k}{D}\left[2.0 + 0.60\,(Re)^{\frac{1}{2}}\,(Pr)^{\frac{1}{3}}\right] . \qquad (8)$$

In Eq. 8 k is the thermal conductivity of the gas, D is the drop diameter, Re is the particle

reynolds number ($D\langle v\rangle\rho/\mu$), and Pr is the Prandtl number of the gas ($C_p\mu/k$). Gas properties were evaluated at the bulk gas temperature of 750°C. An increase in gas velocity from 0.61 to 1.83 m/s (2 to 6 ft/s) would result in a 32% increase in convective heat transfer coefficient as calculated by Eq. 8. For this system a radiant heat transfer coefficient (h_r) can be defined:[81]

$$h_r = 4\varepsilon\sigma T_D^3 \quad , \tag{9}$$

where the liquor emissivity (ε) was assumed to be 0.95, σ is the Stefan-Boltzman constant, and T_D is the drop temperature.

Drop temperature (T_D) was calculated by an iterative solution of a heat balance accounting for combined radiative and convective heat transfer. Average wall temperature was estimated to be 720°C. This calculation showed that tripling gas velocity would result in less than a 1% increase in actual drop temperature. This result implies that there was no cooling of the drop due to increased flow. The overall heat transfer coefficient ($h_c + h_r$) would increase only 12% for the increase in gas velocity from 0.31 to 1.83 m/s. Identical drying and devolatilization stage times, given in Table 3, verify the assumption that the increase in velocity did not substantially affect drop heating rate.

Assuming the sodium loss resulted from physical ejection of liquor and char, caused by escaping gases, then higher flow rate may have reduced ejection by suppressing bubble formation. However, any effect caused by increased pressure on the leading of the drops should have been balanced by a corresponding pressure decrease on the trailing edge. A review of the video images revealed no visible differences in surface activity or swelling

behavior between chars produced at 750°C with ⟨v⟩ = 0.31 m/s or 1.83 m/s. Furthermore, the specific volume of chars produced at both conditions could not be statistically differentiated.[77] A study of the physics of bubble formation and bursting is necessary to understand the effect of gas velocity on the extent of material loss during these experiments.

Drop Thermal History Model

Significant sodium losses were measured at minimum exposure times; thus, it was suspected that particle temperatures were substantially below the furnace temperature during the period of initial sodium loss. Since direct measurement of drop temperature was not made during the sodium loss experiments, a thermocouple was used to approximate the heating and cooling history of a liquor drop in the laboratory furnace. The 0.81 mm diameter thermocouple, connected to a digital data acquisition system, was inserted into the reaction chamber for a given exposure time and then withdrawn to cool in the quench stream. Figure 16 is a typical plot of thermocouple response as a function of exposure time.

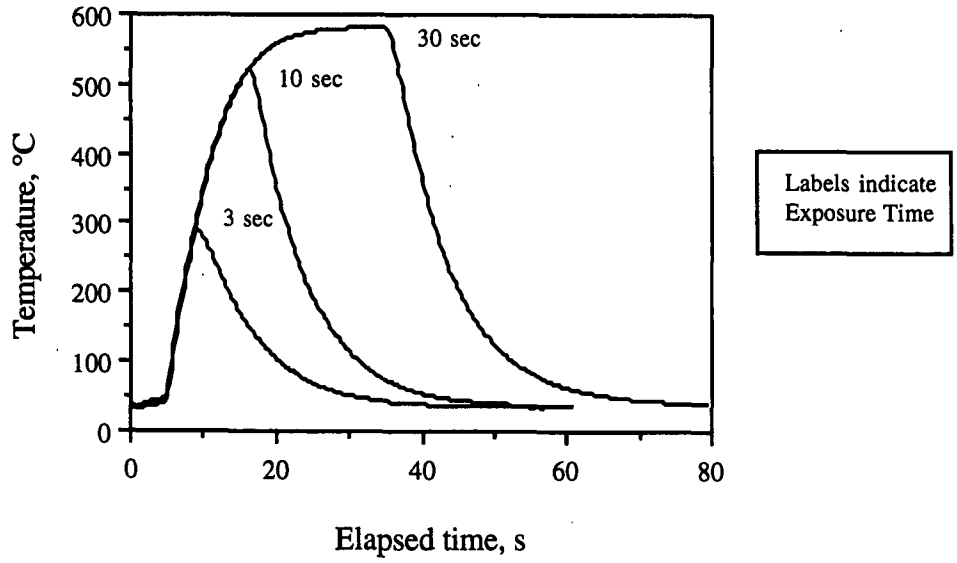

Figure 16. Thermocouple response as a function of exposure time. Furnace conditions: air at 600°C and 0.61 m/s; quench flow: 5 L/min N_2.

Drop heating rates were estimated from the elapsed time required for the thermocouple temperature to increase from 100°C to 80% of the maximum (ultimate) temperature; this corresponds to the nearly linear region of the curves in Fig. 16. This "average linear heating rate" ranged from 36°C/s at 500°C to 106°C/s at 900°C. In a similar experimental system, Frederick et al.[82] measured the surface temperature of liquor drops with a two-color pyrometer. For a 17 mg drop, pyrolyzed at 800°C in 95% N_2 with 5% CO, the surface temperature increased at a rate of approximately 100°C/s during devolatilization.[82] Heat transfer to a swelling black liquor drop may be substantially greater than to a thermocouple junction; thus, this technique only provides an approximate thermal history for a drop. The average time to reach maximum swollen volume at 600°C was 5.7 ± 0.7 s (see Table 3). The data in Fig. 16 suggest that particle temperature would have reached 320-390°C after this elapsed time. Miller[20] measured somewhat higher liquor temperatures (400-500°C) during the period of rapid swelling. It can be concluded that the actual drop heating rate was probably greater than that predicted by the thermocouple model.

The time required to fully withdraw a drop from the center of the reaction chamber to the quench zone was approximately 0.2 seconds. Assuming that pyrolysis reactions are quenched at temperatures below 200°C, a cooling time can be defined as the elapsed time between the maximum temperature measured by the thermocouple and 200°C. The average of 24 determinations of cooling rate (taken from eight measurements at furnace temperatures of 500, 600 and 900°C) was 11.2 ± 2.0 seconds.

The understanding gained from this experiment is that there was a finite heating and cooling period during the drop exposures, and that the char reached the furnace

temperature only after 15 to 25 seconds exposure time. Additional mass loss may have occurred during the quench period of the drop experiments; therefore, the actual pyrolysis time was greater than the reported drop exposure time. This error is not expected to effect interpretation of the results because it was manifest in all determinations.

Sodium Loss in Muffle Furnace Experiment

It was suspected that the violent boiling action observed during drying was responsible for part of the initial sodium loss measured during single drop experiments. A procedure was therefore devised to isolate the sodium release during drying from that occurring during devolatilization. The outcome of this muffle furnace experiment -- no sodium loss from either liquor or dried solids samples pyrolyzed at identical conditions -- was not expected. Comparison of the results from this experiment with the individual drop experiments is convoluted by differences in liquor sample geometry; however, this result provides evidence that sodium release during pyrolysis is not an evaporative process.

Approximately 100 mg of liquor was applied in a 5 cm line along the bottom of twelve ceramic combustion boats. Half of these samples were dried overnight at 105°C. Three boats each of dried solids and wet liquor were pyrolyzed for 60 seconds in the quartz tube apparatus, as described in the Experimental chapter. Behavior of the liquor was similar to that observed for pyrolyzing single drops. There was a period of boiling and bursting immediately after insertion of the wet liquor samples; bursting was not observed for the oven dried samples. After exposure for a few seconds, swelling liquor was visible above the top of the boat. Because the char surface was exposed to flowing gas, devolatilization products would have been carried away by the flow as in the drop furnace. No accidental material

losses were noted during these experiments and the swollen liquor never touched the inside surface of the quartz tube.

Results of the muffle furnace experiment are summarized in Table 4. Calculated solids contents agree well with the standard determination[75] of 72.3% solids for this liquor sample; thus, samples dried in the ceramic boats reached total dryness. There was a substantial amount of volatiles released during these experiments. In fact, the volatiles yield in Table 4 is somewhat higher than the values of 15-25% determined for pyrolysis of individual drops at 750°C. The results in Table 4 show that there was no statistically-significant difference in the sodium contents of the black liquor, dried solids, or the pyrolyzed char samples. Constant sodium content, on an initial solids basis, implies that there was *no sodium loss* during devolatilization in these experiments. For comparison, the results in Fig. 15 indicate there was a 20% ultimate sodium loss for single drops pyrolyzed in 95% N_2 with 5% CO at 750°C.

Table 4. Results of muffle furnace liquor pyrolysis experiment. 100 mg sample size; pyrolysis conditions: 95% N_2 with 5% CO at 750°C and 0.61 m/s. All values reported as average ± 95% confidence limit.

Sample	Na cont., %[a]	Liquor solids, %	Char mass loss, %
Liquor	16.2 ± 0.4	-	-
Solids	16.2 ± 0.2	72.0 ± 2.5	-
Pyrolyzed liquor	16.5 ± 0.6	-	29.6 ± 1.0[b]
Pyrolyzed solids	16.4 ± 0.6	72.2 ± 1.2	32.1 ± 2.0

[a] Reported as % of initial black liquor solids.
[b] Estimated from liquor sample solids content.

There were several significant differences between the two experiments which may account for the disagreement of the results: sample geometry, initial specific surface area, and geometric surface area. Effects of these variables on sodium release are considered below. An individual 5-mg liquor drop, 2-mm in diameter, had a geometric surface area of 12.6 mm^2 and an initial specific surface area of approximately 2.5 mm^2/mg. A 100-mg stripe of liquor at the bottom of a ceramic boat had a geometric surface area of 100 mm^2; thus, the initial specific surface area of the stripe was 2.5 times less than the drop.

The geometry of the liquor samples in the muffle furnace could have significantly affected the sodium release during pyrolysis. A flowing gas stream caused the heating rate to be higher along the upstream surface of individual liquor drops in the tubular furnace. Gas bubbles generated within the heating drops were observed to burst preferentially on the downstream free surface. Liquor samples contained in the alumina boats were heated entirely from above. The lower surface of the sample was thermally insulated and physically restrained by the boat. There was no free surface opposing the heated surface which may have suppressed bubble bursting and consequently reduced material loss by physical ejection.

In Fig. 3 the average sodium loss for pyrolysis from one experiment reported by Frederick and Hupa[13] was compared with results of another set of experiments conducted at identical conditions. The drop size in the first experiment was 10-20 mg, while 5-12 mg drops were formed in the second set;[70] the *larger* drops would have had approximately 15-20% *lower* initial specific surface area. It is expected that the statistically lower sodium loss in the first experiment was caused by the lower initial specific surface area. During black liquor combustion, sodium mass loss was found to decrease with increasing drop size[11] (see

Fig. 1). It is possible that the lower initial specific surface area of the liquor samples in the muffle furnace experiment reduced sodium mass loss to below measurable limits. Sodium mass loss during pyrolysis must be evaluated over a range of controlled drop sizes in order to verify the effects of surface area.

Evaporative sodium loss should be governed by heat and mass transfer processes; such a mechanism would be proportional to geometric surface area. The liquor samples in the alumina combustion boats had approximately eight times greater geometric surface area than individual drops, but there was dramatically less sodium released during pyrolysis in the muffle furnace experiment. It can therefore be inferred that the initial sodium loss from single drops was not a result of evaporation.

Mechanisms of Sodium Loss During Pyrolysis

In a thermogravimetric study of model organic alkali compounds, Stewart et al.[71] demonstrated that no alkali loss occurred over the temperature range 450-550°C. However, substantial amounts of alkali were vaporized as a result of Na_2CO_3 reduction at 750-900°C. These findings support the result of the muffle furnace experiment, which leads one to question if the sodium mass loss measured during the single drop experiments was not merely an artifact of the technique. Nevertheless, the single drop results reported in this thesis, and those of other researchers,[12,13] suggest that 5-30% of the sodium is lost during the initial stages of black liquor combustion. Two mechanisms were proposed to explain this sodium loss: evaporation and convection.[83] Evaporation implies there is a partial pressure of a sodium species above a condensed sodium-containing phase. Convection is defined as physical transport of sodium-containing material by gases escaping from a reacting particle.

Evaporation of Sodium

Based on TGA results, sodium release must occur either before all the organically-bound sodium is converted to Na_2CO_3 or after sufficiently high particle temperatures have been reached for Na_2CO_3 to decompose.[12,71] It is unlikely that sodium vapor is produced during devolatilization because particle temperature is expected to reach only 400-500°C, and thermodynamic data indicate that the vapor pressures of all inorganic sodium species (including elemental sodium) are very low at these temperatures.[26,58,59] It may be argued that the fugitive sodium is associated with volatile organic compounds. A low molecular weight organo-sodium compound that has substantial vapor pressure and thermal stability at devolatilization temperatures could be swept from the boundary layer surrounding the black liquor particle into the bulk phase. The compound would there decompose to low molecular weight gases and elemental sodium. Subsequent reactions with O_2, H_2O, and CO_2 would produce submicron-sized fume.[26,65] While this may seem plausible, any mechanism depending on a volatile intermediate is subject to criticism; thermally stable organo-sodium compounds must be identified before such a mechanism can be considered tenable.

Figure 17 confirms a result noted in the last section, that increasing average gas velocity greatly reduced sodium mass loss. The results of the drop experiments at 750°C, given in Fig. 15, are compared with similar values reported by Frederick and Hupa[13] in Fig. 17. The Åbo Akademi experiments were conducted at 800°C with no forced convection; the 50°C temperature difference is not expected to significantly affect the sodium loss values. All points are from 10 seconds pyrolysis of 5-12 mg drops in N_2 with 5% CO. Figure 17 clearly indicates there was greater sodium retention at higher flow rates. While the reason for the velocity effect is unknown, the argument remains that if the sodium mass loss was due to

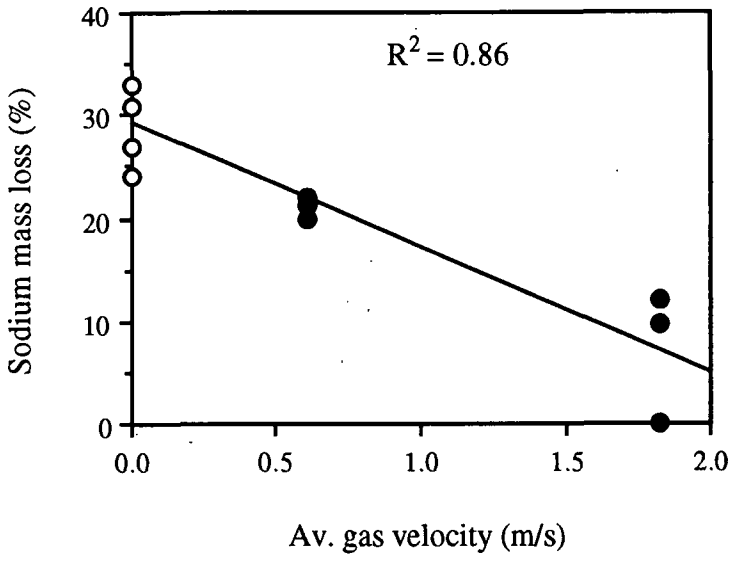

Figure 17. Effect of average gas velocity on sodium loss after 10 s pyrolysis. Data at 0 m/s were from 800°C,[13] filled circles are from this work at 750°C.

direct vaporization, then the increased removal rate (mass transfer) of the alkali species by the higher gas velocity should have resulted in greater sodium release.

There was no sodium loss during pyrolysis of liquor samples in the muffle furnace apparatus, yet there were substantial total mass losses resulting from devolatilization in the same experiments. Comparison of these results with the single drop experiments requires a better understanding of the differences in the physical processes occurring in the two systems. Nevertheless, the gas velocity effect (described above) and results of the muffle furnace experiment clearly support the hypothesis that sodium loss during devolatilization is not an evaporative process.

Physical Ejection of Liquor and Char

The above results suggest that evaporation is not the mechanism of sodium loss

during black liquor pyrolysis. During the first observations of spent liquor drop combustion, researchers noted that the drops bubbled violently during drying.[1,16,18] Bubble formation and erupting jets of gases were also observed in photographic images of devolatilizing black liquor solids and coal particles.[20,34] These eruptions of water vapor and pyrolysis gases from the surface film of a liquor drop could result in ejection of tiny particles of liquor and char. Convection of sodium-containing material has been overlooked as a possible mechanism of sodium loss during the gas evolution stages of drop combustion. Under reducing conditions, organic alkali compounds in ejected liquor and char would rapidly decompose to low molecular weight gases and sodium carbonate aerosol. If the gaseous environment supported combustion, then the mechanisms of char burning and sulfide oxidation, discussed in the Introduction, would produce sodium vapor from the burning bits of ejecta. Sodium vapor would further react with O_2, H_2O, and CO_2 in the gas phase and condense as fume.

The average sodium mass loss from all the single drop experiments are plotted versus furnace temperature in Fig. 18. Each point represents the average sodium mass loss measured for all exposure times at each condition. Clearly, there was a significant effect of temperature on sodium loss during pyrolysis in 95% N_2 with 5% CO. Higher particle heating rates caused by higher furnace temperature would produce more rapid drying and devolatilization.[20] Björkman[18] noted the violence of liquor bursting during heating increased with furnace temperature. The rate of gas release may explain the effect of heating rate on initial sodium loss apparent in Fig. 18.

At 500°C in an oxygen-containing atmosphere, sodium loss was greater than at 600°C in an oxygen-free atmosphere. This is likely a thermal effect caused by particle

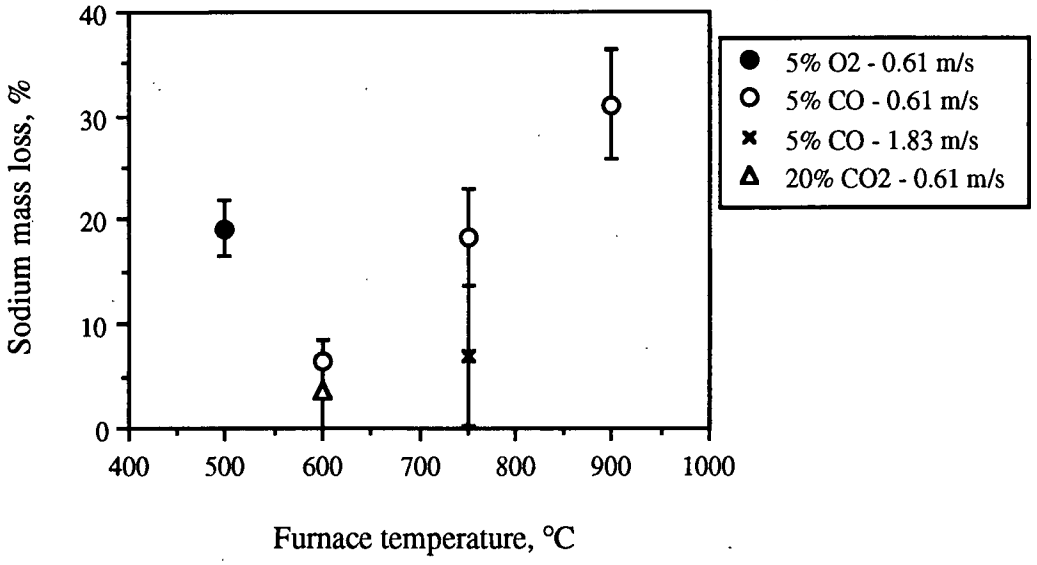

Figure 18. Summary of the effects of process variables on sodium mass loss for all experiments given in Table 3. Plotted points represent mean sodium loss for each condition ± one standard deviation.

heating from slow char oxidation. Oxygen should enhance the rate of sodium loss if an evaporative mechanism was responsible for sodium loss prior to char burning.[65,66] From the limited number of experiments conducting in oxidizing atmospheres, it was not possible to determine if this effect, apparent in Fig. 18, was due to particle heating or chemical reaction enhanced vaporization.

If the initial sodium loss during the individual drop experiments is due to physical ejection, then liquor properties affecting swelling behavior would be expected to affect sodium loss. Results presented in Fig. 3 do not clearly indicate a substantial effect of black liquor type on sodium mass loss. Analyses of the Finnish liquors were not reported; thus, it is not certain if the chosen samples represent a wide enough range of properties to cause significant differences in devolatilization behavior. van Heiningen et al.[28] made a series

of black liquor chars for gasification experiments; a significant effect of liquor type on sodium loss can be calculated from their reported data. While white pine liquors experienced a 15 ± 10% sodium loss during pyrolysis, birch liquors apparently did not release sodium at all. Viscosity, surface tension, extractive content, extent of oxidation, and inorganic content would be expected to affect the physical processes occurring during drying and devolatilization.[20] The effect of these variables on sodium mass loss remains to be systematically investigated.

AEROSOL COLLECTION

Regardless of the mechanism of sodium release during devolatilization, the impact of this sodium loss on fume formation can be evaluated by collection of generated aerosol as a function of exposure time. The first part of this section compares aerosols collected during the pyrolysis experiments described above with those from liquor combustion in air. The second part contains pertinent drop combustion observations and important results from the dynamic aerosol collection experiments. This section concludes with a discussion of the significance of initial sodium loss on fume formation in industrial recovery furnaces. Appendix V contains additional results from static aerosol collection experiments. The technique of time resolution of dynamic aerosol collection data is described in Appendix VI. Consideration of losses due to collection efficiency limitations and deposition within the equipment are contained in Appendix VII.

Aerosol Collection on Stationary Filters

The design of the aerosol collection system was based on the use of borosilicate glass fiber (BGF) filters as the collection medium. For reasons detailed in the

Appendices, these filters were found to be unsuitable for quantitative analysis of inorganic aerosol. However, BGF filters worked well for investigating the morphology of captured particulate matter. The following SEM photomicrographs are indicative of the material found during extensive searches of random samples cut from exposed BGF filters. No evidence of the fine particles, shown in Figs. 19-26, was seen on unexposed filters.

Appendix V indicates that the aerosol collection configuration, particularly the distance of the filters above the drop location, greatly affected the amount of material collected. While more material was collected closer to the combustion source, the higher gas temperature and volumetric flow rate damaged the filters during dynamic collection experiments. To facilitate comparison, all of the photomicrographs presented in this section are of aerosols collected with the dynamic aerosol collection equipment in a fixed mode. Additional SEM images obtained during preliminary collection experiments are presented in Appendix V.

In several of the sodium mass loss determinations, aerosols generated during liquor pyrolysis were collected on BGF filters. The dynamic aerosol collection system was used to place a BGF filter over the drop furnace exit. The filter remained in place during the first five individual drop exposures of each determination. Before additional drops were pyrolyzed, the collection medium carriage was activated to carry the filter past the exhaust flow. The total mass of black liquor solids pyrolyzed for a given filter exposure is given in parenthesis in the captions of Figs. 19-24. A nominal vacuum flow of 14 L/min was maintained for all static aerosol collections during pyrolysis experiments except for the trial at 750°C; in that instance there was no induced flow.

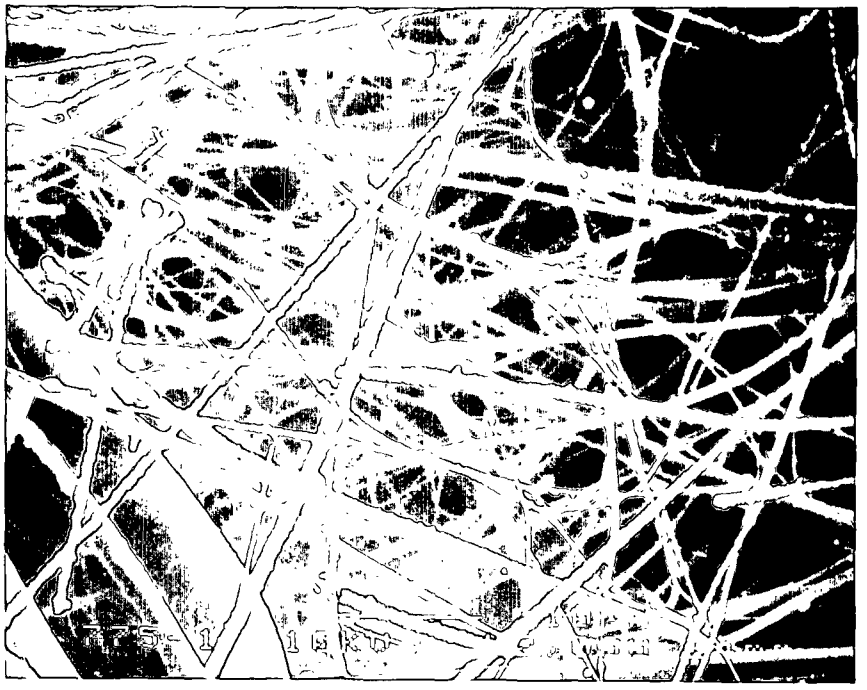

Figure 19. SEM photomicrograph showing aerosol on BGF filter. 10 s pyrolysis of 5 drops (18.9 mg) in 95% N_2/5% CO at 900°C and 0.61 m/s. Magnification 2,000 ×.

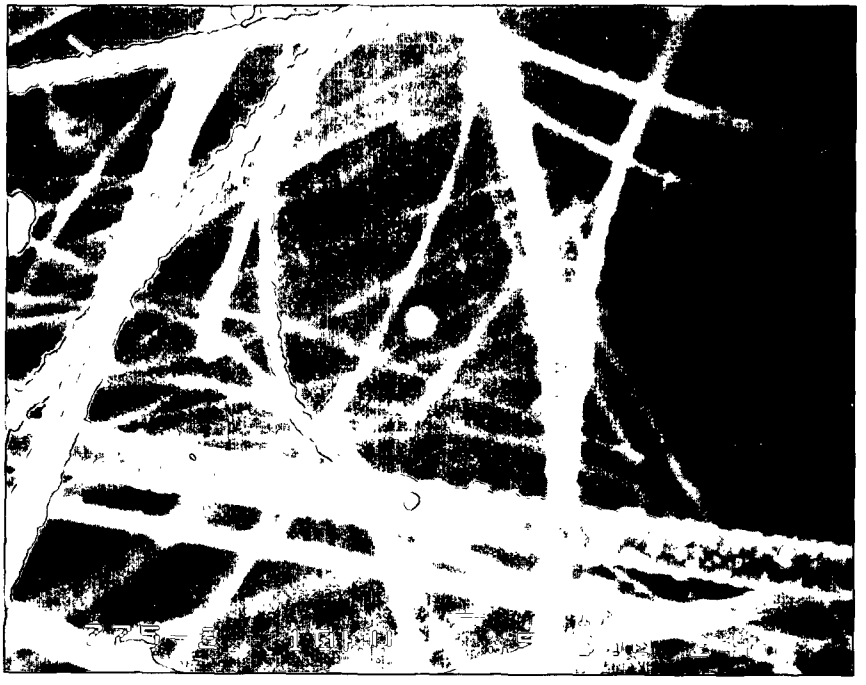

Figure 20. SEM photomicrograph showing fume on surface fibers of BGF filter. Conditions given in Fig. 19. Magnification 5,000 ×.

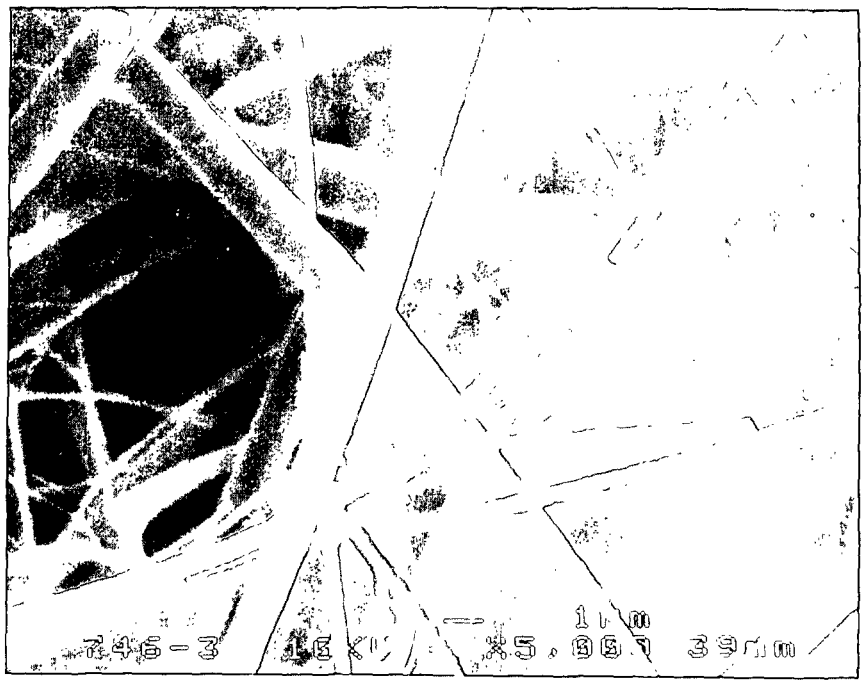

Figure 21. SEM photomicrograph showing no apparent fume on BGF filter. 10 s pyrolysis of 5 drops (24.4 mg) in 95% N_2/5% CO at 750°C and 0.61 m/s. Magnification 5,000 ×.

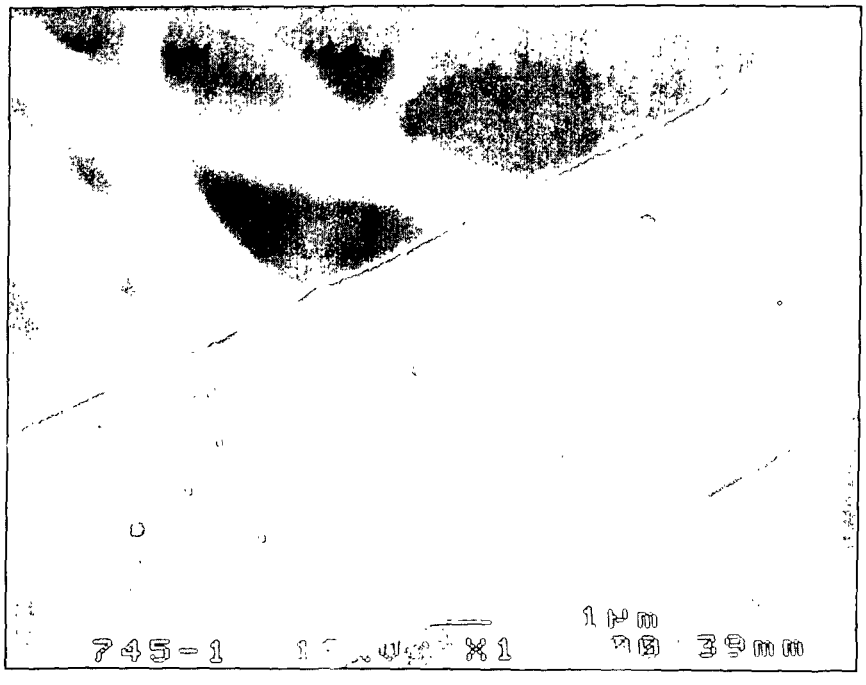

Figure 22. SEM photomicrograph showing very fine aerosol on BGF filter. 28 s pyrolysis of 5 drops (24.0 mg) in 95% N_2/5% CO at 750°C and 0.61 m/s. Magnification 10,000 ×.

Figure 19 is an example SEM photomicrograph of the material collected during liquor pyrolysis at 900°C in 95% N_2 with 5% CO. Numerous 1-2 μm scale-like deposits and submicron-sized globular deposits are visible on the filter fibers. A few 10-20 μm smooth-surfaced spheres were observed on other filter samples; the appearance of these large aerosol particles was similar to those shown in Fig. 32 of Appendix V. This material may have resulted from ejection of liquor or char during drop drying and devolatilization. Deposits of the fume-like aerosol were concentrated on surface fibers, as shown in Fig. 20; this material did not appear to deeply penetrate the fiber mat. TGA results[12,71] suggest that the fume collected on the filters during pyrolysis at 900°C resulted from sodium released during Na_2CO_3 decomposition by reaction with char carbon, as shown in Eqs. 1 and 2.

Despite similar total sodium mass loss values, there were fewer submicron-sized deposits on the filters from pyrolysis at 600°C and 750°C in N_2 with 5% CO than what was observed at 900°C. Figure 21 is a typical representation of what was found at these conditions; little or no fume-like material was evident at 5,000 × magnification. At 10,000 × magnification (Fig. 22), particles smaller than 0.1 μm can clearly be seen on the surface of a glass fiber. While not shown in these figures, a few large (25 μm) smooth spheres and irregular agglomerated deposits were observed on some regions of the filters produced during these experiments.

Figure 23 indicates that gasification of liquor drops at 500°C in 95% N_2 with 5% O_2 produced somewhat more 0.2-1.0 μm fume than did pyrolysis at 750°C. However, the majority of the material collected during the gasification experiment was very similar to the fine aerosol (< 0.1 μm) obtained during pyrolysis at 600 and 750°C (compare Figs. 22 and

Figure 23. SEM photomicrograph showing sparse aerosol on BGF filter. 15 s gasification of 5 drops (19.2 mg) in 95% N_2/5% O_2 at 500°C and 0.61 m/s. Magnification 5,000 ×.

Figure 24. SEM photomicrograph showing very fine aerosol on BGF filter. 30 s gasification of 5 drops (28.1 mg) in 95% N_2/5% O_2 at 500°C and 0.61 m/s. Magnification 10,000 ×.

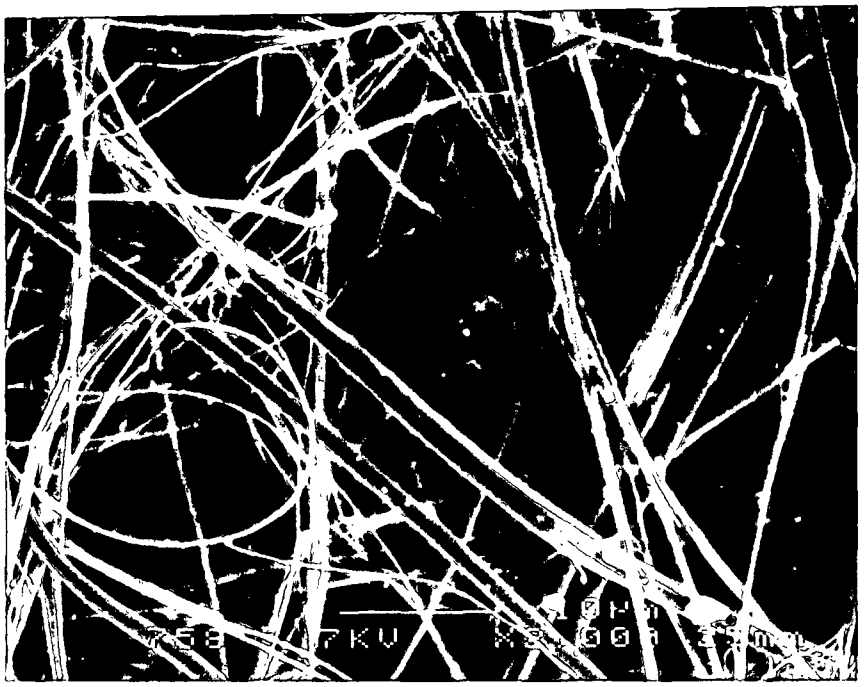

Figure 25. SEM photomicrograph showing aerosol on BGF filter. Combustion of a single 6.2 mg drop in air at 750°C and 0.31 m/s. Magnification 2,000 ×.

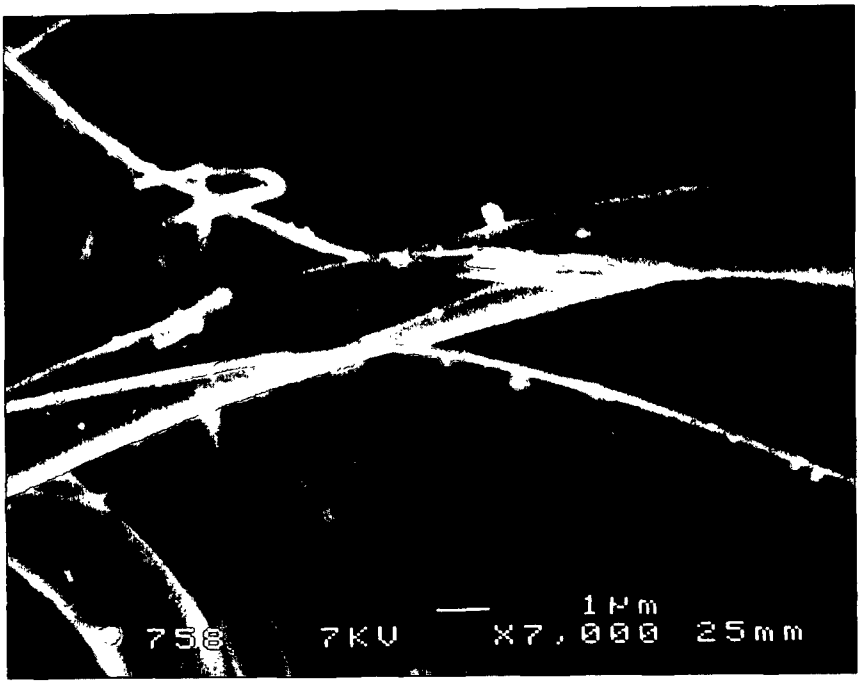

Figure 26. SEM photomicrograph showing fume on BGF filter fibers. Conditions given in Fig. 25. Magnification 7,000 ×.

24). It may be argued that the sodium released during pyrolysis experiments would not have been collected as fume if it had escaped as sodium vapor. Clearly, the presence of oxygen during liquor gasification at 500°C should have created condensed fume from sodium vapor, as described by Cameron.[65] While there was some fume-like material collected during this experiment; there was more material collected on the filters from pyrolysis at 900°C in a reducing atmosphere (compare Figs. 20 and 23). It is therefore unlikely that material escaped the collection system as alkali vapor.

For comparison to the above photomicrographs, Figs. 25 and 26 show the aerosol collected during combustion of single drops of the same liquor in air at 750°C. There was a sparse but uniform coverage of 0.1-1.0 μm irregular fume and a few >10 μm spherical particles on all of the filters exposed in this experiment. Furnace gas velocity was 0.15 m/s (1 ft/s) for the collections shown in Figs. 25 and 26. Analysis of material captured at 0.61 m/s (2 ft/s) in the same experiment revealed similar occurrence and morphology to that shown in Fig. 25. Comparing these last two photomicrographs with Figs. 21 and 22 indicates that less fume was collected during the pyrolysis of 5 drops as during the combustion of a single drop of the same liquor at 750°C.

These SEM photomicrographs provide qualitative evidence that less submicron-sized aerosol was formed during pyrolysis at temperatures below 900°C than during combustion in air at 750°C. Sodium mass loss during the determinations represented in Figs. 19 to 24 ranged from 20.0 to 23.0%. Interestingly enough, the *minimum* sodium mass loss measured from single drops of liquor burned in 92.5% N_2 with 7.5% O_2 at 750°C was 7-9%. This agrees remarkably well with field data of Borg et al.[5] that indicate total sodium loss

from the lower furnace (as fume) is 9% of the sodium entering with the black liquor. These results suggest that sodium release prior to char burning is not a significant source of submicron-size fume in the recovery furnace.

Drop Combustion Behavior

Liquor drops were fixed in place in a flowing gas stream in the IPST drop furnace. Convection was necessary to rapidly carry any generated aerosol to the collection surface, the resulting combustion stage overlap was accounted for by careful analysis of the video images. This section contains a description of the combustion behavior of black liquor drops and observations of the material ejected during combustion.

In the dynamic collection experiments, described in the next section, drops of liquor no. 2B were burned in 92.5% N_2 with 7.5% O_2 at 750°C. This liquor exhibited significant overlap of combustion stages, e.g., bursting during drying was observed on the downstream side of the drop simultaneous with ignition on upstream edge, and char burning started before maximum swollen volume was reached. Incidentally, there was less overlap observed during the combustion of liquor no. 3 at the same conditions. An interesting characteristic of liquor no. 2B was that it maintained a roughly spherical shape throughout the stages of combustion. The burning volatiles flame only appeared at the end of swelling and persisted a few seconds after maximum volume was reached. The swelling of liquor no. 3 was rapid and serpentine; burning volatiles persisted for about one second after maximum swollen volume was reached.

Events observed during combustion of both liquors, at 750°C in 7.5% O_2, were similar to what has been described in the literature.[1,11,16,18] These events are presented

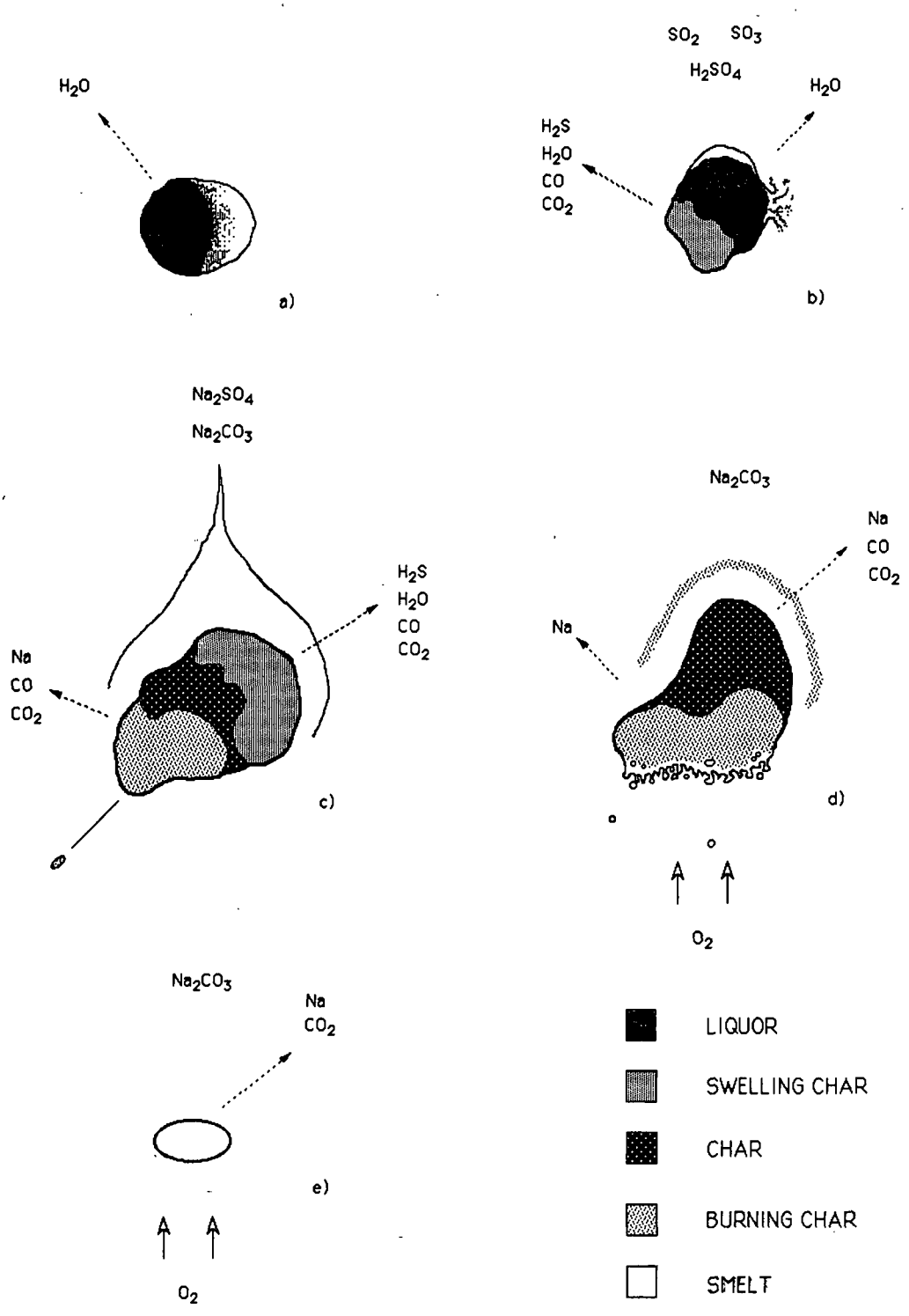

Figure 27. Phases of liquor drop combustion in 7.5% O_2 at 750°C and 0.61 m/s: a) drying; b) drying/devolatilization; c) devolatilization/char burning; d) char burning/ smelting; e) sulfide oxidation.

diagrammatically in Fig. 27; expected products of each combustion stage[23] are shown evolving from corresponding regions of the particle. In all cases there was a brief period of drying which exhibited pronounced bubble bursting (Fig. 27a). While the trailing edge of the drop was still bubbling, the leading edge began to swell and ignition flashes were seen along the surface (Fig. 27b). Swelling proceeded rapidly to the downstream side of the particle as the volatiles flame appeared and the glow of char burning was seen on the leading edge (Fig. 27c). Bright sparks occasionally erupted from regions of the particle undergoing char burning. This material was ejected radially and at high initial velocity. Occasionally the sparks were seen to turn and follow the gas flow. In most instances it appeared that they collided with the quartz reactor tube walls.

After extinction of the volatiles flame, there were a few seconds of heterogeneous char burning, characterized by a shrinking diameter and a gaseous combustion "halo" (Fig. 27d). As carbon burnout progressed tiny droplets of molten smelt formed on the upstream side of the char particles. This process occurred at all combustion conditions with more than 5% O_2. Most of the droplets of smelt disappeared into the char residue or collapsed into what appeared to be a molten smelt layer on the char surface. Some of the depending droplets detached from the char and dropped out of the field of view. This process is referred to herein as smelt shedding. When very little of the char remained, surface tension forces drew the smelt together into a single bead (Fig. 27e).

Under certain conditions material was ejected from the molten smelt bead after coalescence had occurred. This "sparking" phenomenon was suppressed if the furnace environment contained less than 10% oxygen. Two distinct periods of sparking were noted

during drop combustion in air (21% O_2). In all cases there was a period of intense sparking immediately following smelt coalescence; for some drops a stream or cloud of haze persisted until the residue began to visibly cool.

In previous experiments, smelt bead oxidation has been dismissed as an unimportant artifact of the single drop combustion technique.[1,21] Most of the smelt is indeed removed from the char bed of the recovery furnace with little sulfide oxidation. However, airborne smelt droplets would undergo complete sulfide oxidation in the oxidizing conditions of the upper furnace. The degree of smelt entrainment depends on combustion conditions, but could be substantial in overloaded or suspension fired furnaces. It is therefore necessary to consider spark ejection and fume formation occurring during this stage as potential sources of aerosol in the recovery furnace.

Dynamic Aerosol Collection

In the static collection experiments, all of the particulate matter generated during the course of combustion was collected on a small area of filter. The technique of determining the time during combustion when inorganic aerosols were generated required coordinating drop combustion progress with continuous collection of the aerosols as they were produced. Details of this procedure are included in Appendix VI. BGF filters were found to be an unsuitable material for analytical determination of fume species. The amount of soluble Na_2O in the filter fibers was greater than the expected amount of sodium to be collected as aerosol. Furthermore, reaction between acidic combustion gases and alkaline earth contaminants in the filters confounded interpretation of sulfate ion analysis. Silver membranes were chosen as a more suitable aerosol collection medium for the dynamic

aerosol collection experiments. Accurate determination of microgram quantities of sodium was possible with silver membranes because the levels of soluble contaminants in the membranes were extremely low. The quantity of extractable sodium was approximately 5.3×10^{-3} mg per gram of silver membrane material, as compared to a value of 16.5 mg Na per gram of the BGF filter material.

SEM Analysis of Aerosol Collected on Silver Membranes

The performance of the silver membranes was evaluated in one exploratory trial using the dynamic aerosol collection system. A single 7.6-mg drop of liquor no. 3 was burned in 92.5% N_2 with 7.5% O_2 at 750°C and 0.61 m/s. A carriage speed of 305 mm/min (12 in./min) was chosen to expose as much of the 89 by 229-mm (3.5 by 9-in.) membrane as possible to combustion products during the short combustion time. Eight consecutive 13-mm (0.5-in.) square samples were cut from the centerline of the exposed membrane. A traverse along each section in the direction of motion represented approximately 2.5 seconds of elapsed combustion time.

SEM analysis revealed 0.10-0.25 μm fume on all samples. Figure 28 shows that this material is similar to that observed during the static aerosol collection experiments described in the previous section. These fine white specks were not observed on unexposed sections of silver membrane. There were no large spheres (1-30 μm) on the silver membrane samples. Deposit density was observed to increase over the first six samples and then remain constant. The overwhelming presence of silver precluded elemental analysis of the collected material by EDS.

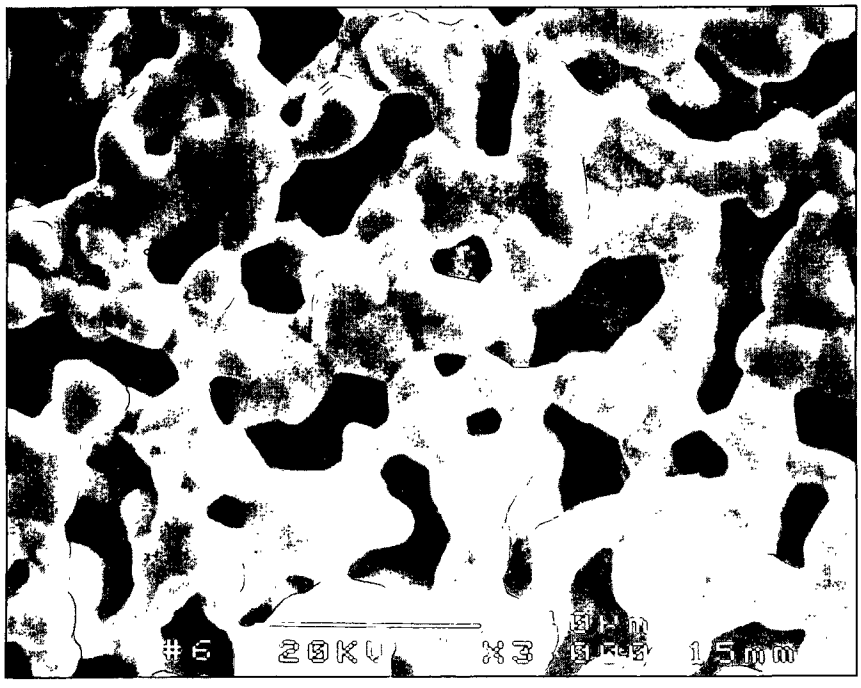

Figure 28. SEM photomicrograph showing submicron-sized aerosol on silver membrane. Combustion of 7.6 mg drop in 92.5% N_2/7.5% O_2 at 750°C and 0.61 m/s. Magnification 3,000 ×.

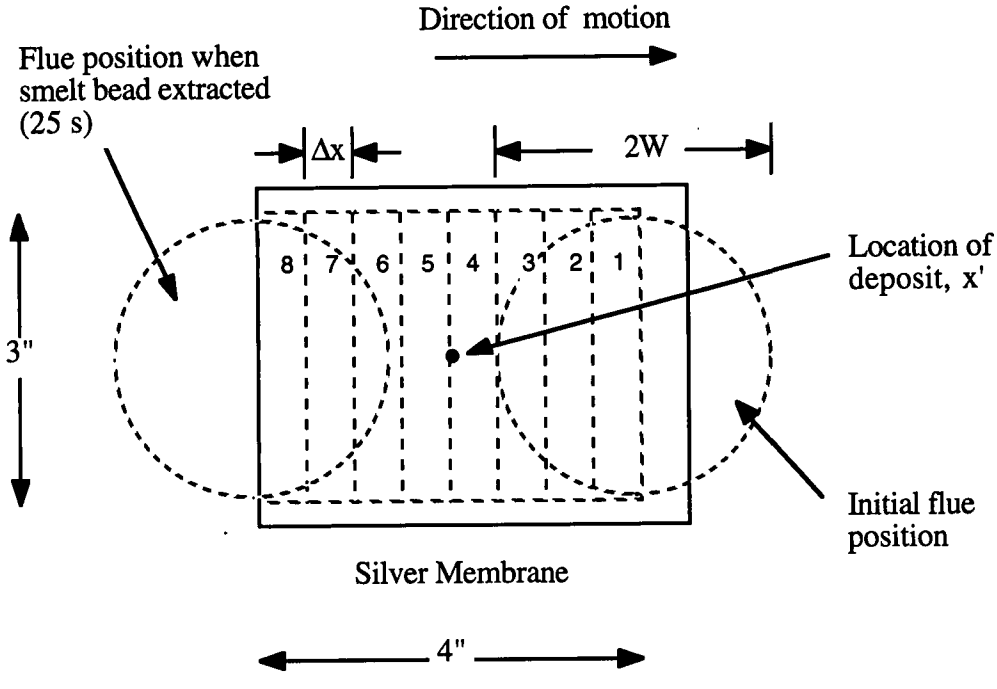

Figure 29. Schematic of silver membrane showing locations of analyzed sections and reference points for discussion of time resolution.

Dynamic Aerosol Collection on Silver Membranes

As described in Appendix VI, the exhaust flow director was replaced with a 76.2-mm (3-in.) diameter metal flue prior to the dynamic aerosol collection experiment. Exhaust gases from drop combustion were impinged on two 89 by 229-mm (3.5 by 9-in.) moving silver membranes. After exposure each membrane was divided into eight 12.7-mm (0.5-in.) sections, as indicated in Fig. 29. All sections were agitated in 45 ml of Type I water; sodium concentration was determined by ICP. The measured species concentrations are reported in Appendix VI.

The following discussion summarizes the analysis of dynamic aerosol collection data. The collection time (t_x) of an inorganic aerosol deposit, located a given displacement (x') from the leading edge of the silver membrane depicted in Fig. 29, can be calculated by

$$t_x = \frac{x}{s_l} \quad , \tag{10}$$

where x is displacement along the membrane and s_l is the linear speed of carriage. When analyzing an area corresponding to time t_x, material collected at t_x was measured but also a fraction of the material collected at all other times the cylindrical flue opening was under the point on the membrane corresponding to t_x. This region of potential overlap is x' ± W in Fig. 29. The time resolution (δ) is set by the width and shape of the flow director opening:

$$\delta_C = \pm \frac{W}{s_l} \quad , \tag{11}$$

where δ_C is the time resolution for a circular opening and W is the half-width or radius of the

flue. For this experiment the time resolution was 9 seconds. The width of each membrane section (Δx) was 13 mm; therefore, the time interval represented by a filter segment ($t_{\Delta x}$) was 3 seconds.

Time during combustion when the sodium-containing species were formed (t_{DC}) was estimated from the locations of the membrane sections, the speed of the carriage drive mechanism, and a calculated average residence time (Θ) between drop and collection surface:

$$t_{DC} = t_x - \Theta \quad . \tag{12}$$

Residence time was calculated from the steady state heat transfer model described in Appendix VI. For these experiments, reactor dynamics was not the factor limiting the time resolution of the results. The estimated residence time was 1.0 s for an average gas velocity of 0.61 m/s at 750°C in the drop reactor. This time lag was less than 5% of the mean duration of drop combustion; a small error compared to the uncertainty arising from spatial overlap of the collected aerosol on the filter.

If a spark, ejected during char burning, followed the center streamline of the exhaust gases, it would strike the membrane at $x = s_l(t_{DC} + \Theta)$. Due to mixing in the exhaust flue, the ejected particle could strike the filter anywhere within the spatial range of the flue opening ($x \pm W$). The temporal uncertainty of determining the origin of instantaneous combustion events from filter analysis is therefore $\pm W/s_l$; exactly the same as the time resolution for this geometry.

Fume Formation Rate During Drop Combustion

The rate of sodium deposition is plotted against elapsed drop combustion time in Fig. 30. Rate of deposition was calculated from the mass of sodium collected during each 3 second time interval (corresponding to the 12.7 mm sections of the membrane). Equation 12 was used to calculate the drop combustion time associated with each membrane section. The horizontal bars in Fig. 30 indicate elapsed combustion stage times with the 9 second temporal uncertainty added and subtracted from either end of each stage time ranges.

The entrainment and collection efficiency calculations in Appendix VII indicate that submicron-sized fume should have been collected preferentially to larger aerosol on the silver membranes. Therefore, the sodium deposition rate history shown in Fig. 30 approximately represents the rate of fume formation. This important result demonstrates that maximum sodium release, leading to fume formation, occurred during the char burning and sulfide oxidation stages of combustion. The primary inorganic product during these stages would have been Na_2CO_3 (see Fig. 27 d) as there were no oxidized sulfur gases evolved after the completion of devolatilization.

Observations of combustion and the results of the dynamic aerosol collection experiments suggest that there were two potential phases of aerosol formation during combustion at 7.5% O_2 at 750°C. The first phase occurred during the overlapped devolatilization and char burning stages, possibly producing Na_2CO_3/Na_2SO_4 fume and inorganic ejecta. The second phase extended from char burning through smelt oxidation and produced primarily sodium carbonate fume and ejecta. At high enough oxygen partial pressure there would have been a third phase of aerosol generation resulting from sparking

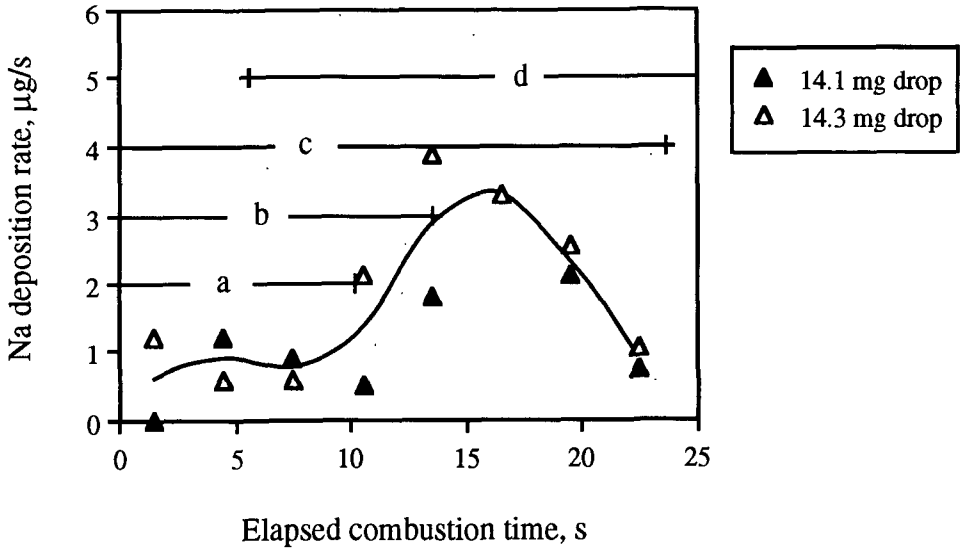

Figure 30. Sodium deposition rate from dynamic aerosol collection; combustion in 7.5% O_2 at 750°C. Bars show stage times: a) drying, b) devolatilization, c) char burning, d) smelt oxidation.

during smelt coalescence. This phase would have produced 10-100 µm sized particles characterized by typical smelt composition.

Collection Efficiency and Material Losses in System

During the drop combustion experiments, the mass flow of gas was adjusted to produce a desired average gas velocity at the set temperature of the quartz reaction chamber. Gas velocity decreased as a result of progressive cooling with displacement past the top of the drop reactor heating elements. As discussed in Appendix VII, entrained material would have fallen out of the gas stream when its settling velocity exceeded the upward gas velocity. It was concluded from this analysis that particles larger than 0.1-0.2 mm in size (smelt ejecta, shedded smelt droplets) fell to the bottom of the furnace.

Particles smaller than 57-80 µm could have reached the silver membrane in the

dynamic aerosol collection experiment. The minimum particle size with sufficient inertia to be collected by impaction on the silver membrane was estimated to be greater than 150 μm. Clearly there would have been no aerosol collection by impaction because the minimum particle size necessary for inertial impaction was substantially larger than the maximum size expected to be carried to the collection plane. As the exhaust flow contacted the surface of the silver membrane, some of the submicron-sized aerosol would have been collected by electrostatic attraction and diffusion.[84] This conclusion is substantiated by the absence of large particulate (d_p > 1 μm) in SEM images of silver membrane samples, as shown in Fig. 28. Loss of aerosol by reentrainment after contact is unlikely for particles smaller than 10 μm because the adhesive forces that act on the particle are two orders of magnitude greater than the removal force of a 10 m/s air current.[78]

During the aerosol collection experiments, the relative change in sodium content from the original liquor to the smelt residue was 25-48%. It is not certain how much of the sodium loss was in the form of fume and how much was as shed smelt droplets; however, it is expected that only a fraction of the airborne material was collected on the silver membrane. Material balance calculations in Appendix VII show that between 5 and 7% of the total sodium "lost" during drop combustion could be accounted for on the silver membranes; this can be considered an indication of the minimum collection efficiency. Assuming 8% of the sodium present in the liquor became fume, total sodium loss for these drops was partitioned into vaporized and shed fractions. The total amount of sodium collected on all sections of each silver membranes accounted for 22-29% of the estimated vaporized fraction; this value can be taken as an estimate of the maximum collection efficiency.

The range of 6-25% collection efficiency for the silver membranes does not seem unreasonable for this experiment. There was no collection of large particles because the minimum particle size necessary for inertial impaction was substantially larger than the maximum expected to be carried to the collection plane. Only submicron-sized aerosol would have been light enough to be collected by electrostatic forces or diffusion as the exhaust flow contacted the silver membrane surface.

This thesis proposes that physical ejection of sodium containing material was responsible for the sodium loss observed during drop pyrolysis. However, there was little physical evidence of this material collected on BGF filters and silver membranes. The experimental system was designed to collect submicron-sized material; therefore, it is expected that most of the larger aerosol was lost within the drop furnace. Figure 31 suggests the fate of the ejected material; it was spattered on the walls of the quartz reactor tube. The tube shown in Fig. 31 was replaced after approximately 360 individual drops had been pyrolyzed or burned at various conditions. The most dense deposits, slightly above the port elevation, were probably a result of ejecta impaction. Thermophoretic fume deposition and sodium vapor crystallization on the unheated portion of the tube are likely causes of the light fog near the quartz reactor exit.[85]

Significance of Initial Sodium Loss on Fume Formation

It is not certain if the initial sodium loss, measured during drop pyrolysis experiments, produces submicron-sized fume in recovery furnaces. Frederick and Hupa[13] suggested that sodium release during devolatilization may be the most significant source of fume. Their justification was that the amount of sodium evolved during single drop pyrolysis

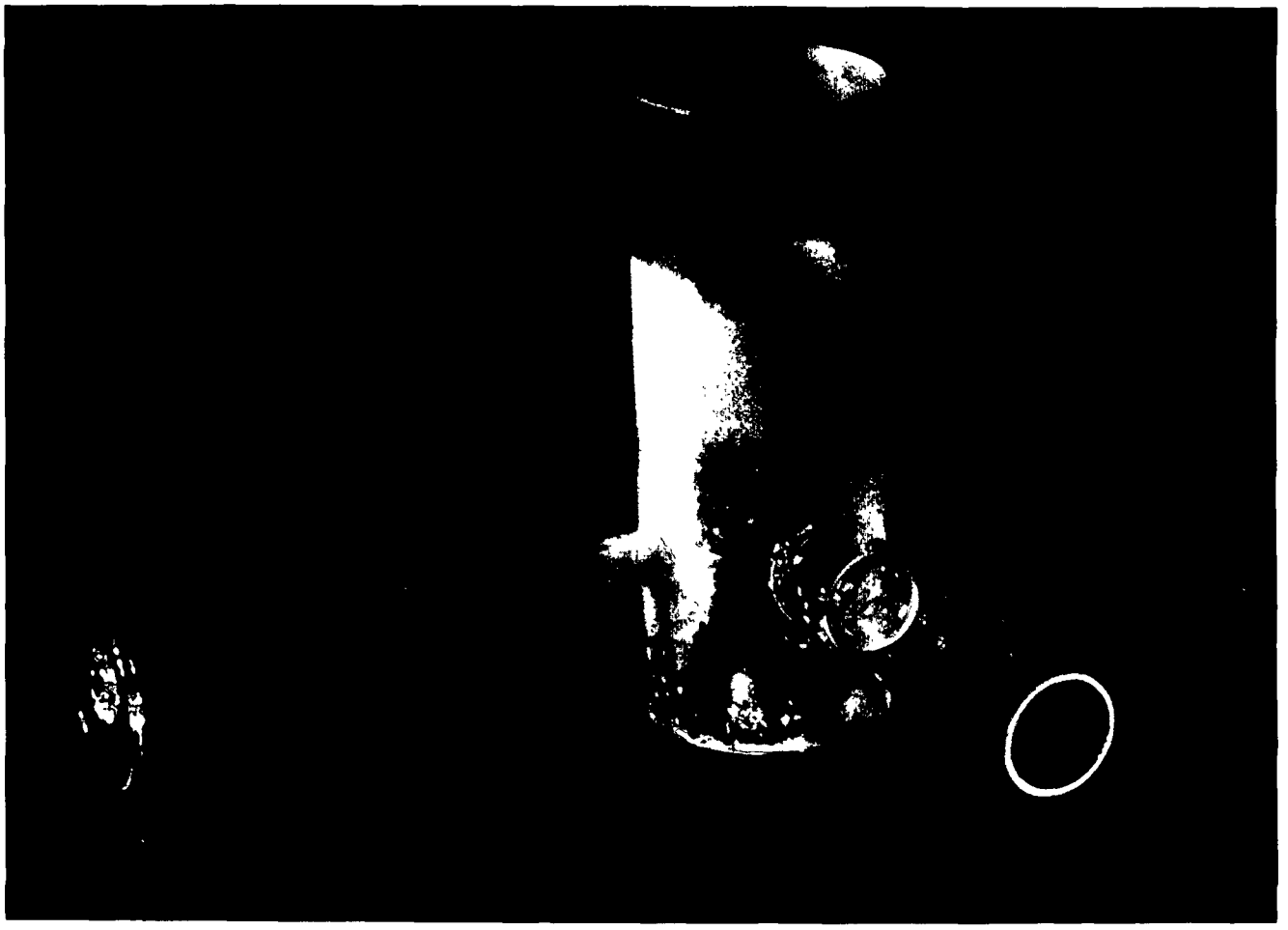

Figure 31. Photograph of quartz reactor tube after combustion of approximately 110 individual drops and pyrolysis of an additional 250 drops.

was an order of magnitude higher than that released during char burning and smelt oxidation experiments. Operational experience indicates that 10% of the sodium in the fired liquor is captured as fume in the electrostatic precipitator; sodium losses measured during the pyrolysis experiments were commonly greater than 10%. While this is a striking comparison, Frederick and Hupa[13] did not consider the fate of the lost sodium in a global furnace environment. If the material was lost by ejection, it could be entrained and produce fume; however, it could also deposit on other liquor drops or fall to the char bed.

SEM analysis of aerosol samples collected during this thesis indicate that little.

submicron-sized fume was formed during the pyrolysis experiments. Only at temperature high enough for Na_2CO_3 decomposition to occur were substantial quantities of fume collected. Some 1-100 μm particles were collected on filters left in place during drop pyrolysis and combustion experiments. The appearance of the combustion chamber after numerous drop exposures and results of entrainment calculations indicate that a significant amount of material was lost within the drop furnace. However, calculations showed that collection efficiency for submicron-sized aerosol was reasonably high. Results of dynamic aerosol collection on silver membranes indicated that the majority of the sodium collected as fume was released during the char burning and smelt oxidation stages of black liquor drop combustion.

A Third Category of Particulate

It has been established that fume and carryover are two distinct types of solid material that reach the heat transfer surfaces in the recovery furnace.[26] Results of this thesis suggest that a third category, ejecta, should also be considered. Furnace particulate samples contained a significant fraction of 1-100 μm inorganic aerosol.[53,55] This was postulated to result from entrainment of smelt beads remaining at the end of airborne drop combustion.[55] Smelt beads should be about half the initial diameter of liquor drops (0.25-2.5 mm);[26] therefore, the collected particles were too small to support the stated hypothesis.

It is more likely that the large aerosol originated as ejecta. During the early stages of drop combustion bits of liquor and char are ejected by erumpent gases. If smelt coalescence occurs in regions of high oxygen concentration, then numerous smelt droplets are ejected by escaping CO_2. This material has been overlooked as an important aspect of furnace chemistry and fouling. Mill experience has shown that electrostatic precipitator catch

from overloaded suspension-fired boilers contains a substantial amount of inorganic material larger than 10 μm.[86] At the high gas velocities encountered within the steam generating section of the furnace, these larger particles may deposit on boiler tubes by inertial impaction.[85] Analysis of furnace dust samples from this region should verify the presence of this intermediate-sized inorganic aerosol.

CONCLUSIONS

Approximately 5-30% of the sodium present in black liquor was released during the drying and devolatilization stages of single drop pyrolysis and gasification experiments. The extent of this initial loss increased with increasing furnace temperature. Exposure to an oxygen-containing atmosphere at 500°C resulted in significant particle heating and higher sodium loss than would be expected in a reducing environment. Higher relative gas velocity resulted in a substantial decrease in sodium release.

After the initial loss, continued sodium release was only measured during pyrolysis at 900°C. A substantial amount of submicron-sized fume was collected on stationary filters during this experiment. The additional sodium loss and fume formation at 900°C resulted from Na_2CO_3 reduction by char carbon. This continued loss was not observed at lower temperatures because carbon monoxide in the gas stream suppresses Na_2CO_3 decomposition up to 800°C.[12]

There was no sodium loss during pyrolysis of liquor films at 750°C, yet there was a 30% volatile yield during this experiment. The liquor film samples had approximately eight times the surface area of the individual drops. This result and the effect of gas velocity suggest that sodium loss prior to the char burning stage of black liquor combustion is not a evaporative process, i.e., it does not result from vaporization of a sodium species. There were fewer results to support the hypothesis that physical transport of alkali-containing material is responsible for sodium loss during black liquor drying and devolatilization. However, eruptions of water vapor and pyrolysis gases through the surface film of rapidly heated drops were observed; this process would be expected to eject small black liquor and char particles.

There was evidence of physically ejected material during all stages of drop combustion in N_2 with 7.5% O_2 at 750°C. Much of this material deposited on the reactor tube walls during the experiments. Within the kraft recovery furnace, the ejecta may react to produce fume, collide with other airborne particles, fall to the char bed, or deposit on furnace heat transfer surfaces.

Inorganic aerosols were collected during the respective stages of black liquor drop combustion. Time resolution of the results was limited by spatial overlap of the aerosol on the collection media. However, the measured sodium deposition history was representative of submicron-sized fume formation from a burning drop. Results of these experiments demonstrate that a maximum in fume formation occurred during the char burning and smelt oxidation stages of combustion.

SEM photomicrographs showed that more submicron-sized fume was produced during the combustion of a single drop of black liquor than during the pyrolysis of five drops at similar furnace conditions. While initial sodium loss during devolatilization may contribute to fume formation, these aerosol collection results suggest that it is not necessarily the most significant source of submicron-sized fume in the recovery furnace.

RECOMMENDATIONS FOR FUTURE WORK

MODELING SODIUM LOSS

Additional experiments are required before the process of sodium loss during pyrolysis can be modeled. A factorial experimental design would allow quantification of the effects of process variables. The influence of gas velocity should be evaluated at a different temperature to conclusively isolate the effects of heating rate from relative velocity. As heating rate is a function of both furnace temperature and drop size, a range of controlled drop sizes should be exposed to constant furnace conditions. A larger insertion port may be required to withdraw large swollen char particles from the furnace. It is well known that solids content greatly affects liquor viscosity,[87] this should be the first liquor composition variable studied. Wood species and extractives content have been shown to have dramatic effects on liquor properties and swelling behavior.[20] It is recommended that sodium loss be measured from two or more additional liquors, having a wide range of physical properties, for at least one set of furnace conditions.

Determination of the significance of sodium release during each stage of combustion on overall fume formation will require a global consideration of the complex physical and chemical processes occurring within the kraft recovery furnace. This may best be investigated by incorporating experimental results in a complex recovery furnace model and evaluating the response to specified changes in process conditions.

The relative contributions of drying and devolatilization to total sodium loss during pyrolysis remains to be determined. This could be accomplished by measuring the

sodium loss at different solids contents for identical furnace conditions and initial drop size. The liquor used in this thesis had a solids content of 71-73%. Forming drops from a diluted sample (60% solids) and pelletizing 100% solids should provide a sufficient range for comparison to the thesis results.

IDENTIFICATION OF FUGITIVE SODIUM

Single drop pyrolysis experiments provide fundamental information about the processes occurring during black liquor combustion. However, it is possible that the large sodium losses measured in the single drop studies may be an artifact of the experimental technique. While the aerosol collection experiments suggest that ejection of black liquor and char from the reacting particles contributed to the measured sodium loss, it was not possible to close the material balance. The form(s) of the lost sodium must be conclusively identified. The dynamic aerosol collection system can be modified to better collect submicron-sized fume on silver membranes. Another technique must be developed to independently capture the larger ejected material.

Collection efficiency for submicron-sized aerosol on silver membranes could be improved by inducing flow through the membrane with a vacuum source; however, furnace flow would have to be drastically reduced. Another option would be to establish a potential difference between the quartz reactor tube and the collection surface, thereby charging the aerosol and enhancing electrostatic aerosol collection forces. The analysis in Appendix VI suggests that a narrow rectangular opening is necessary for accurate time resolution; the original flow director should therefore be used in subsequent experiments. Increasing the platform drive speed would also improve resolution as long as it does not reduce deposit

density to below analysis detection limits. Optimization of these equipment parameters is expected to improve the accuracy of the results.

One possibility for collecting the ejected material close to its point of origin would be to encircle the liquor drop with a cylinder of metallic foil, oriented parallel to the furnace gas flow. Inserting this assembly into the drop furnace would allow the fume to escape while collecting spattered material on the inside surface. SEM analysis of the foil surface should reveal the nature of the deposits.

RECOVERY FURNACE PARTICULATE ANALYSIS

An industrial furnace study should be directed towards size classification of inorganic aerosol, and determination of the role of ejecta in fouling. A multistage low pressure cascade impactor would best be utilized to isolate the various aerosol size fractions. Samples should be taken as close to the combustion zone as possible to minimize loss of certain classes of aerosol. Such a study would also provide data for validating a computational model of the aerosol mechanics and chemistry within the kraft recovery furnace.

LITERATURE CITATIONS

1. Hupa, M.; Solin, P.; Hyöty, P., Combustion behavior of black liquor droplets. J. Pulp Paper Sci. 13(2):J67-J72 (1987).

2. Björkman, A.; Warnqvist, B., Basic processes in gasification/burning of kraft liquors. Pulp Paper Can. 89(11):T374-T380 (1988).

3. Tran, H., How does a kraft recovery furnace become plugged? Tappi Kraft Recovery Operations Seminar Notes. Orlando, FL, p. 183-191 (1989).

4. Rizhinshvili, G.V.; Kaplun, L.V., Means to reduce furnace emissions of soda recovery boilers. Bumazh. Prom. (1):26-28 (1983).

5. Borg, A.; Teder, A.; Warnqvist, B., Inside a kraft recovery furnace - studies on the origins of sulfur and sodium emission. Tappi 57(1):126-129 (1974).

6. Björklund, H.; Warnqvist, B.; Pettersson, B., Inside a kraft recovery boiler - combustion of black liquor at high dry solids. Proc. TAPPI/CPPA Int. Chemical Recovery Conf. Ottawa, Ontario, p. 177-181 (1989).

7. Hyöty, P.; Hupa, M.; Skrifvars, B.-J.; Kärki, R., Latest experiences of high solids firing. Proc. TAPPI/CPPA Int. Chemical Recovery Conf. Ottawa, Ontario, p. 169-175 (1989).

8. Jones, A.K.; Stewart, R.I., The high solids breakpoint - a trade-off between SO_2 and NO_x. Proc. TAPPI/CPPA Int. Chemical Recovery Conf. Seattle, WA, p. 365-370 (1992).

9. Lang, C.J.; DeHaas, G.G.; Gommi, J.V.; Nelson, W., Recovery furnace operating parameter effects on SO_2 emissions. Tappi 56(6):115-119 (1973).

10. Clay, D.T.; Grace, T.M.; Kapheim, R.J., Fume formation from synthetic sodium salt melts and commercial kraft smelts. AIChE Symposium Series 80(239):99-106 (1984).

11. Volkov, A.D.; Evseev, O.D.; Ibatullina, R.I.; Dravolina, E.I., Sodium loss during burning of moist particles of black liquor. Mezhuz. Sb. Nauchn. Tr. Ser. Khim. Teknol. Tsellyul. (7):72-75 (1980).

12. Li, J.; van Heiningen, A.R.P., Sodium emission during pyrolysis and gasification of black liquor char. Tappi 73(12):213-219 (1990).

13. Frederick, W.J.; Hupa, M., Evidence of sodium fuming during pyrolysis of black liquor. Tappi 74(11):192-194 (1991).

14. Frederick, W.J.; Forssén, M.; Hupa, M.; Hyöty, P., Sulfur and sodium volatilization during black liquor pyrolysis. Proc. TAPPI/CPPA Int. Chemical Recovery Conf. Seattle, WA, p. 599-608 (1992).

15. Masdin, E.G.; Thring, M.W., Combustion of single droplets of liquid fuel. J. Inst. Fuel 35:251-260 (1962).

16. Monaghan, M.T.; Siddall, R.G., The combustion behavior of waste sulfite liquor - a preliminary investigation. Tappi 46(2):89-91 (1963).

17. Huldén, B., Combustion behavior of spent liquor drops. Proc. IUPAC/EUCEPA Symp. on Recovery of Pulping Chemicals. Helsinki, Finland, p 375-383 (1969).

18. Björkman, A., Pyrolysis of spent liquors. Proc. IUPAC/EUCEPA Symp. Recovery of Pulping Chemicals. Helsinki, Finland, p. 235-267 (1969).

19. Grace, T.M.; Cameron, J.H.; Clay, D.T., Char Burning. Project 3473-6 Summary Technical Report. The Institute of Paper Chemistry, Appleton, WI (1985).

20. Miller, P.T., Swelling of kraft black liquor. An understanding of the associated phenomena during pyrolysis. Ph.D. Dissertation. The Institute of Paper Chemistry, Appleton, WI (1986).

21. Kulas, K.A., An overall model of the combustion of a single droplet of kraft black liquor. Ph.D. Dissertation. Institute of Paper Science and Technology, Atlanta, GA (1990).

22. Noopila, T.; Hupa, M., Measuring the combustion properties of black liquors by different techniques. Combustion Chemistry Research Group Report 88-5. Åbo Akademi, Turku, Finland (1988).

23. Frederick, W.J., Combustion Processes in Black Liquor Recovery: Analysis and Interpretation of Combustion Rate Data and an Engineering Design Model. Report No. One for U.S. Dept. of Energy, DOE/CE/40637-T8 (DE90012712). (March, 1990).

24. Clay, D.T.; Lien, S.J.; Grace, T.M.; Macek, A.; Semerjian, H.G.; Amin, N.; Charagundla, S.R., Fundamental Studies of Black Liquor Combustion. Report No. 2. for U.S. Dept. of Energy, DE88005756. (January, 1987).

25. Frederick, W.J.; Noopila, T.; Hupa, M., Swelling of spent pulping liquor droplets during combustion. J. Pulp Paper Sci. 17(5):J164-J170 (1991).

26. Adams, T.N.; Frederick, W.J., Kraft Recovery Boiler Physical and Chemical Processes. The American Paper Institute, New York, NY (1988).

27. Li, J.; van Heiningen, A.R.P., Kinetics of CO_2 gasification of fast pyrolysis black liquor char. Ind. Eng. Chem. Res. 29(9):1776-1785 (1990).

28. Heiningen, A.R:P; Arpiainen, V.T.; Alén, R., Effect of liquor type and pyrolysis rate on the steam gasification reactivities of black liquors. Proc. TAPPI/CPPA Int. Chemical Recovery Conf. Seattle, WA, p. 641-649 (1992).

29. Elliott, M.A.; Yohe, G.R., The coal industry and coal research and development in perspective. Chemistry of Coal Utilization, Second Supplementary Volume. Elliott, M.A., ed., John Wiley & Sons, New York, p. 1-54 (1981).

30. Hendrickson, T.A., ed., Synthetic Fuels Data Handbook. Cameron Engineers, Inc., Denver, CO, p. 117-125 (1975).

31. Singer, J.G., Combustion Fossil Power Systems. Combustion Engineering, Inc., Windsor, CT, p. 7-1 - 8-52 (1981).

32. Smoot, L.D.; Smith, P.J., Coal Combustion and Gasification. Plenum Press, New York (1985).

33. Laurendeau, N.M., Heterogeneous kinetics of coal char gasification and combustion. Progr. Energy Combust. Sci. 4:221-270 (1979).

34. Anthony, D.B.; Howard, J.B., Coal devolatilization and hydrogasification. AIChE J 22(4):625-656 (1976).

35. Ragland, K.W.; Weiss, C.A., Combustion of single coal particles in a jet. Energy 4:341-348 (1979).

36. Raask, E., Mineral Impurities in Coal Combustion. Hemisphere Publishing Corp., Washington, DC (1985).

37. Sarofim, A.F.; Howard, J.B.; Padia, A.S., The physical transformations of the mineral matter in pulverized coal under simulated combustion conditions. Comb. Sci. Tech. 16:187-205 (1977).

38. Grace, T.M.; Sachs, D.G.; Grady, H.J., Determination of the inorganic composition of alkaline black liquors. Tappi 60(4):122-125 (1977).

39. Huffman, G.P.; Huggins, F.E., Reactions and transformations of coal mineral matter at elevated temperatures. Mineral Matter and Ash in Coal: ACS Symp. Series 301, Vorres, K.S., ed. American Chemical Society, Washington, DC, p. 101-113 (1986).

40. Neville, M.; Sarofim, A.F.,The fate of sodium during pulverized coal combustion. Fuel 64(3) (1985).

41. Reid, W.T., Coal ash - its effect on combustion systems. Chemistry of Coal Utilization, Second Supplementary Volume. Elliott, M.A., ed. John Wiley & Sons, New York, NY, p. 1389-1445 (1981).

42. Ondov, J.M.; Ragini, R.C.; Bierman, A.H., Emissions and particle-size distributions of minor and trace elements at two Western coal-fired power plants equipped with cold-side electrostatic precipitators. Environ. Sci. Technol. 13(8):946-953 (1979).

43. Raask, E.; Goetz, L., Characteristics of captured ash, chimney solids, and trace elements. J. Inst. Energy 54:163-173 (1981).

44. Kauppinen, E.I.; Pakkanen, T.A., Coal combustion aerosols: a field study. Environ. Sci. Technol. 24(12):1811-1818 (1990).

45. Flagan, R.C.; Taylor, D.D., Laboratory studies of submicron particles from coal combustion. Symp. (Int.) on Combustion. 18th:1227-1237 (1980).

46. Neville, M.; Quann, R.J.; Haynes, B.S.; Sarofim, A.F., Vaporization and condensation of mineral matter during pulverized coal combustion. Symp. (Int.) on Combustion. 18th:1267-1274 (1981).

47. Linak, W.P.; Peterson, T.W., Effect of coal type and residence time on the submicron aerosol distribution from pulverized coal combustion. Aerosol. Sci. Technol. 3:77-96 (1984).

48. Quann, R.J.; Sarofim, A.F., Vaporization of refractory oxides during pulverized coal combustion. Symp. (Int.) on Combustion. 19th:1429-1440 (1982).

49. Green, H.L.; Lane, W.R., Particulate Clouds: Dusts, Smokes and Mists. D. Van Nostrand Co., Princeton, NJ, p. 3-7 (1957).

50. Smith, R.D.; Campbell, J.A.; Nielson, K.K., Characterization and formation of submicron particles in coal-fired plants. Atmos. Environ. 13:607-617 (1979).

51. Faist, M.B.; Davidovits, P., Formation of submicron ash particles in coal combustion. Proc. Int. Conf. on Residual Solid Fuels, Portland OR, p. 808-830 (1981).

52. Bosch, J.C.; Pilat, M.J.; Hrutfiord, B.F., Size distribution of aerosols from a kraft mill recovery furnace. Tappi 54(11):1871-1875 (1971).

53. Nguyen, X.T.; Rowbottom, R.S., Characterizing particulates from kraft recovery boilers. Pulp Paper Can. 80(10):T318-T324 (1979).

54. Reeve, D.W.; Tran, H.N.; Barham, D., The effluent-free bleached kraft pulp mill - Part XI. Pulp Paper Can. 82(9):T315-T320 (1981).

55. Tran, H.N.; Reeve, D.W.; Barham, D., Formation of kraft recovery boiler superheater fireside deposits. Pulp Paper Can. 84(1):T7-T12 (1983).

56. Zhuchkov, P.A.; Volkov, A.D.; Evseev, O.D., Influence of soda recovery boiler operating parameters on carryover of mineral salts. Mezhuz. Sb. Nauchn. Tr. Khim. Teknol. Tsellyul.:74-77 (1983).

57. Hyöty, P.A.; Ojala, S.T., High-solids black liquor combustion, tampella's super combustion system. Tappi 71(6):108-111 (1988).

58. Kohl, F.J.; Stearns, C.A.; Fryburg, G.C., Sodium sulfate: vaporization thermodynamics and role in corrosive flames. NASA Technical Memorandum NASA TM X-71641. Presented at the Electrochem. Soc. Int. Symp. on Metal-Slag-Gas Reactions and Processes (May, 1975).

59. Andresen, R.E., Solubility of oxygen and sulfur dioxide in molten sodium sulfate and oxygen and carbon dioxide in molten sodium carbonate. J. Electrochem. Soc. 126(2):328-334 (1973).

60. Pejryd, L.; Hupa, M., Bed and furnace gas compositions in recovery boilers - advanced equilibrium calculations. Proc. Tappi Pulping Conf. San Francisco, CA, p. 579-590 (1984).

61. Blackwell, B.; King, T., Chemical Reactions in Kraft Recovery Boilers. Sandwell and Co.; Vancouver, British Columbia (1985).

62. Warnqvist, B., Chemical equilibria in the soda unit - connection between operating conditions and emission. Svensk Papperstidning 76(12):463-466 (1973).

63. Cameron, J.H., Vaporization from alkali carbonate melts with reference to the kraft recovery furnace. J. Pulp Paper Sci. 14:J76-J81 (1988).

64. Cameron, J.H.; Grace, T.M., Fume Generation from Alkali Carbonate/Sulfide Melts. Project 3473-1 Progress Report Four. The Institute of Paper Chemistry, Appleton, WI (1986).

65. Cameron, J.H., Reaction enhanced vaporization of molten salt. Chem. Eng. Comm. 59:243-257 (1987).

66. Turkdogan, E.T.; Grieveson, P.; Darken, L.S., Enhancement of diffusion-limited rates of vaporization of metals. J. Phys. Chem. 67:1647-1654 (1963).

67. Shivgulam, N.; Barham, D.; Rapson, H., Sodium chloride, potassium: their effects on kraft smelt. Pulp Paper Can. 80(9):T282-T285 (1979).

68. Gilbert, A.F.; Rapson, H., Accumulation of potassium in a closed mill cycle. Pulp Paper Can. 81(2):T43-T47 (1980).

69. Reeve, D.W.; Tran, H.N.; Barham, D., Superheater fireside deposits and corrosion in kraft recovery boilers. Tappi 64(5):109-113 (1981).

70. Forssén, M., Personal communication. (June, 1992).

71. Stewart, G.W.; Chakrabarti, A.; Moore, W.R., Reactions of alkali containing species in combustion streams. U.S. Dept. of Energy Proc.: High-Temperature, High-Pressure Particulate and Alkali Control in Coal Combustion Process Streams. Science Applications, Inc., McLean, VA, p. 275-300 (1981).

72. Srinivasachar, S.; Helble, J.J.; Ham, D.O.; Domazetis, G., A kinetic description of vapor phase alkali transformations in combustion systems. Prog. Energy Combust. Sci. 16:303-309 (1990).

73. Alén, R.; Sjöström, E., Utilization of black liquor organics as chemical feedstocks. Proc. 6th Ann. Int. Symp. on Wood and Pulping Chemistry. Melbourne, Australia, p. 357-360 (1991).

74. TAPPI Test Method T 699 om-87. Analysis of pulping liquors by suppressed ion chromatography.

75. TAPPI Test Method T 650 om-89. Solids content of black liquor.

76. EPA Test Method 200.7. Inductively Coupled Plasma - Atomic Emission Spectrometric Method for Trace Element Analysis of Water and Wastes. (December, 1982).

77. Lee, S.R.; Verrill, C.L.; Nichols, K.M., Kraft black liquor char density. AIChE Forest Products Div. Symp. Proc., Tappi Press, Atlanta, GA, p. 1-26 (1992).

78. Hinds, W.C., Aerosol Technology: Properties, Behavior, and Measurement of Airborne Particles. John Wiley and Sons, New York, NY (1982).

79. Brown, C.A.; Grace, T.M.; Lien, S.J.; Clay, D.T., Char bed burning rates - experimental results. Tappi 72(10):175-181 (1989).

80. McCabe, W.L.; Smith, J.C., Unit Operations of Chemical Engineering. Third Edition. McGraw-Hill, New York, NY (1976).

81. Özişik, M.N., Heat Transfer: A Basic Approach. McGraw-Hill, New York, NY (1985).

82. Frederick, W.J.; Wåg, K.; Hupa, M.; Stenberg, J.; Hernberg, R., Optical pyrometer measurements of surface temperature during black liquor combustion and implications to black liquor combustion processes. Prepared for presentation at the AIChE Annual Meeting, Miami Beach, FL (1992).

83. Verrill, C.L.; Nichols, K.M., Fume formation during black liquor drop combustion: the importance of sodium release during devolatilization. Proc. TAPPI/CPPA Int. Chemical Recovery Conf. Seattle, WA, p. 609-615 (1992).

84. Fuchs, N.A., The Mechanics of Aerosols. Pergamon Press, Macmillan Co., New York, NY (1964).

85. Goerg, K.A., A Study of Fume Particle Deposition. Ph.D. Dissertation. The Institute of Paper Chemistry, Appleton, WI (1989).

86. Samuelsson, I.L.; Bradburn, K.M., Electrostatic precipitator design and operation, to meet particulate emission control requirements, for today's trends in recovery boiler operation. Presented at TAPPI/CPPA Int. Chemical Recovery Conf., Seattle, WA, (June, 1992).

87. Söderhjelm, L., Viscosity of strong black liquor from sulphate mills. Proc. TAPPI/CPPA Int. Chemical Recovery Conf. Ottawa, Ontario, p. 95-99 (1989).

ACKNOWLEDGEMENTS

I sincerely thank the Institute of Paper Science and Technology and its member companies not only for financial support, but also for an excellent education and the opportunity to live in two fine cities. I am proud to be a veteran of The Move and look forward to following the growth of the Institute in its new home.

I thank my advisor, Dr. Ken Nichols, for his constant enthusiasm, motivational inspiration, and fresh perspective. My thesis advisory committee - Drs. Jeff Empie, Jeff Lindsay, and Dave Orloff - provided essential support and guidance during my project. I wish to acknowledge Dr. John Cameron for introducing me to the mysteries of fume formation. Special thanks are due Dr. Tom Grace who has always maintained interest in this project as well as offering the wisdom of his experience and careful review of my work. Dr. Robert Damon deserves special mention for providing me with a practical knowledge of kraft recovery operations. Drs. Terry Adams, Jim Frederick, Dave Clay, Mikko Hupa, and Adriaan van Heiningen have all offered significant suggestions during my project. Drs. Frederick and Hupa are also thanked for the opportunity to work at Åbo Akademi.

My special thanks go to all the Institute staff who have helped along the way, especially the world class Chemical Recovery Group technicians: Orlin Kuehl, Don Sachs, and Doug Samuels. The image analysis of the drop videos was done by my fellow Ph.D. candidate, Stacy Lee; his contribution is gratefully acknowledged. I thank Mr. Mikael Forssén for sharing the preliminary results of his work at Åbo Akademi. The University of New Brunswick and the Babcock and Wilcox Company are thanked for providing the computing and copying resources necessary to complete the corrections to this dissertation.

The friendship of my fellow students has made this experience all the more enjoyable. My years at the Institute will be remembered most fondly for the good times shared with my friends. My parents, my brother, and his family have provided me enduring support; their love is gratefully acknowledged. I thank my other friends and relatives who put up with my intermittent correspondence and always had a kind word to offer. Most of all I thank Colleen Walker, my companion and colleague. Not only has Colleen's constant love and encouragement helped me through emotionally difficult times, but also her insightful suggestions have helped me solve my most difficult technical problems.

APPENDIX I. GLOSSARY

Aerosol A general term describing a dispersion of solid or liquid particles in a gas. Most correctly, this definition implies that particle size is small enough to form a stable colloidal suspension.[48]

Black Liquor The by-product of the kraft, or sulfate, pulping process. In this dissertation other spent pulping liquors will be specifically referred to as **soda** or **sulfite** liquor to avoid confusion.

Char The porous, friable material remaining at the end of devolatilization. Black liquor char contains carbon and finely dispersed inorganic compounds.

Combustion The process of burning fuel. When sufficient oxygen is present for complete combustion the reaction products are H_2O, CO_2, and inorganic residue or ash.

Drop A liquid entity that is on the order of 1 mm in size, e.g., a black liquor drop.

Droplet A liquid entity that is on the order of 0.1 mm in size, e.g., an ejected smelt droplet.

Dust Solid particles of widely variable size formed by disintegration processes.

Ejecta The fine solid or liquid material physically ejected by erupting gases from a burning drop of liquid fuel or a solid fuel particle.

Exposure Generic term used herein to refer to combustion or pyrolysis of a single drop of black liquor.

Fume Submicron-sized solid particles produced by physicochemical reactions such as combustion, sublimation, or distillation.

Mist Droplets produced by liquid atomization or vapor condensation; the size of mist droplets is generally considered to be less than 100 μm.

Gasification The thermal conversion of a solid or liquid fuel to a gaseous fuel of relatively high heating value. Gasification is commonly thought of as incomplete combustion with O_2, H_2O, or CO_2, as the oxidizer.[32]

Pyrolysis The thermal decomposition of organic material conducted in an oxidizer-free environment that yields volatile substances and a carbonaceous solid residue.[32]

Shedding The loss of molten smelt droplets during char burning and smelt coalescence; differentiated from sparking by lower velocity and downward trajectory.

Smelt The molten mixture of Na_2S and Na_2CO_3 remaining at the end of char burning.

Smoke A cloud of particles, from 5 to less than 0.1 μm in size, usually considered to originate from combustion of carbonaceous material.

Solids Oven dry black liquor solids or the material left at the end of drop drying.

Sparking Violent ejection of molten smelt droplets during the char burning and smelt coalescence stages of drop combustion. Spark trajectory is random.

Stage A characteristic event during black liquor drop combustion, namely: drying, devolatilization, char burning, and inorganic reactions (smelt oxidation).[1]

APPENDIX II. LIST OF EXPERIMENTAL EQUIPMENT

Table 5. List of major components of drop furnace and aerosol collection system.

COMPONENT	DESCRIPTION	VENDOR
Gas heater tube	Cast mullite tube: single reduced end, 2.75 in. OD, 2.5 in. ID, 29-in. total length, cat. no. 66329.	Coors Ceramics Co., Golden, CO
Ceramic joining section	902 Machinable ceramic rod: 4 by 12 in., cat. no. 902-24. Section machined by GTRI machine shop.	Cotronics Corp., Brooklyn, NY
Quartz drop reactor tube	Custom assembly of Vitreosil® tubing: 69 mm OD DA4XMO2 reactor tube, 7-in. long; 31.4 mm OD NCO2800 view port, 4.5-in. long; 15.6 mm OD NCO1300 insertion port, 6-in. long.	Thermal American Fused Quartz Co., Montville, NJ
Heating elements: gas preheater section	Watlow ceramic fiber heaters: semicylindrical, 3.5 in. ID, 7.5 in. OD, 6-in. heated length, high emissivity surface coating, model no. VS403J06S.	Ash Equipment Co., Bensenville, IL
Heating elements: main gas heater section	Watlow ceramic fiber heaters: semicylindrical, 3.5 in. ID, 7.5 in. OD, 18-in. heated length, high emissivity surface coating, model no. VS403J18S.	Ash Equipment Co., Bensenville, IL
Heating elements: drop reactor section	Watlow ceramic fiber heaters: semicylindrical, 3.5 in. ID, 7.5 in. OD, 6-in. heated length, high emissivity surface coating, custom fabricated to accommodate reactor ports.	Ash Equipment Co., Bensenville, IL
Temperature controllers (2)	Watlow series 910 microprocessor-based PID auto-tuning control: 6 A @ 115 V mech. relay output, model no. 910C-KDAO-0000	Ash Equipment Co., Bensenville, IL
Temperature control thermocouples	Type K, exposed junction, 1/16-in. sheath diam., cat. no. TJ36-CAIN-116E-12.	Omega Engineering, Inc., Stamford, CT
External insulation	T-12 calcium silicate pipe covering: 7.5 in. ID by 10.5 in. OD.	Industrial Insulation Corp., Appleton, WI

Table 5 (cont.). List of major components of drop furnace and aerosol collection system.

COMPONENT	DESCRIPTION	VENDOR
Mass flowmeter: Air/N_2 flow	Hastings Mass Flowmeter: model HS-10S flow transducer, model NALL flow monitor, 0-9.99 std. ft^3/min air capacity.	Teledyne-Hastings-Raydist, Hampton, VA
Mass flowmeter: vacuum flow	Hastings Mass Flowmeter: model STH-200K flow transducer, model PR-4 four channel flow monitor, 0-200 std. L/min air capacity.	Teledyne-Hastings-Raydist, Hampton, VA
Mass flowmeter: CO/CO_2 flow	Hastings Mass Flowmeter: model ST-10K flow transducer, model PR-4 four channel flow monitor, 0-10 std. L/min air capacity.	Teledyne-Hastings-Raydist, Hampton, VA
Aerosol collection system	Custom fabricated components: collection medium platform; exhaust flow director; vacuum flow director.	Georgia Tech Research Institute, Atlanta, GA
Carriage drive system	Pacific Science 1/4 hp 90 V dc motor; Fenner M-Trim PID digital speed control; Danfoss VariSpeed A2000 motor controller w/ reversing option: Red Lion proximity feedback sensor, model ARCJ; Grove Flexaline® gearbox, 7.5:1 ratio.	J.W. Vaughn Co., Inc., Columbia, SC
Carriage hardware	2 linear motion rail assemblies; 4 bearing blocks; Acme lead screw, 1/4-20-1st thread; Acme lead screw nut.	Techno, A DSG Co., New Hyde Park, NY
Vacuum source	PIAB™ M125D multi-ejector pneumatically-driven vacuum pump, cat. no. PFC-M125D-1.	Davis Airtech, Inc., Atlanta, GA
BGF filters	Whatman EPM-2000 Air Sampling Medium: borosilicate glass fiber filters, 8 by 10-in. sheets, Whatman cat. no. 1882 866.	Baxter Scientific Products Div., Stone Mountain, GA
Silver membranes	Silver membrane filters: 1.2 μm pore size, 293 mm circles, cat. no. 59258.	Poretics Corp., Livermore, CA
Video system	Panasonic WV-3260 color video camera; Panasonic AG-2400 portable VHS video cassette recorder.	Available at IPST

APPENDIX III. DROP PYROLYSIS DATA

There were over 700 individual drop pyrolysis videos recorded during the sodium mass loss determinations. Many of the char particles produced during the experiments were lost or damaged during extraction from the furnace. Approximately 100 of the videos were from exploratory experiments or used to determine minimum exposure time necessary to prevent drops from being extracted prior to the end of drying. A total of 409 char particles were collected for the mass loss determinations reported in the text (see Table 3).

Table 6 contains the complete list of drop data and calculations of total liquor solids mass and average stage times for each of the 66 mass loss determinations. The data are presented in chronological order. Each grouping of 4,5, or 20 drop exposures represents a single determination. Letters in the drop identification code (a, b, c, etc.) indicate the individual drop exposures which yielded intact char particles for a given determination. Variation of the mean is expressed as 95% confidence limits for each grouping with three or more observations. Drop dry solids mass ("Drop o.d. mass" in Table 6) was determined by the amount of liquor applied to an insertion wire (weighed by difference) and the appropriate liquor solids content. As explained in the Experimental chapter, liquor solids content was measured periodically during the experiments. "Loss on wire" was the final mass of an insertion wire (after char removal) minus its initial mass (before liquor application). The Total Mass Loss section of the Results and Discussion explains why this quantity was determined for the entire group of wires in later experiments (DPT5.5-DPT5.41 in Table 6).

Stage times and total exposure times, given in Table 6, were determined from

the elapsed time indicated on the video record of each individual drop exposure. The first appearance of the drop in the field of view was used to denote the start of drying. The first sign of swelling indicated the onset of devolatilization. The maximum swollen volume of the char particle was taken as the end of devolatilization. Complete disappearance of the particle from the field of view denoted the end of exposure. Note that for many of the drops extracted at minimum exposure time the drying or devolatilization stages were not complete.

Table 6. Drop mass and stage time data for individual mass loss determinations.

Furnace conditions	Drop no.		Mass drop, mg	Drop o.d. mass, mg	Loss on wire, mg	Drying time, s	Devol. time, s	Exposure time, s
600 C	DPT2.6	a	4.4	3.2	1.9		2.0	
0.61 m/s	DPT2.6	b	8.9	6.4	-1.5	3.1	4.5	11.4
5% CO	DPT2.6	c	3.5	2.5	0.8	2.6	2.3	10.4
	DPT2.6	d	4.0	2.9	1.8	2.8	2.8	12.2
	DPT2.6	f	8.4	6.0	0.6		4.8	12.4
	sum:		29.2	21.0	3.6			
	av.:		5.8	4.2	0.7	2.8	3.3	11.6
	95% c.l.:		3.2	2.3	1.7	0.6	1.6	1.4
600 C	DPT2.7	a	6.5	4.7	1.4	3.0	3.9	29.7
0.61 m/s	DPT2.7	b	6.7	4.8	0.3	3.1	3.2	29.7
5% CO	DPT2.7	c	7.4	5.3	1.2	3.4	3.0	30.1
	DPT2.7	d	13.4	9.6	1.8	4.4	3.7	29.9
	DPT2.7	e	10.9	7.8	-1.6	3.8	3.2	30.0
	sum:		44.9	32.3	3.1			
	av.:		9.0	6.5	0.6	3.5	3.4	29.9
	95% c.l.:		3.8	2.7	1.7	0.7	0.5	0.2
600 C	DPT2.8	a	5.8	4.2				3.5
0.61 m/s	DPT2.8	b	3.1	2.2		2.1		3.3
5% CO	DPT2.8	c	5.8	4.2				3.2
	DPT2.8	d	5.0	3.6		3.0		4.1
	DPT2.8	e	4.4	3.2		2.7		3.7
	sum:		24.1	17.4	-			
	av.:		4.8	3.5	-	2.6	-	3.6
	95% c.l.:		1.4	1.0	-	1.1	-	0.4
900 C	DPT2.10	a	4.4	3.2	0.8	0.6	1.3	9.6
0.61 m/s	DPT2.10	c	2.2	1.6	1.1	0.4	1.1	9.3
5% CO	DPT2.10	e	4.6	3.3	-1.0	0.9	1.5	9.7
	DPT2.10	f	4.1	3.0	1.5	0.9	1.2	9.9
	DPT2.10	k	2.4	1.7	1.1	0.6	1.2	10.6
	sum:		17.7	12.9	3.5			
	av.:		3.5	2.6	0.7	0.7	1.3	9.8
	95% c.l.:		1.4	1.0	1.2	0.3	0.2	0.6

Table 6 (cont.). Drop mass and stage time data for individual mass loss determinations.

Furnace conditions	Drop no.		Mass drop, mg	Drop o.d. mass, mg	Loss on wire, mg	Drying time, s	Devol. time, s	Exposure time, s
900 C	DPT2.11	f	2.1	1.5	-1.2	0.6	1.1	30.0
0.61 m/s	DPT2.11	h	2.1	1.5	1.5	0.4	1.3	30.3
5% CO	DPT2.11	i	2.2	1.6	-1.0	0.6	1.5	29.8
	DPT2.11	l	2.6	1.9	0.0	1.1	0.9	30.1
	DPT2.11	q	7.0	5.1	-1.1	0.6	1.3	30.5
	sum:		16.0	11.8	-1.8			
	av.:		3.2	2.4	-0.4	0.7	1.2	30.1
	95% c.l.:		2.7	1.9	1.4	0.3	0.3	0.3
900 C	DPT2.12	a	4.9	3.6	-0.9	1.2	1.3	3.0
0.61 m/s	DPT2.12	b	4.5	3.3	-0.5	1.2	1.3	3.4
5% CO	DPT2.12	c	3.9	2.9	0.3	0.5	1.2	3.5
	DPT2.12	d	2.9	2.1	-1.2	0.7	1.0	3.3
	DPT2.12	f	2.6	1.9	0.1	0.6	1.0	2.9
	sum:		18.8	13.8	-2.2			
	av.:		3.8	2.8	-0.4	0.8	1.2	3.2
	95% c.l.:		1.2	0.9	0.8	0.4	0.2	0.3
600 C	DPT2.13	a	5.3	3.9	0.9	3.2	3.3	9.7
0.61 m/s	DPT2.13	b	4.2	3.1	2.5	3.5	2.4	9.4
5% CO	DPT2.13	c	3.3	2.5	0.7	3.3	1.5	9.6
	DPT2.13	d	3.6	2.7	1.9	3.6	2.1	10.0
	DPT2.13	e	2.5	1.9	0.3	3.0	2.1	9.9
	sum:		18.9	14.0	6.3			
	av.:		3.8	2.8	1.3	3.3	2.3	9.7
	95% c.l.:		1.3	1.0	1.1	0.3	0.8	0.3
600 C	DPT2.14	a	4.5	3.3	-1.9	3.4	3.1	30.0
0.61 m/s	DPT2.14	b	1.9	1.4	-1.1	1.8	1.7	29.6
5% CO	DPT2.14	c	4.4	3.3	-0.1	3.0	2.2	30.0
	DPT2.14	d	3.1	2.3	-1.6	2.7	2.4	30.0
	DPT2.14	e	2.9	2.2	0.7	3.0	1.6	29.9
	sum:		16.8	12.5	-4.0			
	av.:		3.4	2.5	-0.8	2.8	2.2	29.9
	95% c.l.:		1.4	1.0	1.3	0.7	0.8	0.2

Table 6 (cont.). Drop mass and stage time data for individual mass loss determinations.

Furnace conditions	Drop no.		Mass drop, mg	Drop o.d. mass, mg	Loss on wire, mg	Drying time, s	Devol. time, s	Exposure time, s
600 C	DPT2.15	a	3.6	2.7		2.9		3.3
0.61 m/s	DPT2.15	b	3.6	2.7		2.8		3.0
5% CO	DPT2.15	c	2.7	2.0		2.7		3.2
	DPT2.15	d	7.0	5.2				2.9
	DPT2.15	e	3.2	2.4				3.4
	sum:		20.1	14.9	-			
	av.:		4.0	3.0	-	2.8	-	3.2
	95% c.l.:		2.1	1.6	-	0.2	-	0.3
900 C	DPT2.19	a	2.6	2.0	-0.9	0.6	0.8	10.2
0.61 m/s	DPT2.19	b	5.4	4.1	1.6	0.8	1.3	10.2
5% CO	DPT2.19	c	8.9	6.7	-0.1	0.9	1.7	10.3
	DPT2.19	d	2.8	2.1	0.4	0.6	1.1	10.1
	DPT2.19	e	5.6	4.2	-0.1	0.9	0.8	10.5
	sum:		25.3	19.0	0.9			
	av.:		5.1	3.8	0.2	0.8	1.1	10.3
	95% c.l.:		3.2	2.4	1.1	0.2	0.5	0.2
900 C	DPT2.20	a	6.1	4.6	1.3	0.8	1.8	3.1
0.61 m/s	DPT2.20	b	6.7	5.0	-1.8	0.8	1.4	3.4
5% CO	DPT2.20	c	4.9	3.7	1.8	0.9	1.4	3.5
	DPT2.20	d	2.0	1.5	-1.5	0.5	0.9	3.0
	DPT2.20	e	3.1	2.3	2.2	0.7	1.2	3.1
	sum:		22.8	17.1	2.0			
	av.:		4.6	3.4	0.4	0.7	1.3	3.2
	95% c.l.:		2.5	1.8	2.4	0.2	0.4	0.3
900 C	DPT2.23	a	3.8	2.9	-0.5	1.0	1.2	30.2
0.61 m/s	DPT2.23	h	1.6	1.2	-0.8	0.6	0.7	29.8
5% CO	DPT2.23	j	2.7	2.0	-0.7	0.9	0.9	30.4
	DPT2.23	k	1.9	1.4	-0.5	0.9	0.8	30.4
	DPT2.23	l	3.2	2.4	-0.4		1.0	
	sum:		13.2	9.9	-2.9			
	av.:		2.6	2.0	-0.6	0.9	0.9	30.2
	95% c.l.:		1.1	0.8	0.2	0.3	0.2	0.5

Table 6 (cont.). Drop mass and stage time data for individual mass loss determinations.

Furnace conditions	Drop no.		Mass drop, mg	Drop o.d. mass, mg	Loss on wire, mg	Drying time, s	Devol. time, s	Exposure time, s
500 C	DPT3.3	c	4.3	3.1	0.2	5.8	3.2	15.5
0.61 m/s	DPT3.3	e	3.8	2.7	-0.2	5.8	2.1	15.0
5% O_2	DPT3.3	g	5.0	3.6	1.1	5.1	2.3	15.7
	DPT3.3	i	3.9	2.8	-0.8	5.0	2.8	15.5
	DPT3.3	j	1.6	1.2	-1.8	4.5	1.6	14.9
	sum:		18.6	13.4	-1.5			
	av.:		3.7	2.7	-0.3	5.2	2.4	15.3
	95% c.l.:		1.6	1.1	1.3	0.7	0.8	0.4
500 C	DPT3.4	a	8.0	5.7				7.2
0.61 m/s	DPT3.4	b	8.8	6.3				6.9
5% O_2	DPT3.4	c	6.4	4.6				6.9
	DPT3.4	d	10.0	7.1				6.9
	DPT3.4	e	4.2	3.0				6.9
	sum:		37.4	26.7	-			
	av.:		7.5	5.3	-	-	-	7.0
	95% c.l.:		2.8	2.0	-	-	-	0.2
500 C	DPT3.5	a	2.8	2.0	1.4	5.2	2.7	30.0
0.61 m/s	DPT3.5	d	4.5	3.2	0.9	6.2	2.6	29.7
5% O_2	DPT3.5	j	3.8	2.7	0.8	5.8	3.2	29.9
	DPT3.5	k	3.5	2.5	-1.3	6.0	2.6	30.4
	DPT3.5	l	7.2	5.1	-0.1	7.3	4.0	30.1
	sum:		21.8	15.5	1.7			
	av.:		4.4	3.1	0.3	6.1	3.0	30.0
	95% c.l.:		2.1	1.5	1.3	1.0	0.7	0.3
500 C	DPT3.6	a	4.7	3.4	-1.1	6.2	2.1	14.7
0.61 m/s	DPT3.6	d	4.2	3.0	-0.3	5.7	2.6	15.2
5% O_2	DPT3.6	e	4.7	3.4	-1.0	6.3	2.4	14.9
	DPT3.6	g	7.5	5.3	-1.1	7.0	4.1	14.7
	DPT3.6	i	4.4	3.1	0.3	5.7	2.9	15.8
	sum:		25.5	18.2	-3.2			
	av.:		5.1	3.6	-0.6	6.2	2.8	15.1
	95% c.l.:		1.7	1.2	0.8	0.7	1.0	0.6

Table 6 (cont.). Drop mass and stage time data for individual mass loss determinations.

Furnace conditions	Drop no.		Mass drop, mg	Drop o.d. mass, mg	Loss on wire, mg	Drying time, s	Devol. time, s	Exposure time, s
500 C	DPT3.7	a	3.9	2.8		6.0		7.2
0.61 m/s	DPT3.7	b	3.8	2.7		5.9		7.2
5% O_2	DPT3.7	c	4.1	2.9				6.7
	DPT3.7	d	6.7	4.8				7.0
	DPT3.7	e	4.4	3.1				6.9
	sum:		22.9	16.3	-			
	av.:		4.6	3.3	-	6.0	-	7.0
	95% c.l.:		1.5	1.1	-	0.6	-	0.3
500 C	DPT3.9	b	3.5	2.5	-1.0	5.7	2.7	30.1
0.61 m/s	DPT3.9	d	4.8	3.4	0.1	5.7	3.3	30.3
5% O_2	DPT3.9	f	4.7	3.4	-0.4	6.4	2.6	30.1
	DPT3.9	g	5.2	3.7	-0.6	4.4	4.5	30.3
	DPT3.9	j	2.4	1.7	0.4	5.7	2.1	29.9
	sum:		20.6	14.8	-1.5			
	av.:		4.1	3.0	-0.3	5.6	3.0	30.1
	95% c.l.:		1.4	1.0	0.7	0.9	1.1	0.2
900 C	DPT3.11	a	4.6	3.3	0.1	1.0	0.7	20.2
0.61 m/s	DPT3.11	b	6.9	5.0	0.7	1.0	1.5	20.1
5% CO	DPT3.11	c	4.9	3.5	-0.8	1.2	0.8	20.2
	DPT3.11	d	5.1	3.7	0.5	1.1	0.7	20.4
	DPT3.11	e	3.9	2.8	-0.6		1.4	20.2
	sum:		25.4	18.2	-0.1			
	av.:		5.1	3.6	-0.0	1.1	1.0	20.2
	95% c.l.:		1.4	1.0	0.8	0.2	0.5	0.1
900 C	DPT3.12	d	4.6	3.3	-0.2	1.4	1.6	20.1
0.61 m/s	DPT3.12	e	5.8	4.2	-1.2	1.3	1.3	20.6
5% CO	DPT3.12	f	5.0	3.6	-2.2	1.0	1.4	20.4
	DPT3.12	g	4.1	3.0	-1.4	1.2	0.8	20.4
	DPT3.12	h	5.9	4.3	1.4	0.7	1.8	19.8
	sum:		25.4	18.3	-3.6			
	av.:		5.1	3.7	-0.7	1.1	1.4	20.3
	95% c.l.:		1.0	0.7	1.7	0.3	0.5	0.4

Table 6 (cont.). Drop mass and stage time data for individual mass loss determinations.

Furnace conditions	Drop no.		Mass drop, mg	Drop o.d. mass, mg	Loss on wire, mg	Drying time, s	Devol. time, s	Exposure time, s
900 C	DPT3.13	a	6.2	4.5	0.2	1.2	1.2	15.2
0.61 m/s	DPT3.13	b	5.9	4.3	-1.2	1.1	1.3	14.9
5% CO	DPT3.13	c	9.1	6.6	1.7	1.5	0.9	14.7
	DPT3.13	d	5.1	3.7	-1.1	1.3	1.3	15.3
	DPT3.13	e	4.7	3.4	1.4	1.2	1.4	15.4
	sum:		31.0	22.4	1.0			
	av.:		6.2	4.5	0.2	1.3	1.2	15.1
	95% c.l.:		2.1	1.6	1.7	0.2	0.2	0.4
900 C	DPT3.14	b	4.2	3.0	1.6	1.1	0.8	15.2
0.61 m/s	DPT3.14	c	5.2	3.8	-2.0	1.5	1.2	15.1
5% CO	DPT3.14	d	8.1	5.8	-0.2	1.3	1.4	15.3
	DPT3.14	e	4.7	3.4	-1.5	1.1	0.9	15.0
	DPT3.14	g	3.2	2.3	-1.7	1.1	1.1	15.3
	sum:		25.4	18.3	-3.8			
	av.:		5.1	3.7	-0.8	1.2	1.1	15.2
	95% c.l.:		2.3	1.7	1.8	0.2	0.3	0.2
600 C	DPT4.14	a	6.0	4.3		4.2	3.1	30.1
0.61 m/s	DPT4.14	b	7.0	5.0		4.6	2.8	30.2
5% CO	DPT4.14	c	7.0	5.0		4.5	3.4	30.3
	DPT4.14	d	5.3	3.8		4.8	2.2	30.3
	DPT4.14	g	5.6	4.0		4.3	2.7	30.3
	DPT4.14	h	5.6	4.0		4.5	2.1	30.2
	DPT4.14	i	7.0	5.0		4.5	3.7	30.1
	DPT4.14	j	6.3	4.5		5.0	2.7	29.8
	DPT4.14	k	6.9	4.9		4.2	3.1	30.3
	DPT4.14	l	5.5	3.9			2.8	
	DPT4.14	m	5.2	3.7		3.1	3.5	30.3
	DPT4.14	n	6.9	4.9		5.1	3.5	30.0
	DPT4.14	o	5.3	3.8		4.1	3.3	30.3
	DPT4.14	r	5.6	4.0		4.1	2.6	30.5
	DPT4.14	t	5.4	3.9		4.4	3.1	30.1
	DPT4.14	u	6.6	4.7		4.3	3.3	30.1
	DPT4.14	v	6.2	4.4		4.1	3.1	29.9
	DPT4.14	w	6.4	4.6		4.7	2.9	30.0
	DPT4.14	x	6.3	4.5		4.9	2.6	30.1
	DPT4.14	z	6.6	4.7		4.9	3.0	30.1
	sum:		122.7	87.9	-			
	av.:		6.1	4.4	-	4.4	3.0	30.2
	95% c.l.:		0.3	0.2	-	0.2	0.2	0.1

Table 6 (cont.). Drop mass and stage time data for individual mass loss determinations.

Furnace conditions	Drop no.	Mass drop, mg	Drop o.d. mass, mg	Loss on wire, mg	Drying time, s	Devol. time, s	Exposure time, s
600 C	DPT4.15 b	6.0	4.3		4.5	3.1	10.3
0.61 m/s	DPT4.15 d	5.5	3.9		4.4	2.6	10.4
5% CO	DPT4.15 e	5.0	3.6		4.4	2.6	10.4
	DPT4.15 h	6.0	4.3		4.6	3.0	10.1
	DPT4.15 i	5.5	3.9		4.4	3.0	10.2
	DPT4.15 j	5.5	3.9		3.7	3.6	10.0
	DPT4.15 k	5.9	4.2		4.7	2.8	10.1
	DPT4.15 m	5.1	3.7		4.6	2.6	10.2
	DPT4.15 n	5.9	4.2		4.5	3.0	10.2
	DPT4.15 o	5.9	4.2				10.7
	DPT4.15 q	6.8	4.9			3.7	
	DPT4.15 r	5.6	4.0		4.0	3.2	9.9
	DPT4.15 v	7.0	5.0		5.2	3.4	10.4
	DPT4.15 w	5.9	4.2		4.5	3.0	10.5
	DPT4.15 y	6.8	4.9		4.8	2.7	11.1
	DPT4.15 aa	5.7	4.1		4.4	3.3	10.1
	DPT4.15 bb	5.0	3.6			2.0	
	DPT4.15 cc	6.3	4.5		4.2	3.5	10.0
	DPT4.15 dd	5.2	3.7		4.4	2.8	10.5
	DPT4.15 ee	6.1	4.4		4.7	2.1	10.4
	sum:	116.7	83.6	-			
	av.:	5.8	4.2	-	4.5	2.9	10.3
	95% c.l.:	0.3	0.2	-	0.2	0.2	0.1
600 C	DPT4.16 b	5.2	3.7				3.3
0.61 m/s	DPT4.16 c	5.7	4.1				3.2
5% CO	DPT4.16 d	6.0	4.3				3.2
	DPT4.16 e	5.8	4.2				
	DPT4.16 f	6.2	4.4				3.3
	DPT4.16 g	5.5	3.9				3.6
	DPT4.16 h	5.2	3.7				3.2
	DPT4.16 i	5.8	4.2				
	DPT4.16 j	6.4	4.6				3.2
	DPT4.16 k	6.5	4.7				3.6
	DPT4.16 l	5.9	4.2				3.1
	DPT4.16 m	6.4	4.6				
	DPT4.16 o	4.1	2.9				3.5
	DPT4.16 p	5.5	3.9				3.3
	DPT4.16 q	5.1	3.7				3.5
	DPT4.16 r	5.4	3.9				3.5
	DPT4.16 s	5.6	4.0				3.2
	DPT4.16 t	6.8	4.9				3.2
	DPT4.16 u	4.8	3.4				3.7
	DPT4.16 v	5.4	3.9				3.4
	sum:	113.3	81.1	-			
	av.:	5.7	4.1	-	-	-	3.4
	95% c.l.:	0.3	0.2	-	-	-	0.1

Table 6 (cont.). Drop mass and stage time data for individual mass loss determinations.

Furnace conditions	Drop no.	Mass drop, mg	Drop o.d. mass, mg	Loss on wire, mg	Drying time, s	Devol. time, s	Exposure time, s
600 C	DPT4.17 a	5.2	3.7		3.9	2.6	29.9
0.61 m/s	DPT4.17 b	5.4	3.9		3.9	2.2	30.1
5% CO	DPT4.17 c	5.0	3.6		3.3	2.1	30.3
	DPT4.17 d	5.0	3.6				30.0
	DPT4.17 f	6.3	4.5		4.0	2.1	30.1
	DPT4.17 g	5.0	3.6		3.6	2.0	30.0
	DPT4.17 h	5.0	3.6		3.8	1.8	30.1
	DPT4.17 j	5.9	4.2		3.7	2.3	30.1
	DPT4.17 k	6.6	4.7		4.4	1.9	30.2
	DPT4.17 l	5.3	3.8		3.7	2.6	30.0
	DPT4.17 m	6.6	4.7		3.1	3.0	29.9
	DPT4.17 n	6.0	4.3		4.0	3.2	30.0
	DPT4.17 o	5.3	3.8		3.4	2.7	30.1
	DPT4.17 p	6.0	4.3		3.8	2.0	29.9
	DPT4.17 q	5.3	3.8		3.2	1.7	30.1
	DPT4.17 r	5.1	3.7		3.4	2.0	30.1
	DPT4.17 s	6.6	4.7		3.4	3.2	30.0
	DPT4.17 t	5.9	4.2		3.5	2.3	30.0
	DPT4.17 u	5.9	4.2		3.8	2.4	29.8
	DPT4.17 w	5.8	4.2		3.7	2.3	30.0
	sum:	113.2	81.4	-			
	av.:	5.7	4.1	-	3.7	2.3	30.0
	95% c.l.:	0.3	0.2	-	0.2	0.2	0.1
600 C	DPT4.18 b	5.3	3.8		3.4	2.2	10.1
0.61 m/s	DPT4.18 c	5.1	3.7		3.3	3.2	10.0
5% CO	DPT4.18 d	6.0	4.3		3.6	1.6	9.8
	DPT4.18 e	6.9	5.0		3.4	3.4	10.2
	DPT4.18 f	5.7	4.1		3.2	2.4	10.1
	DPT4.18 h	6.6	4.7		3.1	2.4	10.0
	DPT4.18 i	5.0	3.6		3.3	2.9	10.2
	DPT4.18 k	5.4	3.9		3.0	2.8	10.3
	DPT4.18 l	6.3	4.5		3.6	1.8	10.2
	DPT4.18 m	5.7	4.1		3.4	2.1	10.3
	DPT4.18 n	6.0	4.3		3.9	2.2	10.0
	DPT4.18 p	5.3	3.8		3.7	2.5	10.0
	DPT4.18 q	5.3	3.8		3.5	1.7	10.3
	DPT4.18 r	5.4	3.9		3.4	2.9	10.1
	DPT4.18 s	5.0	3.6		3.0	3.0	9.9
	DPT4.18 t	6.0	4.3		4.0	1.8	10.2
	DPT4.18 u	5.6	4.0			1.6	
	DPT4.18 v	6.5	4.7		3.7	3.4	10.4
	DPT4.18 w	6.1	4.4		3.4	3.2	10.0
	DPT4.18 x	5.4	3.9		3.8	2.4	10.1
	sum:	114.6	82.4	-			
	av.:	5.7	4.1	-	3.5	2.5	10.1
	95% c.l.:	0.3	0.2	-	0.1	0.3	0.1

Table 6 (cont.). Drop mass and stage time data for individual mass loss determinations.

Furnace conditions	Drop no.	Mass drop, mg	Drop o.d. mass, mg	Loss on wire, mg	Drying time, s	Devol. time, s	Exposure time, s
600 C	DPT4.19 a	7.0	5.0				3.0
0.61 m/s	DPT4.19 b	5.0	3.6				3.1
5% CO	DPT4.19 c	5.8	4.2				3.0
	DPT4.19 d	5.9	4.2				3.0
	DPT4.19 e	5.0	3.6				3.3
	DPT4.19 f	6.5	4.7				3.0
	DPT4.19 g	5.4	3.9				2.9
	DPT4.19 h	6.8	4.9				3.2
	DPT4.19 i	6.2	4.5				3.2
	DPT4.19 j	5.1	3.7				2.8
	DPT4.19 k	6.8	4.9				3.1
	DPT4.19 l	6.2	4.5				3.1
	DPT4.19 m	5.7	4.1				2.9
	DPT4.19 n	5.8	4.2				3.0
	DPT4.19 o	6.7	4.8				2.9
	DPT4.19 p	6.8	4.9				2.9
	DPT4.19 q	6.0	4.3				3.3
	DPT4.19 r	7.0	5.0				3.2
	DPT4.19 s	6.8	4.9				2.9
	DPT4.19 t	5.8	4.2				3.0
	sum:	122.3	87.9	-			
	av.:	6.1	4.4	-	-	-	3.0
	95% c.l.:	0.3	0.2	-	-	-	0.1
600 C	DPT4.21 b	6.3	4.6	1.4	3.3	2.2	10.4
0.61 m/s	DPT4.21 c	6.0	4.4	-0.1	3.3	2.7	10.0
5% CO	DPT4.21 d	6.9	5.0	1.6	3.1	3.2	10.1
	DPT4.21 e	5.5	4.0	0.6	3.2	2.3	10.1
	DPT4.21 g	6.6	4.8	1.4	4.0	2.2	10.1
	sum:	31.3	22.7	4.9			
	av.:	6.3	4.5	1.0	3.4	2.5	10.1
	95% c.l.:	0.7	0.5	0.9	0.4	0.5	0.2
600 C	DPT4.22 a	4.3	3.1	-1.1	3.1	1.6	30.3
0.61 m/s	DPT4.22 b	6.7	4.9	0.7	3.9	2.5	30.0
5% CO	DPT4.22 c	6.6	4.8	1.2	3.9	2.4	29.9
	DPT4.22 d	6.0	4.4	1.6	3.1	2.3	29.9
	DPT4.22 e	6.4	4.6	1.0	3.4	2.8	29.9
	sum:	30.0	21.8	3.4			
	av.:	6.0	4.4	0.7	3.5	2.3	30.0
	95% c.l.:	1.2	0.9	1.3	0.5	0.6	0.2

Table 6 (cont.). Drop mass and stage time data for individual mass loss determinations.

Furnace conditions	Drop no.		Mass drop, mg	Drop o.d. mass, mg	Loss on wire, mg	Drying time, s	Devol. time, s	Exposure time, s
600 C	DPT4.23	a	5.4	4.0		3.1	2.0	5.5
0.61 m/s	DPT4.23	b	6.8	5.0		3.6		5.4
5% CO	DPT4.23	f	5.3	3.9		3.1		5.3
	DPT4.23	g	3.9	2.9		2.9		5.0
	DPT4.23	h	6.9	5.1		3.4	2.5	6.2
	sum:		28.3	20.7	-			
	av.:		5.7	4.1	-	3.2	2.3	5.5
	95% c.l.:		1.5	1.1	-	0.3	3.2	0.6
600 C	DPT4.24	b	5.9	4.3	0.4	3.3	2.7	10.3
0.61 m/s	DPT4.24	d	6.0	4.4	2.5	3.7	2.1	10.1
5% CO	DPT4.24	e	6.5	4.8	1.1	4.0	2.0	10.3
	DPT4.24	f	6.2	4.5	0.3	3.7	2.4	10.3
	DPT4.24	g	6.5	4.8	-1.0	3.0	2.1	10.4
	sum:		31.1	22.8	3.3			
	av.:		6.2	4.6	0.7	3.5	2.3	10.3
	95% c.l.:		0.3	0.3	1.6	0.5	0.4	0.1
600 C	DPT4.25	a	5.7	4.2	-0.9	3.2	2.1	30.1
0.61 m/s	DPT4.25	b	5.4	4.0	0.7	2.8	2.5	29.9
5% CO	DPT4.25	c	5.8	4.3	-1.6	3.6	2.4	30.1
	DPT4.25	d	5.3	3.9	0.7	3.0	2.3	29.9
	DPT4.25	e	6.4	4.7	1.3	4.1	1.4	30.2
	sum:		28.6	21.0	0.2			
	av.:		5.7	4.2	0.0	3.3	2.1	30.0
	95% c.l.:		0.5	0.4	1.5	0.6	0.5	0.2
600 C	DPT4.26	d	5.9	4.3		3.7		5.3
0.61 m/s	DPT4.26	e	5.6	4.1		3.4		5.2
5% CO	DPT4.26	f	5.1	3.7		3.5		5.1
	DPT4.26	g	6.7	4.9		3.2		5.0
	DPT4.26	i	7.0	5.1		3.5		5.2
	sum:		30.3	22.2	-			
	av.:		6.1	4.4	-	3.5	-	5.2
	95% c.l.:		1.0	0.7	-	0.2	-	0.1

Table 6 (cont.). Drop mass and stage time data for individual mass loss determinations.

Furnace conditions	Drop no.		Mass drop, mg	Drop o.d. mass, mg	Loss on wire, mg	Drying time, s	Devol. time, s	Exposure time, s
750 C	DPT5.7	a	4.0	2.8		1.6	1.7	10.0
0.61 m/s	DPT5.7	b	5.2	3.7		1.8	1.8	10.1
5% CO	DPT5.7	c	5.0	3.5		1.9	1.3	9.9
	DPT5.7	d	5.0	3.5		1.7	1.1	10.2
	DPT5.7	e	4.7	3.3		1.9	1.5	10.3
	sum:		23.9	16.8	0.4			
	av.:		4.8	3.4	-	1.8	1.5	10.1
	95% c.l.:		0.6	0.4	-	0.2	0.4	0.2
750 C	DPT5.8	a	5.2	3.7		2.2	0.8	29.9
0.61 m/s	DPT5.8	c	4.3	3.0		1.6	1.6	30.0
5% CO	DPT5.8	d	4.3	3.0		1.9	1.1	29.9
	DPT5.8	e	4.9	3.4		1.9	1.0	30.1
	sum:		18.7	13.1	0.3			
	av.:		4.7	3.3	-	1.9	1.1	30.0
	95% c.l.:		0.7	0.5	-	0.4	0.5	0.2
750 C	DPT5.9	a	4.7	3.3		1.7	0.9	3.1
0.61 m/s	DPT5.9	b	4.9	3.4		2.0		3.0
5% CO	DPT5.9	c	4.2	2.9		1.9	1.0	3.1
	DPT5.9	d	4.5	3.2		1.7		3.0
	DPT5.9	e	4.8	3.4		2.0		3.0
	sum:		23.1	16.2	0.1			
	av.:		4.6	3.2	-	1.9	1.0	3.0
	95% c.l.:		0.3	0.2	-	0.2	0.6	0.1
750 C	DPT5.10	a	5.1	3.6		2.2	1.7	9.8
0.61 m/s	DPT5.10	b	5.0	3.5		2.0	1.1	10.1
5% CO	DPT5.10	c	4.7	3.3		1.9	1.4	9.9
	DPT5.10	d	5.4	3.8		2.0	1.4	9.9
	DPT5.10	e	4.3	3.0		1.5	1.3	9.8
	sum:		24.5	17.2	0.3			
	av.:		4.9	3.4	-	1.9	1.4	9.9
	95% c.l.:		0.5	0.4	-	0.3	0.3	0.2

Table 6 (cont.). Drop mass and stage time data for individual mass loss determinations.

Furnace conditions	Drop no.		Mass drop, mg	Drop o.d. mass, mg	Loss on wire, mg	Drying time, s	Devol. time, s.	Exposure time, s
750 C	DPT5.11	a	5.4	3.8		2.1	1.0	30.1
0.61 m/s	DPT5.11	b	5.5	3.9		1.9	1.2	30.0
5% CO	DPT5.11	c	5.2	3.7		2.0	1.7	30.0
	DPT5.11	d	4.4	3.1		1.7	1.0	29.9
	DPT5.11	e	5.1	3.6		2.2	1.0	30.1
	sum:		25.6	18.1	0.1			
	av.:		5.1	3.6	-	2.0	1.2	30.0
	95% c.l.:		0.5	0.4	-	0.2	0.4	0.1
750 C	DPT5.12	a	5.3	3.8		2.2		3.1
0.61 m/s	DPT5.12	b	4.7	3.3		2.1	0.8	3.4
5% CO	DPT5.12	c	4.3	3.0		1.8	1.2	3.1
	DPT5.12	d	5.3	3.8		2.1		3.0
	DPT5.12	e	5.1	3.6		2.2		3.0
	sum:		24.7	17.5	0.4			
	av.:		4.9	3.5	-	2.1	1.0	3.1
	95% c.l.:		0.5	0.4	-	0.2	2.5	0.2
750 C	DPT5.13	a	5.3	3.8		1.7	1.5	10.0
0.61 m/s	DPT5.13	b	4.8	3.4		2.0	1.5	10.0
5% CO	DPT5.13	c	4.7	3.3		1.9	1.0	10.2
	DPT5.13	d	4.8	3.4		2.0	1.3	10.2
	DPT5.13	e	4.8	3.4		2.0	1.3	10.2
	sum:		24.4	17.4	-0.2			
	av.:		4.9	3.5	-	1.9	1.3	10.1
	95% c.l.:		0.3	0.2	-	0.2	0.3	0.1
750 C	DPT5.14	a	4.5	3.2		1.9	1.5	30.0
0.61 m/s	DPT5.14	b	4.6	3.3		2.0	1.2	29.9
5% CO	DPT5.14	c	5.1	3.6		2.0	1.4	20.0
	DPT5.14	d	4.6	3.3		2.0	1.0	29.8
	DPT5.14	e	5.2	3.7		2.1	1.4	30.0
	sum:		24.0	17.1	0.5			
	av.:		4.8	3.4	-	2.0	1.3	27.9
	95% c.l.:		0.4	0.3	-	0.1	0.2	5.5

Table 6 (cont.). Drop mass and stage time data for individual mass loss determinations.

Furnace conditions	Drop no.		Mass drop, mg	Drop o.d. mass, mg	Loss on wire, mg	Drying time, s	Devol. time, s	Exposure time, s
750 C	DPT5.15	a	5.4	3.8		1.9		3.3
0.61 m/s	DPT5.15	b	4.8	3.4		2.1	1.1	3.5
5% CO	DPT5.15	c	5.3	3.8		2.1		2.9
	DPT5.15	d	4.6	3.3		2.0	1.0	3.2
	DPT5.15	e	5.2	3.7		2.2		3.0
	sum:		25.3	18.0	-0.5			
	av.:		5.1	3.6	-	2.1	1.1	3.2
	95% c.l.:		0.4	0.3	-	0.1	0.6	0.3
750 C	DPT5.16	a	4.7	3.3		1.7	1.3	9.9
1.83 m/s	DPT5.16	b	5.0	3.6		2.0	1.3	10.0
5% CO	DPT5.16	d	5.2	3.7		1.9	1.2	10.1
	DPT5.16	e	4.9	3.5		1.9	1.3	10.1
	sum:		19.8	14.1	0.0			
	av.:		5.0	3.5	-	1.9	1.3	10.0
	95% c.l.:		0.3	0.2	-	0.2	0.1	0.2
750 C	DPT5.17	a	5.4	3.8		1.9	1.1	30.1
1.83 m/s	DPT5.17	b	4.8	3.4		1.9	0.9	30.0
5% CO	DPT5.17	c	4.9	3.5		1.8	1.0	30.2
	DPT5.17	d	4.7	3.3		1.8	1.2	29.8
	DPT5.17	e	5.2	3.7		1.9	1.2	30.0
	sum:		25.0	17.8	0.0			
	av.:		5.0	3.6	-	1.9	1.1	30.0
	95% c.l.:		0.4	0.3	-	0.1	0.2	0.2
750 C	DPT5.19	b	5.2	3.7		2.0		3.2
1.83 m/s	DPT5.19	c	5.1	3.6		2.0		3.1
5% CO	DPT5.19	d	5.1	3.6		1.9		3.1
	DPT5.19	e	5.0	3.6		2.1		3.1
	sum:		20.4	14.5	-0.2			
	av.:		5.1	3.6	-	2.0	-	3.1
	95% c.l.:		0.1	0.1	-	0.1	-	0.1

Table 6 (cont.). Drop mass and stage time data for individual mass loss determinations.

Furnace conditions	Drop no.		Mass drop, mg	Drop o.d. mass, mg	Loss on wire, mg	Drying time, s	Devol. time, s	Exposure time, s
750 C	DPT5.20	a	5.1	3.6		1.9	1.7	10.2
1.83 m/s	DPT5.20	b	5.2	3.6		2.0	1.2	9.9
5% CO	DPT5.20	c	4.5	3.2		1.8	1.8	10.0
	DPT5.20	d	5.5	3.9		2.4	1.3	10.2
	DPT5.20	e	4.8	3.4		2.1	1.2	10.2
	sum:		25.1	17.6	0.8			
	av.:		5.0	3.5	-	2.0	1.4	10.1
	95% c.l.:		0.5	0.3	-	0.3	0.4	0.2
750 C	DPT5.21	a	5.4	3.8		2.3	1.7	30.2
1.83 m/s	DPT5.21	b	4.6	3.2		1.8	1.5	30.0
5% CO	DPT5.21	c	4.9	3.4		1.4	2.0	29.6
	DPT5.21	d	5.2	3.6		2.0	1.6	30.4
	DPT5.21	e	4.8	3.4		1.7	1.7	30.0
	sum:		24.9	17.5	-0.2			
	av.:		5.0	3.5	-	1.8	1.7	30.0
	95% c.l.:		0.4	0.3	-	0.4	0.2	0.4
750 C	DPT5.22	a	4.7	3.3		1.9		2.9
1.83 m/s	DPT5.22	b	4.8	3.4		2.0		3.2
5% CO	DPT5.22	c	5.0	3.5		1.7		3.1
	DPT5.22	d	5.6	3.9		1.9		2.9
	DPT5.22	e	5.1	3.6		1.8		3.2
	sum:		25.2	17.7	0.1			
	av.:		5.0	3.5	-	1.9	-	3.1
	95% c.l.:		0.4	0.3	-	0.1	-	0.2
750 C	DPT5.23	a	4.6	3.2		1.9	1.5	10.2
1.83 m/s	DPT5.23	b	5.3	3.7		2.0	0.9	10.1
5% CO	DPT5.23	c	5.3	3.7		1.9	1.5	10.0
	DPT5.23	d	5.1	3.6		2.0	1.5	9.9
	DPT5.23	e	5.0	3.5		2.1	1.2	9.9
	sum:		25.3	17.7	-0.3			
	av.:		5.1	3.5	-	2.0	1.3	10.0
	95% c.l.:		0.4	0.3	-	0.1	0.3	0.2

Table 6 (cont.). Drop mass and stage time data for individual mass loss determinations.

Furnace conditions	Drop no.		Mass drop, mg	Drop o.d. mass, mg	Loss on wire, mg	Drying time, s	Devol. time, s	Exposure time, s
750 C	DPT5.24	a	4.4	3.1		1.5	1.0	30.2
1.83 m/s	DPT5.24	b	4.9	3.4		1.7	1.4	29.8
5% CO	DPT5.24	d	4.7	3.3		1.7	1.1	30.4
	DPT5.24	e	5.6	3.9		2.1	1.0	30.3
	sum:		19.6	13.7	-0.7			
	av.:		4.9	3.4	-	1.8	1.1	30.2
	95% c.l.:		0.8	0.6	-	0.4	0.3	0.4
750 C	DPT5.25	a	5.3	3.7		2.0		2.9
1.83 m/s	DPT5.25	b	4.5	3.2		1.7	1.0	3.3
5% CO	DPT5.25	c	4.4	3.1		1.7		2.7
	DPT5.25	d	4.8	3.4		1.8		3.1
	DPT5.25	e	5.1	3.6		1.8		2.9
	sum:		24.1	17.0	-0.5			
	av.:		4.8	3.4	-	1.8	1.0	3.0
	95% c.l.:		0.5	0.3	-	0.2	-	0.3
600 C	DPT5.26	a	5.3	3.7		2.9	2.9	10.7
0.61 m/s	DPT5.26	b	4.9	3.5		2.9	2.2	9.7
20% CO_2	DPT5.26	d	5.1	3.6		2.9	1.9	10.0
5% CO	DPT5.26	e	4.6	3.2		2.6	2.6	10.0
	sum:		19.9	14.0	-0.1			
	av.:		5.0	3.5	-	2.8	1.9	10.1
	95% c.l.:		0.5	0.3	-	0.2	1.4	0.7
600 C	DPT5.28	b	5.1	3.6		3.2	2.5	19.8
0.61 m/s	DPT5.28	c	4.4	3.1		2.6	2.2	20.0
20% CO_2	DPT5.28	d	4.6	3.3		3.1	2.6	20.3
5% CO	DPT5.28	e	4.6	3.3		2.5	2.4	19.9
	sum:		18.7	13.3	0.8			
	av.:		4.7	3.3	-	2.9	2.4	20.0
	95% c.l.:		0.5	0.3	-	0.6	0.3	0.3

Table 6 (cont.). Drop mass and stage time data for individual mass loss determinations.

Furnace conditions	Drop no.		Mass drop, mg	Drop o.d. mass, mg	Loss on wire, mg	Drying time, s	Devol. time, s	Exposure time, s
600 C	DPT5.29	a	4.8	3.4		2.8	1.9	5.0
0.61 m/s	DPT5.29	b	5.2	3.7		3.5		5.3
20% CO_2	DPT5.29	c	4.5	3.2		2.8		4.9
5% CO	DPT5.29	d	4.9	3.5		2.8		5.0
	DPT5.29	e	4.6	3.3		2.9		5.1
	sum:		24.0	17.0	-0.3			
	av.:		4.8	3.4	-	3.0	1.9	5.1
	95% c.l.:		0.3	0.2	-	0.4	-	0.2
600 C	DPT5.30	a	4.5	3.2		2.9	1.9	39.9
0.61 m/s	DPT5.30	b	5.1	3.6		3.0	2.3	40.4
20% CO_2	DPT5.30	c	4.9	3.5		3.0	2.8	40.3
5% CO	DPT5.30	d	4.2	3.0		2.6	2.0	39.9
	DPT5.30	e	4.5	3.2				40.0
	sum:		23.2	16.4	-0.9			
	av.:		4.6	3.3	-	2.9	2.3	40.1
	95% c.l.:		0.4	0.3	-	0.3	0.6	0.3
600 C	DPT5.31	a	4.6	3.3		2.9		9.9
0.61 m/s	DPT5.31	b	5.2	3.7		2.8	2.1	10.0
20% CO_2	DPT5.31	c	5.0	3.5		2.9		10.0
5% CO	DPT5.31	d	4.7	3.3		2.9		10.1
	DPT5.31	e	5.1	3.6		3.3	1.7	10.2
	sum:		24.6	17.4	0.7			
	av.:		4.9	3.5	-	3.0	1.9	10.0
	95% c.l.:		0.3	0.2	-	0.2	2.5	0.1
600 C	DPT5.32	a	4.7	3.3		2.6		20.0
0.61 m/s	DPT5.32	c	5.1	3.6		3.1	2.0	20.0
20% CO_2	DPT5.32	d	5.1	3.6		3.1		20.3
5% CO	DPT5.32	e	4.9	3.5		3.7	1.6	20.0
	sum:		19.8	14.0	-1.0			
	av.:		5.0	3.5	-	3.1	1.8	20.1
	95% c.l.:		0.3	0.2	-	0.7	2.5	0.2

Table 6 (cont.). Drop mass and stage time data for individual mass loss determinations.

Furnace conditions	Drop no.		Mass drop, mg	Drop o.d. mass, mg	Loss on wire, mg	Drying time, s	Devol. time, s	Exposure time, s
600 C	DPT5.33	a	5.0	3.6		3.5		5.1
0.61 m/s	DPT5.33	b	5.1	3.6		2.9		4.8
20% CO_2	DPT5.33	c	4.9	3.5		2.5		4.9
5% CO	DPT5.33	d	5.0	3.6		3.8		5.1
	DPT5.33	e	4.9	3.5		3.2		5.1
	sum:		24.9	17.8	0.0			
	av.:		5.0	3.6	-	3.2	-	5.0
	95% c.l.:		0.1	0.1	-	0.6	-	0.2
600 C	DPT5.34	a	4.9	3.5		3.3		40.1
0.61 m/s	DPT5.34	c	5.1	3.6		3.4		39.8
20% CO_2	DPT5.34	d	5.2	3.7		3.2		40.2
5% CO	DPT5.34	e	5.1	3.6		3.5	2.3	40.2
	sum:		20.3	14.5	-0.1			
	av.:		5.1	3.6	-	3.4	2.3	40.1
	95% c.l.:		0.2	0.1	-	0.2	-	0.3
600 C	DPT5.35	a	4.5	3.2		3.0	1.8	10.0
0.61 m/s	DPT5.35	b	4.6	3.3		3.7	1.9	10.2
5% CO	DPT5.35	c	4.5	3.2		3.5	2.0	10.2
	DPT5.35	e	5.1	3.7		3.9	1.2	10.2
	sum:		18.7	13.4	-0.1			
	av.:		4.7	3.3	-	3.5	1.7	10.2
	95% c.l.:		0.5	0.3	-	0.6	0.6	0.2
600 C	DPT5.36	a	4.4	3.2		3.5	2.2	29.7
0.61 m/s	DPT5.36	b	5.0	3.6		3.3	1.9	31.1
5% CO	DPT5.36	c	4.8	3.4		3.1	2.9	30.0
	DPT5.36	d	4.7	3.4		3.7	1.4	30.2
	DPT5.36	e	4.9	3.5		3.5	1.7	30.2
	sum:		23.8	17.0	0.5			
	av.:		4.8	3.4	-	3.4	2.0	30.2
	95% c.l.:		0.3	0.2	-	0.3	0.7	0.6

Table 6 (cont.). Drop mass and stage time data for individual mass loss determinations.

Furnace conditions	Drop no.		Mass drop, mg	Drop o.d. mass, mg	Loss on wire, mg	Drying time, s	Devol. time, s	Exposure time, s
600 C	DPT5.38	b	4.6	3.3		3.3	1.6	6.1
0.61 m/s	DPT5.38	c	5.1	3.7		4.1		5.8
5% CO	DPT5.38	d	4.9	3.5		3.4		5.2
	DPT5.38	e	4.6	3.3		3.3		5.4
	sum:		19.2	13.7	-0.3			
	av.:		4.8	3.4	-	3.5	1.6	5.6
	95% c.l.:		0.4	0.3	-	0.6	-	0.6
600 C	DPT5.39	a	5.2	3.7		3.4	1.2	10.4
0.61 m/s	DPT5.39	b	4.5	3.2		3.4	1.4	10.0
5% CO	DPT5.39	d	4.5	3.2		3.1	1.6	10.4
	DPT5.39	e	5.2	3.7		3.8	1.6	10.5
	sum:		19.4	13.9	-0.5			
	av.:		4.9	3.5	-	3.4	1.5	10.3
	95% c.l.:		0.6	0.5	-	0.5	0.3	0.4
600 C	DPT5.40	a	5.1	3.7		3.5	1.4	30.1
0.61 m/s	DPT5.40	b	4.9	3.5		3.3	1.9	30.1
5% CO	DPT5.40	c	4.8	3.4		3.3	1.9	30.2
	DPT5.40	d	4.6	3.3		3.1	2.2	30.6
	DPT5.40	e	5.2	3.7		3.3	2.1	30.2
	sum:		24.6	17.6	-0.6			
	av.:		4.9	3.5	-	3.3	1.9	30.2
	95% c.l.:		0.3	0.2	-	0.2	0.4	0.3
600 C	DPT5.41	b	4.8	3.4		4.0		5.5
0.61 m/s	DPT5.41	d	4.4	3.2		3.0		5.1
5% CO	DPT5.41	e	5.2	3.7		3.2		5.4
	DPT5.41	f	5.1	3.7		3.2		5.6
	DPT5.41	g	4.8	3.4		3.4		5.2
	sum:		24.3	17.4	0.4			
	av.:		4.9	3.5	-	3.4	-	5.4
	95% c.l.:		0.4	0.3	-	0.5	-	0.3

APPENDIX IV. SODIUM MASS LOSS DETERMINATION

This appendix contains the ICP sodium concentration measurements and the calculation of volatiles yield (total mass loss) and sodium mass loss for 66 determinations during drop pyrolysis experiments and 20 measurements of sodium content for the muffle furnace experiment and the liquor spiking experiment (described below). The appendix ends with a consideration of the accuracy of the acid digestion procedure.

SODIUM ASSAYS AND MASS LOSS CALCULATIONS

Table 7 contains the sodium concentration measurements for each char sample. The mass of sodium for the drop pyrolysis experiments was determined by subtracting the background level of an appropriate blank from the measured concentration of each digested sample. The difference was then multiplied by the sample volume. These calculations are presented chronologically in Table 7. Sodium mass for the remaining 20 samples was determined by multiplying the sodium concentration by the sample mass and density, then subtracting an average sodium mass from the associated blanks.

Calculations of liquor sodium content are contained in Table 8. A fresh sample of liquor was used after completing several experiments; the number in parenthesis indicates the chronological sequence of 50 ml sample bottles. Two liquor samples and one blank were digested for each determination of liquor sodium concentration.

Table 9 contains results of char solids and sodium mass loss calculations for the individual drop and muffle furnace experiments. See Eqs. 5-7 in the text for a discussion of the calculational procedure. The calculations are grouped by furnace condition and

Table 7. Calculation of char sodium from ICP sodium concentration measurements.

Mass loss determ. no.	Type of exp.	Char Na conc., mg/L	Blank Na conc., mg/L	Net Na conc., mg/L	Sample volume, mL	Mass Na in char., mg
DPT2.6	drop	65	1.4	63.6	50	3.2
DPT2.7	drop	100	1.4	98.6	50	4.9
DPT2.8	drop	59	1.4	57.6	50	2.9
DPT2.10	drop	37	0.3	36.7	50	1.8
DPT2.11	drop	30	0.3	29.7	50	1.5
DPT2.12	drop	44	0.3	43.7	50	2.2
DPT2.13	drop	42	0.3	41.7	50	2.1
DPT2.14	drop	43	0.3	42.7	50	2.1
DPT2.15	drop	47	0.3	46.7	50	2.3
DPT2.19	drop	52	0.3	51.7	50	2.6
DPT2.20	drop	45	0.3	44.7	50	2.2
DPT2.23	drop	28	0.3	27.7	50	1.4
DPT3.3	drop	39	0.2	38.8	50	1.9
DPT3.4	drop	82	0.2	81.8	50	4.1
DPT3.5	drop	48	0.2	47.8	50	2.4
DPT3.6	drop	60	0.2	59.8	50	3.0
DPT3.7	drop	50	0.2	49.8	50	2.5
DPT3.9	drop	47	0.2	46.8	50	2.3
DPT3.11	drop	43	0.2	42.8	50	2.1
DPT3.12	drop	50	0.2	49.8	50	2.5
DPT3.13	drop	62	0.2	61.8	50	3.1
DPT3.14	drop	51	0.2	50.8	50	2.5
DPT4.2	drop	55	0.22	54.8	50	2.7
DPT4.3	drop	62	0.22	61.8	50	3.1
DPT4.4	drop	51	0.22	50.8	50	2.5
DPT4.5	drop	61	0.22	60.8	50	3.0
DPT4.6	drop	64	0.22	63.8	50	3.2
DPT4.7	drop	59	0.22	58.8	50	2.9
DPT4.8	drop	52	0.2	51.8	50	2.6
DPT4.9	drop	66	0.2	65.8	50	3.3
DPT4.10	drop	50	0.2	49.8	50	2.5
DPT4.11	drop	66	0.2	65.8	50	3.3
DPT4.12	drop	66	0.2	65.8	50	3.3
DPT4.13	drop	60	0.2	59.8	50	3.0
DPT4.14	drop	340	0.2	339.8	50	17.0
DPT4.15	drop	350	0.2	349.8	50	17.5
DPT4.16	drop	310	0.2	309.8	50	15.5
DPT4.17	drop	330	0.2	329.8	50	16.5
DPT4.18	drop	330	0.2	329.8	50	16.5
DPT4.19	drop	370	0.2	369.8	50	18.5

Table 7 (cont.). Calculation of char sodium from ICP sodium concentration measurements.

Mass loss determ. no.	Type of exp.	Char Na conc., mg/L	Blank Na conc., mg/L	Net Na conc., mg/L	Sample volume, mL	Mass Na in char., mg
DPT5.7	drop	53	0.16	52.8	50	2.6
DPT5.8	drop	43	0.16	42.8	50	2.1
DPT5.9	drop	56	0.16	55.8	50	2.8
DPT5.10	drop	53	0.16	52.8	50	2.6
DPT5.11	drop	55	0.16	54.8	50	2.7
DPT5.12	drop	61	0.16	60.8	50	3.0
DPT5.13	drop	54	0.77	53.2	50	2.7
DPT5.14	drop	52	0.77	51.2	50	2.6
DPT5.15	drop	60	0.77	59.2	50	3.0
DPT5.16	drop	49	0.77	48.2	50	2.4
DPT5.17	drop	57	0.77	56.2	50	2.8
DPT5.19	drop	49	0.15	48.9	50	2.4
DPT5.20	drop	61	0.15	60.9	50	3.0
DPT5.21	drop	67	0.15	66.9	50	3.3
DPT5.22	drop	65	0.15	64.9	50	3.2
DPT5.23	drop	68	0.15	67.9	50	3.4
DPT5.24	drop	51	0.15	50.9	50	2.5
DPT5.25	drop	64	0.15	63.9	50	3.2
DPT5.26	drop	55	0.15	54.9	50	2.7
DPT5.28	drop	46	0.07	45.9	50	2.3
DPT5.29	drop	60	0.07	59.9	50	3.0
DPT5.30	drop	64	0.07	63.9	50	3.2
DPT5.31	drop	64	0.07	63.9	50	3.2
DPT5.32	drop	54	0.07	53.9	50	2.7
DPT5.33	drop	67	0.07	66.9	50	3.3
DPT5.34	drop	51	0.07	50.9	50	2.5
DPT5.35	drop	49	0.20	48.8	50	2.4
DPT5.36	drop	61	0.20	60.8	50	3.0
DPT5.39	drop	50	0.20	49.8	50	2.5
DPT5.40	drop	64	0.20	63.8	50	3.2
DPT5.41	drop	66	0.20	65.8	50	3.3

Table 7 (cont.). Calculation of char sodium from ICP sodium concentration measurements.

Mass loss determ. no.	Type of exp.	Na conc., mg/L	Sample mass, mg	Sample volume, ml	Mass Na in sample, mg	Net Mass Na in sample, mg
Liquor 1	boat	297.8	51.05	49.47	14.7	14.3
Liquor 2	boat	264.7	49.75	48.21	12.8	12.3
Liquor 3	boat	397.3	48.77	47.26	18.8	18.3
Solids 1	boat	332.4	47.86	46.37	15.4	15.0
Solids 2	boat	436.3	47.42	45.95	20.0	19.6
Solids 3	boat	399.5	49.19	47.67	19.0	18.6
Pyr. liq. 1	boat	416.3	48.00	46.51	19.4	18.9
Pyr. liq. 2	boat	303.9	49.68	48.14	14.6	14.2
Pyr. liq. 3	boat	255.1	47.62	46.15	11.8	11.3
Pyr. sol. 1	boat	385.8	49.03	47.51	18.3	17.9
Pyr. sol. 2	boat	351.8	49.80	48.25	17.0	16.5
Pyr. sol. 3	boat	374.6	51.87	50.26	18.8	18.4
Blank 1	boat	1.0	49.50	47.96	0.05	
Blank 2	boat	12.5	48.37	46.87	0.59	
Blank 3	boat	13.4	50.51	48.94	0.66	0.43
Liquor 1	spike	479.4	49.49	47.96	23.0	22.9
Liquor 2	spike	450.8	51.15	49.57	22.3	22.2
Na_2CO_3 1	spike	682.6	50.94	49.36	33.7	33.6
Na_2CO_3 2	spike	555.6	50.67	49.10	27.3	27.1
Na_2CO_3 3	spike	596.3	50.85	49.27	29.4	29.2
Acetate 1	spike	591.4	49.93	48.38	28.6	28.5
Acetate 2	spike	691.2	51.13	49.55	34.2	34.1
Acetate 3	spike	606.7	48.99	47.47	28.8	28.7
	spike					
Blank 1	spike	2.4	51.67	50.06	0.12	
Blank 2	spike	2.9	51.35	49.76	0.14	0.13

Table 8. Calculation of liquor sample sodium content from ICP sodium concentration measurements.

Liquor sample (a)	Liquor Na cont., mg/L	Blank Na cont., mg/L	Net Na cont., mg/L	Mass Na in liquor, mg	Mass of liquor, mg	Liquor solids, %	Mass liquor solids, mg	Liquor Na cont., % solids	Av. liquor Na cont., % solids
#3(2)-1	1640	0.20	1639.8	82.0	566.7	75.0	425.0	19.29	
#3(2)-2	1300	0.20	1299.8	65.0	501.9	75.0	376.4	17.27	18.28
#3(3)-1	1290	0.30	1289.7	64.5	471.8	72.3	341.1	18.90	
#3(3)-2	1280	0.30	1279.7	64.0	484.6	72.3	350.4	18.26	18.58
#3(4)-1	1040	0.30	1039.7	52.0	378.7	72.5	274.6	18.93	
#3(4)-2	1420	0.30	1419.7	71.0	502.4	72.5	364.2	19.49	19.21
#3(5)-1	330	0.40	329.6	16.5	122.0	71.6	87.4	18.87	
#3(5)-2	360	0.40	359.6	18.0	135.6	71.6	97.1	18.52	18.69
#3(5)-3	340	0.40	339.6	17.0	125.7	72.2	90.8	18.71	
#3(5)-4	300	0.40	299.6	15.0	108.9	72.2	78.6	19.05	18.88
#3(6)-1	680	0.50	679.5	34.0	215.3	71.9	154.8	21.95	
#3(6)-2	700	0.50	699.5	35.0	226.0	71.9	162.5	21.52	21.74
#3(8)-1	500	0.32	499.7	25.0	176.5	71.1	125.5	19.91	
#3(8)-2	500	0.32	499.7	25.0	181.1	71.1	128.8	19.40	19.66
#3(8)-3	680	0.24	679.8	34.0	248.6	71.3	177.3	19.17	
#3(8)-4	630	0.24	629.8	31.5	223.9	71.3	159.6	19.72	19.45
#3(9)-1	470	0.24	469.8	23.5	176.2	70.3	123.9	18.96	
#3(9)-2	630	0.24	629.8	31.5	231.6	70.3	162.8	19.34	19.15
#3(9)-3	500	0.21	499.8	25.0	182.0	71.8	130.7	19.12	
#3(9)-4	590	0.21	589.8	29.5	211.8	71.8	152.1	19.39	19.26

(a) Number in parenthesis refers to small bottle from liquor batch (see Experimental).

Table 9. Calculation of volatiles yield and sodium mass loss.

Furnace temp., C		Gas composition, % in N_2	Mass loss determ. no.	Av. exposure time, s	Sum drop o.d. mass, mg	Initial mass char, mg	Volatiles yield, %	Liquor Na content, % solids	Mass Na in liquor, mg	Mass Na in char, mg	Na mass loss, %
600	[1]	5% CO	DPT2.8	3.6	17.4	15.8	8.9	18.28	3.2	2.9	9.20
600	[1]	5% CO	DPT2.15	3.2	14.9	15.6	-4.5	18.28	2.7	2.3	14.47
600	[2]	5% CO	DPT4.16	3.4	81.1	101.4	-25.0	21.74	17.6	15.5	12.17
600	[2]	5% CO	DPT4.19	3.0	87.9	96.7	-10.0	21.74	19.1	18.5	3.28
600	[3]	5% CO	DPT4.23	5.5	20.7	17.1	17.6	-	-	-	-
600	[3]	5% CO	DPT4.26	5.2	22.2	18.5	16.7	-	-	-	-
600	[4]	5% CO	DPT5.38	5.6	13.7	11.4	17.0	19.26	2.6	2.5	5.82
600	[4]	5% CO	DPT5.41	5.4	17.4	15.5	10.8	19.26	3.3	3.3	1.68
600	[1]	5% CO	DPT2.6	11.6	21.0	16.0	23.9	18.28	3.8	3.2	17.26
600	[1]	5% CO	DPT2.13	9.7	14.0	9.5	32.3	18.28	2.6	2.1	18.78
600	[2]	5% CO	DPT4.15	10.3	83.6	70.7	15.4	21.74	18.2	17.5	3.72
600	[2]	5% CO	DPT4.18	10.1	82.4	65.2	20.9	21.74	17.9	16.5	7.94
600	[3]	5% CO	DPT4.21	10.1	22.7	16.7	26.4	-	-	-	-
600	[3]	5% CO	DPT4.24	10.3	22.8	17.7	22.4	-	-	-	-
600	[4]	5% CO	DPT5.35	10.2	13.4	11.7	12.6	19.26	2.6	2.4	5.38
600	[4]	5% CO	DPT5.39	10.3	13.9	11.5	17.2	19.26	2.7	2.5	6.93
600	[1]	5% CO	DPT2.7	29.9	32.3	22.7	29.8	18.28	5.9	4.9	16.58
600	[1]	5% CO	DPT2.14	29.9	12.5	7.3	41.5	18.28	2.3	2.1	6.43
600	[2]	5% CO	DPT4.14	30.2	87.9	69.7	20.7	21.74	19.1	17.0	11.04
600	[2]	5% CO	DPT4.17	30.0	81.4	67.6	16.9	21.74	17.7	16.5	6.81
600	[3]	5% CO	DPT4.22	30.0	21.8	17.4	20.0	-	-	-	-
600	[3]	5% CO	DPT4.25	30.0	21.0	15.2	27.5	-	-	-	-
600	[4]	5% CO	DPT5.36	30.2	17.0	13.6	20.2	19.26	3.3	3.0	7.38
600	[4]	5% CO	DPT5.40	30.2	17.6	14.3	18.8	19.26	3.4	3.2	5.97

Table 9 (cont.). Calculation of volatiles yield and sodium mass loss.

Furnace temp., C		Gas composition, % in N_2	Mass loss determ. no.	Av. exposure time, s	Sum drop o.d. mass, mg	Initial mass char, mg	Volatiles yield, %	Liquor Na content, % solids	Mass Na in liquor, mg	Mass Na in char, mg	Na mass loss, %
750	[1]	5% CO	DPT5.9	3.0	16.2	15.4	5.0	19.66	3.2	2.8	12.42
750	[1]	5% CO	DPT5.12	3.1	17.5	16.4	6.2	19.66	3.4	3.0	11.52
750	[1]	5% CO	DPT5.15	3.2	18.0	15.5	14.0	19.45	3.5	3.0	15.47
750	[1]	5% CO	DPT5.7	10.1	16.8	13.5	19.5	19.66	3.3	2.6	19.90
750	[1]	5% CO	DPT5.10	9.9	17.2	14.0	18.6	19.66	3.4	2.6	21.86
750	[1]	5% CO	DPT5.13	10.1	17.4	14.0	19.4	19.45	3.4	2.7	21.23
750	[1]	5% CO	DPT5.8	30.0	13.1	9.9	24.6	19.66	2.6	2.1	17.00
750	[1]	5% CO	DPT5.11	30.0	18.1	15.1	16.7	19.66	3.6	2.7	23.05
750	[1]	5% CO	DPT5.14	27.9	17.1	13.2	22.8	19.45	3.3	2.6	22.93
750	[2]	5% CO	DPT5.19	3.1	14.5	13.7	5.7	19.45	2.8	2.4	13.54
750	[2]	5% CO	DPT5.22	3.1	17.7	16.5	6.6	19.15	3.4	3.2	4.15
750	[2]	5% CO	DPT5.25	3.0	17.0	14.7	13.5	19.15	3.3	3.2	1.88
750	[2]	5% CO	DPT5.16	10.0	14.1	11.4	19.1	19.45	2.7	2.4	12.05
750	[2]	5% CO	DPT5.20	10.1	17.6	13.5	23.3	19.15	3.4	3.0	9.70
750	[2]	5% CO	DPT5.23	10.0	17.7	15.5	12.6	19.15	3.4	3.4	0.11
750	[2]	5% CO	DPT5.17	30.0	17.8	14.4	19.1	19.45	3.5	2.8	18.79
750	[2]	5% CO	DPT5.21	30.0	17.5	14.9	14.6	19.15	3.3	3.3	0.00
750	[2]	5% CO	DPT5.24	30.2	13.7	10.7	22.1	19.15	2.6	2.5	3.37

Table 9 (cont.). Calculation of volatiles yield and sodium mass loss.

Furnace temp., C		Gas composition, % in N_2	Mass loss determ. no.	Av. exposure time, s	Sum drop o.d. mass, mg	Initial mass char, mg	Volatiles yield, %	Liquor Na content, % solids	Mass Na in liquor, mg	Mass Na in char, mg	Na mass loss, %
900	[1]	5% CO	DPT2.12	3.2	13.8	11.1	19.7	18.28	2.5	2.2	13.50
900	[1]	5% CO	DPT2.20	3.2	17.1	10.1	40.9	18.28	3.1	2.2	28.50
900	[1]	5% CO	DPT2.10	9.8	12.9	7.6	40.9	18.28	2.4	1.8	21.99
900	[1]	5% CO	DPT2.19	10.3	19.0	11.5	39.4	18.28	3.5	2.6	25.47
900	[2]	5% CO	DPT3.13	15.1	22.4	14.7	34.3	19.21	4.3	3.1	28.13
900	[2]	5% CO	DPT3.14	15.2	18.3	11.8	35.7	19.21	3.5	2.5	27.90
900	[2]	5% CO	DPT3.11	20.2	18.2	9.0	50.7	19.21	3.5	2.1	38.92
900	[2]	5% CO	DPT3.12	20.3	18.3	11.3	38.4	19.21	3.5	2.5	29.32
900	[1]	5% CO	DPT2.11	30.1	11.8	7.9	32.8	18.28	2.1	1.5	30.92
900	[1]	5% CO	DPT2.23	30.2	9.9	6.9	30.3	18.28	1.8	1.4	23.47
500	[1]	5% O_2	DPT3.4	7.0	26.7	25.8	3.2	19.21	5.1	4.1	20.16
500	[1]	5% O_2	DPT3.7	7.0	16.3	15.9	2.6	19.21	3.1	2.5	20.61
500	[1]	5% O_2	DPT3.3	15.3	13.4	10.4	22.2	18.58	2.5	1.9	21.92
500	[1]	5% O_2	DPT3.6	15.1	18.2	14.4	20.8	19.21	3.5	3.0	14.39
500	[1]	5% O_2	DPT3.5	30.0	15.5	12.0	22.8	19.21	3.0	2.4	19.96
500	[1]	5% O_2	DPT3.9	30.1	14.8	10.5	29.0	19.21	2.8	2.3	17.64

Table 9 (cont.). Calculation of volatiles yield and sodium mass loss.

Furnace temp., C	Gas composition, % in N_2	Mass loss determ. no.	Av. exposure time, s	Sum drop o.d. mass, mg	Initial mass char, mg	Volatiles yield, %	Liquor Na content, % solids	Mass Na in liquor, mg	Mass Na in char, mg	Na mass loss, %
600	[5] 20% CO_2	DPT5.29	5.1	17.0	14.6	14.2	19.20	3.3	3.0	8.28
600	[5] 20% CO_2	DPT5.33	5.0	17.8	17.1	3.7	19.20	3.4	3.3	1.83
600	[5] 20% CO_2	DPT5.26	10.1	14.0	10.8	23.0	19.20	2.7	2.7	-1.81
600	[5] 20% CO_2	DPT5.31	10.0	17.4	13.2	24.3	19.20	3.3	3.2	4.55
600	[5] 20% CO_2	DPT5.28	20.0	13.3	11.1	16.3	19.20	2.5	2.3	9.79
600	[5] 20% CO_2	DPT5.32	20.1	14.0	10.5	25.2	19.20	2.7	2.7	-0.04
600	[5] 20% CO_2	DPT5.30	40.1	16.4	13.1	20.4	19.20	3.2	3.2	-1.21
600	[5] 20% CO_2	DPT5.34	40.1	14.5	9.9	31.6	19.20	2.8	2.5	8.37

Table 9 (cont.). Calculation of volatiles yield and sodium mass loss. (a)

Mass loss determ. no.	Mass liquor, mg	Net Na mass in sample, mg	Calc. Na cont., % solids	Av. calc. Na cont., % solids	Mass solids, mg	Mass char, mg	"Boat solids," %	Volatiles yield, %
Liquor 1	124.9	14.3	16.1					
Liquor 2	106.0	12.3	16.3					
Liquor 3	157.3	18.3	16.4	16.24				
Solids 1	129.1	15.0	16.3		91.6		71.0	
Solids 2	170.7	19.6	16.1		123.0		72.1	
Solids 3	161.0	18.6	16.2	16.20	117.5		73.0	
Pyr. liq. 1	160.0	18.9	16.6		114.1	80.7		29.3
Pyr. liq. 2	122.5	14.2	16.3		87.3	61.1		30.0
Pyr. liq. 3	95.3	11.3	16.7	16.52	67.9	47.6		29.5
Pyr. sol. 1	154.6	17.9	16.2		111.9	76.8	72.4	31.4
Pyr. sol. 2	139.0	16.5	16.7		100.9	68.7	72.6	31.9
Pyr. sol. 3	158.1	18.4	16.3	16.42	113.3	76.0	71.7	32.9

(a) See Results chapter for discussion of sodium mass loss in the muffle furnace experiments.

exposure time. Analysis of the total mass loss results indicated that any material loss incurred during char drying did not cause a systematic error in the calculations of sodium mass loss. In calculating sodium mass loss, liquor sodium concentration values were taken from Table 8 that corresponded to each group of preceding char digestions from Table 7.

EVALUATION OF ACID DIGESTION PROCEDURE

An experiment was conducted to determine if the form of sodium (inorganic or organic salt) affected the measurement of sodium concentration in the acid-digested samples. Such an effect would produce a systematic error in sodium mass loss determination, because the organically bound sodium is converted to Na_2CO_3 during devolatilization.[12,71]

Sodium carbonate was added to three 100 mg black liquor samples as an inorganic spike, sodium acetate was used as the model organically-bound compound. Approximately 30% of the sodium mass was added as the spikes to the liquor samples. The six spiked samples (three of each salt), two of the original black liquor, and two blanks were prepared under identical conditions.

The results in Table 10 show no statistical difference between the sodium contents of the acid-digested spiked samples. Subtracting the known mass of sodium in the spike from the total determined allows an estimation of the sodium in the liquor solids. The 4% lower value than the original liquor was probably a result of moisture in the added chemicals. The results of this experiment indicate that the calculated values of sodium mass loss were not subject to a systematic error in sodium content determination.

Table 10. Results of liquor spiking experiment.

Sample no.	Mass o.d. liquor, mg	Net Na mass in sample, mg	Na conc., % solids	Mass spike, mg	Mass Na in spike, mg	Est. Na in spiked liquor, mg	Est. spiked liquor Na cont., % solids	Actual spiked liq. Na cont., % solids	95% conf. limit
Liquor 1	140.7	22.9	16.2						
Liquor 2	135.3	22.2	16.4					16.3	
Na_2CO_3 1	159.9	33.6	21.0	20.4	8.9	24.7	15.5		
Na_2CO_3 2	126.9	27.1	21.4	16.9	7.3	19.8	15.6		
Na_2CO_3 3	135.1	29.2	21.7	18.8	8.2	21.1	15.6	15.6	0.2
Acetate 1	122.6	28.5	23.2	33.2	9.3	19.2	15.6		
Acetate 2	163.6	34.1	20.9	29.1	8.2	26.0	15.9		
Acetate 3	134.8	28.7	21.3	25.4	7.1	21.5	16.0	15.8	0.4

APPENDIX V. STATIC AEROSOL COLLECTION EXPERIMENTS

A series of preliminary trials were conducted to evaluate and refine the techniques of aerosol collection. The photomicrographs presented in this appendix are indicative of the material found during extensive searches of random samples cut from the BGF filters. Less than 0.1 cm^2 of an exposed filter area of 30-40 cm^2 was investigated by SEM. Therefore, any conclusion drawn from these images is somewhat speculative due to the chance nature of obtaining a representative sample of the total aerosol generated during combustion.

AEROSOL COLLECTION WITH LIMITED VACUUM FLOW

During the first static collection experiment, 76 by 102-mm (3 by 4-in.) BGF filters were located 63.5 mm (2.5 in.) above the quartz reactor tube exit. Filters were held in place by suction on a Teflon® (PTFE) vacuum flow distributor; the vacuum source was a small reciprocating pump. Individual drops of liquor no. 2A (63% dry solids content) were burned in air at 600-750°C with an average gas velocity in the reaction chamber of 0.61-1.22 m/s (2-4 ft/s). Three 5 mm square samples were arbitrarily cut from one filter at each condition for SEM analysis.

A comparison of the aerosol collected from combustion of single liquor drops at two temperatures can be made by inspecting the SEM photomicrographs Figs. 32 to 35. Several large 5-20 μm spheres are visible in both Fig. 32 and 33; small 0.1-0.5 μm irregular deposits on the filter fibers are only apparent in Fig. 32. The higher magnification of Fig. 35 reveals there was sparse but uniform deposition of fine aerosol from the lower temperature

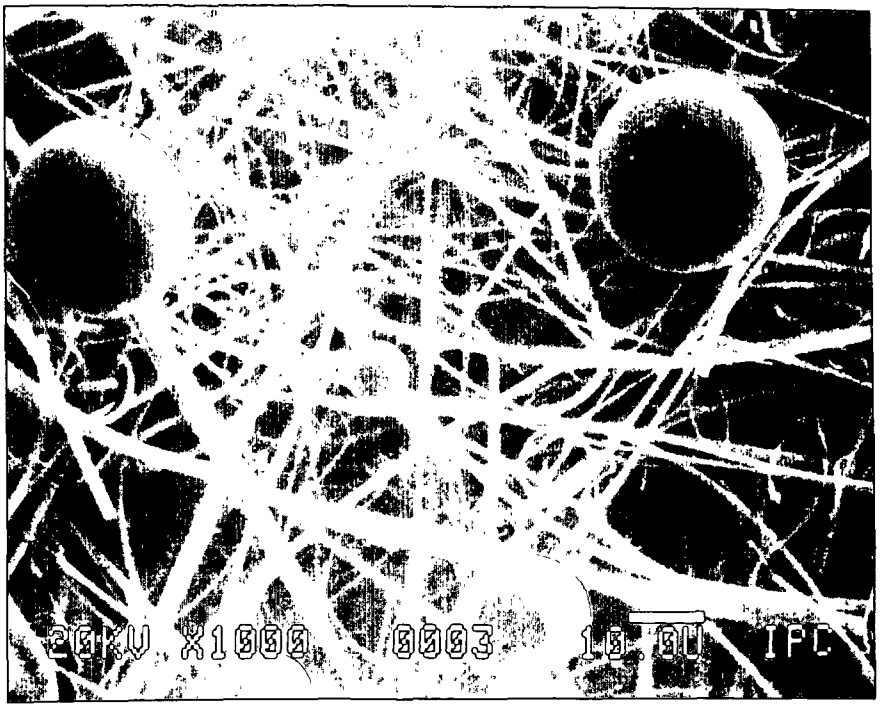

Figure 32. SEM photomicrograph showing particulate on BGF filter. Combustion of 27.1 mg drop of liquor no. 2A in air at 750°C and 0.61 m/s; 14 L/min vacuum flow.

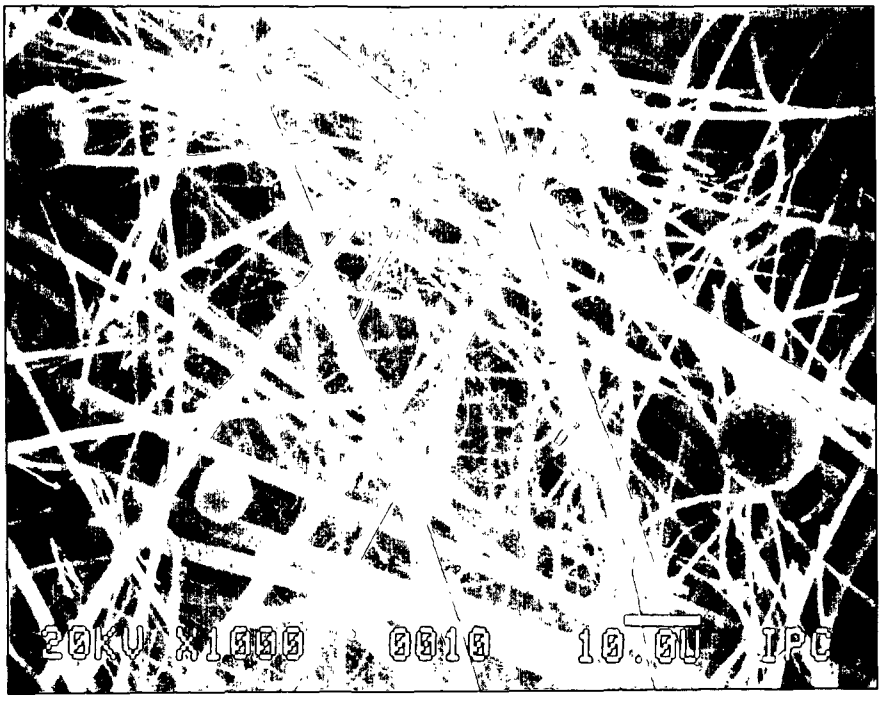

Figure 33. SEM photomicrograph showing particulate on BGF filter. Combustion of 51.6 mg drop of liquor no. 2A in air at 600°C and 0.61 m/s; 14 L/min vacuum flow.

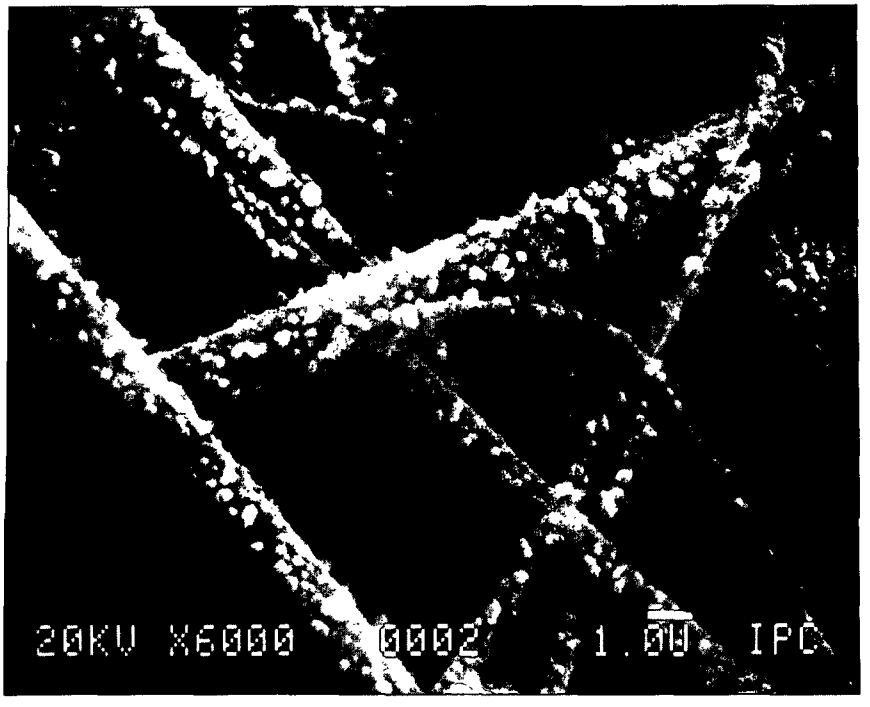

Figure 34. SEM photomicrograph showing submicron-sized aerosol on BGF filter. Conditions given in Fig. 32.

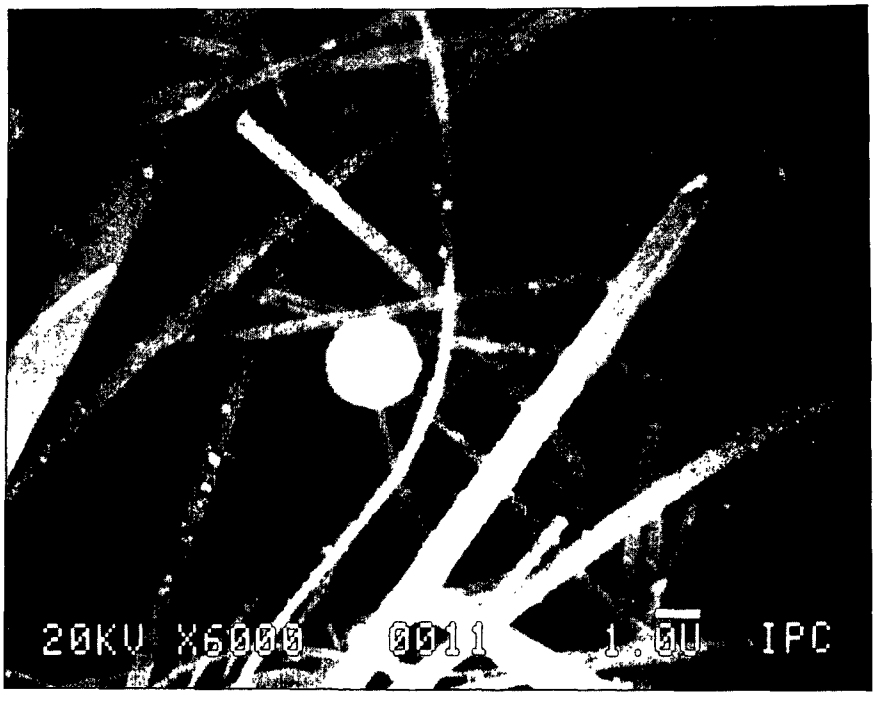

Figure 35. SEM photomicrograph showing submicron-sized aerosol on BGF filter. Conditions given in Fig. 33.

burn. These images suggest that there was more fume-like aerosol produced at 750°C. The large spheres undoubtedly resulted from the ejection of bits of burning char and molten smelt which were observed during the char burning and smelt oxidation stages of combustion.

There was less fine aerosol found on the filters exposed to the higher flow rate at both temperatures; Fig. 36 is an example of this observation. The reciprocating vacuum pump was only capable of drawing 19-45% of the exhaust flow through the filter. The lower percentage of combustion gas drawn through the filter at the higher furnace velocity resulted in fewer submicron-sized particles being collected relative to the larger particles. Submicron-sized particles tend to follow streamlines of a flowing gas. Thus, at the higher flow rate more of the 0.1-0.5 μm aerosol would have been lost because a larger amount of the exhaust gas

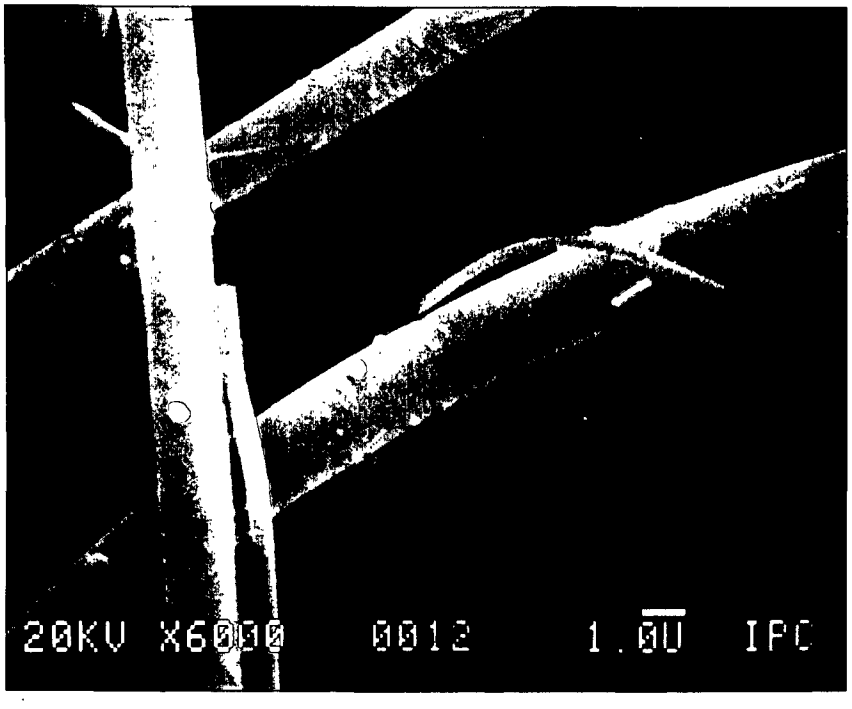

Figure 36. SEM photomicrograph showing submicron-sized aerosol on BGF filter. Combustion of 41.7 mg drop of liquor no. 2A in air at 750°C and 1.22 m/s; 14 L/min vacuum flow.

was diverted at the filter plane. The increased momentum of the 5-20 μm spheres at the higher gas velocity may have increased their chance of collection by impaction on the glass filter fibers.

AEROSOL COLLECTION WITH HIGH CAPACITY VACUUM FLOW

As it was expected that the flow restriction of the reciprocation vacuum pump limited collection efficiency, the experiment was repeated after a high capacity Piab pneumatic vacuum source had been installed. Nine static aerosol collection trials were conducted with drops of liquor no. 3 burned in air at 750°C with an average gas velocity of 0.61 m/s (2 ft/s); the initial filter vacuum flow was varied from 100% of the gas mass flow (33 std. L/min) to the low level used in the previous experiment (14 std L/min). The volume flow rate of gas increased with decreasing gas density after the filters were placed over the hot exhaust gases. Correspondingly, vacuum flow decreased as a result of the increased pressure drop of higher gas velocity through the 0.40-mm (1/64-in.) holes in the PTFE vacuum flow distributor. In all trials the vacuum flow dropped to about 14 L/min after one minute.

Deposits were observed on all the filters with an optical microscope at a 3 × magnification. Samples were taken for SEM analysis -- from regions with and without the visible deposits -- from two filters produced at each level of vacuum flow. All of the samples scanned showed the presence of aerosol despite the poor image quality from the JEOL JSM-35C instrument. Energy dispersive X-ray spectrometry (EDS) indicated that the composition of the particulate was primarily sodium and sulfur.

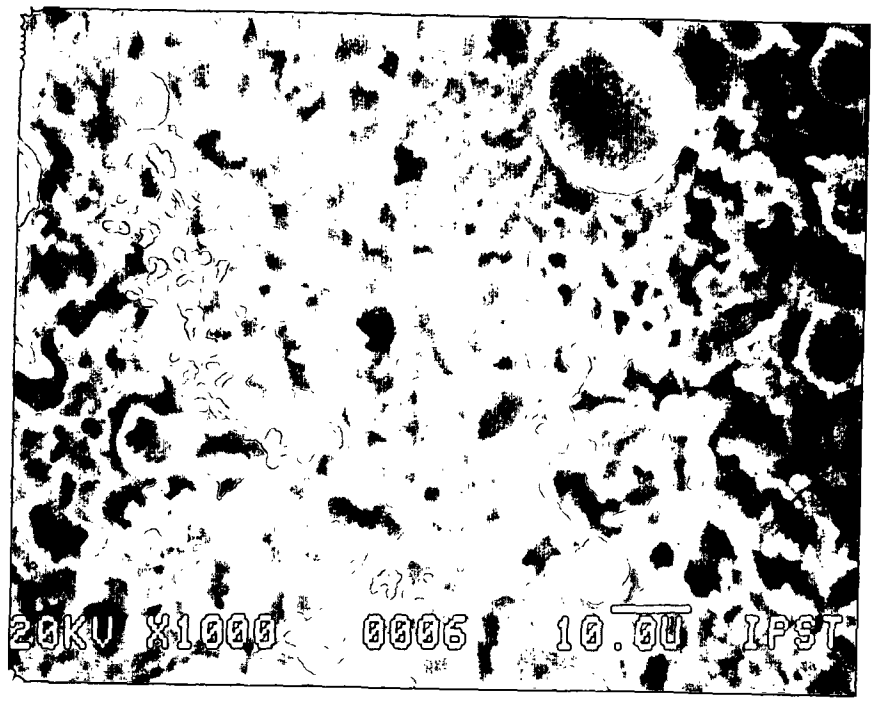

Figure 37. SEM photomicrograph showing dense aerosol deposit on BGF filter. Combustion of 8.9 mg drop of liquor no. 3 in air at 750°C and 0.61 m/s; 31.1 L/min initial vacuum flow.

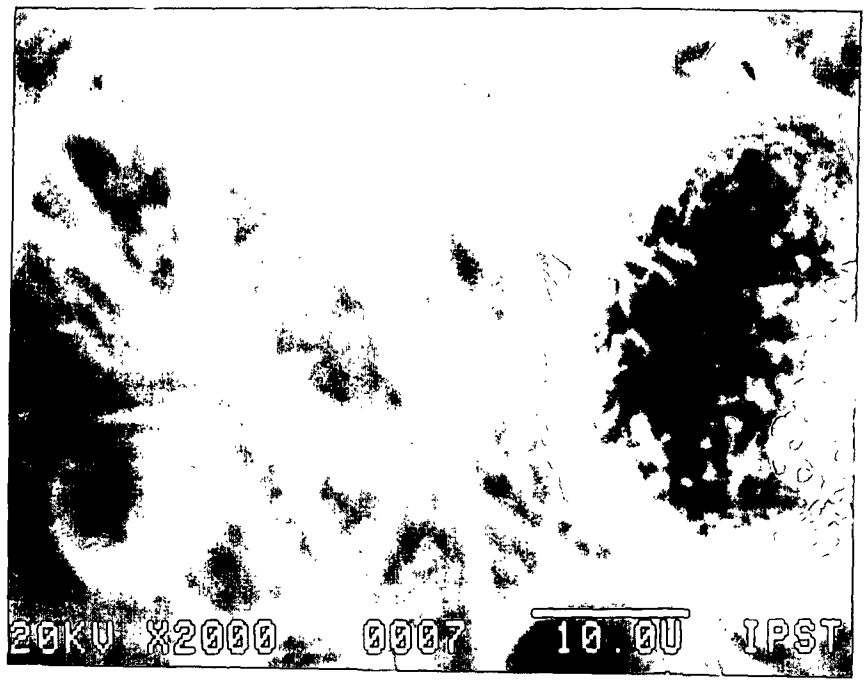

Figure 38. SEM photomicrograph of a large spherical particle with dendritic features. Conditions given in Fig. 37.

Figure 37 shows a region thickly covered with sintered submicron-sized particulate. This material obscured the filter fibers in some areas. Numerous 5 - 20 μm rough-surfaced spheres were distributed on and among the sintered deposits on all of the filter samples. The extent of sintering suggests that the temperature at the filter was higher than in the previous trial. No effect of the initial level of vacuum flow could be determined by comparing the SEM images. There was evidence of dendrite formation on the surface of some spheres, as shown in Fig. 38. Dendrite growth may have resulted from condensation of alkali vapor on the deposited aerosol.

AEROSOL COLLECTION DURING PYROLYSIS

During several of the sodium mass loss determinations, aerosols generated during pyrolysis were collected on BGF filters. The dynamic aerosol collection system, described in the Experimental chapter, was used to place a 102 by 203-mm (4 by 8-in.) BGF filter over the exhaust flow director exit. The filter remained in place during the first five individual drop exposures of each determination. Before additional drops were pyrolyzed, the collection medium carriage was activated to carry the filter past the exhaust flow. The large opening of the vacuum flow director did not restrict the vacuum flow during sampling, as had the PTFE vacuum flow distributor. A nominal vacuum flow of 14 L/min was maintained for all static aerosol collections during pyrolysis except for the trial at 750°C; in that instance there was no induced flow because the vacuum flow director had been removed. Figure 39 is an example of the material collected during pyrolysis at 750°C. Further analysis of the aerosols produced during pyrolysis is contained in the text.

Figure 39. SEM photomicrograph showing fine fume on BGF filter. Pyrolysis of 5 drops (24.0 mg) of liquor no. 3 in 95% N_2/5% CO at 750°C and 0.61 m/s; 14 L/min vacuum flow.

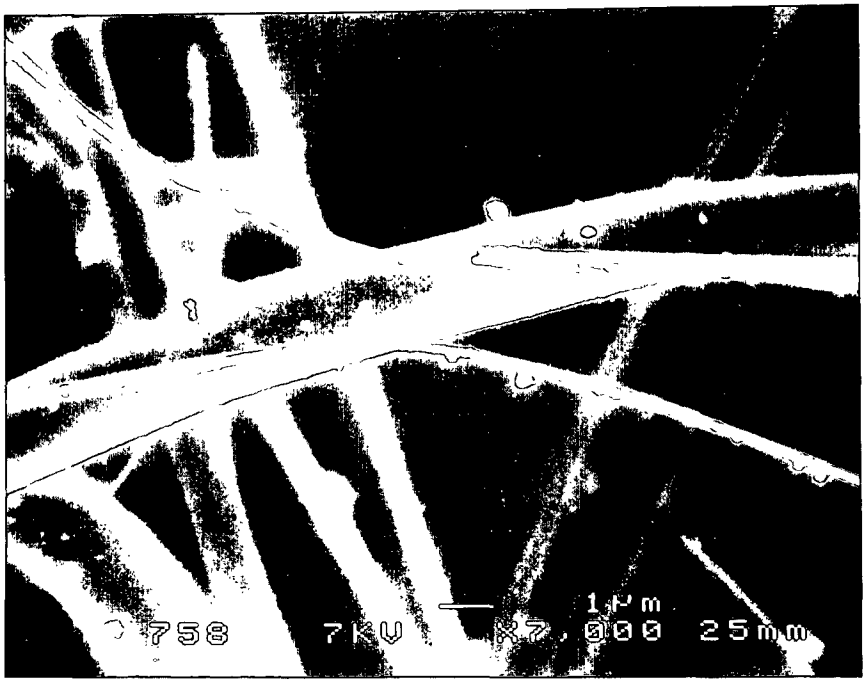

Figure 40. SEM photomicrograph showing collected aerosol on BGF filter. Combustion of 6.2 mg drop of liquor no. 3 in air at 750°C and 0.15 m/s; 0 L/min vacuum flow.

AEROSOL COLLECTION BY IMPACTION

The absence of visible submicron-sized aerosol in the first dynamic aerosol collection experiment (described in Appendix VI) and the unexpectedly small quantities of aerosols captured during pyrolysis were mistakenly blamed on penetration of material through the filters. Fume was not detected on the BGF filter samples from the first dynamic aerosol collection experiment due to limited resolution of the JEOL JSM-35C microscope. It was assumed that collection by impaction on the filters would retain more submicron-sized aerosol than by filtration.

An experiment with 102 by 203-mm filters was conducted using the dynamic aerosol collection system in a fixed mode to evaluate the new collection strategy. Drops of liquor no. 3, 8-12 mg in size, were burned in dry air at 750°C; gas flow rate was adjusted to produce average gas velocities of 0.61, 0.30, and 0.15 m/s in the quartz reactor tube. Vacuum flow was correspondingly set at 14, 6, and 0 L/min. Four 5 by 5-mm samples were cut from the center region of each of five filters for SEM investigation. An example of the material collected from this final group of trials is given in Fig. 40; additional photomicrographs are discussed in the text. Comparing Figs. 39 and 40 indicates that approximately the same amount of fume was collected during the pyrolysis of 5 drops as during the combustion of a single drop of the same liquor.

APPENDIX VI. ANALYSIS OF DYNAMIC AEROSOL COLLECTION DATA

The technique of determining the time during combustion when inorganic aerosols were generated required monitoring drop combustion progress, continuous collection of the aerosols as they were produced, and understanding the material losses and delay time between the source of the aerosol and the collection plane. This appendix contains an analysis of the dynamic aerosol collection data. Evaluation of sources of error in material measurements, and consideration of losses due to collection efficiency limitations and deposition within the equipment are considered in Appendix VII.

Aerosols were separated from the combustion gases by BGF filters in the first dynamic collection experiment; the second utilized silver membranes as an impaction surface for aerosol collection. Differences in equipment configuration, experimental conditions, analysis of captured aerosol, and interpretations of time-resolved results are explained for each experiment.

DYNAMIC AEROSOL COLLECTION ON BGF FILTERS

Experimental conditions used during the dynamic filtration experiment are given in Table 11. Three pairs of BGF filters (203 by 254-mm moving filter and 102 by 102-mm backup) were chosen for inorganic species assays, two that had been exposed to single drop combustion products (DCT3.22, DCT3.23) and one "blank" that had been exposed to combustion gases without burning liquor (DCT3.20). The fourth pair of filters was investigated by SEM (DCT3.24). After exposure each large filter was carefully divided into nine 25-mm (1-in.) sections, as indicated in Fig. 41. Sample preparation for analysis is

Table 11. Furnace conditions and drop combustion data for dynamic aerosol collection on BGF filters.

Furnace Conditions

Furn. temp.	750 C
Av. gas vel.	0.61 m/s
Gas comp.	7.5% O_2 in N_2
Gas flow	2.50 kg/hr
Vacuum flow	3.21 kg/hr
Drive speed	1500 rpm (25.4 cm/min)

Drop Combustion Data

Drop no.	Mass drop, mg	Drop o.d. mass, mg	Loss on wire, mg	Drying time, s	Devol. time, s	Char burning time, s	Smelt oxidation time, s
DCT3.20	-	-	-	-	-	-	-
DCT3.22	19.0	13.6	5.3	1.3	3.7	14.3	24.3
DCT3.23	27.6	19.8	7.9	1.4	4.8	14.6	25.5
DCT3.24	54.3	38.9	1.9	1.2	7.2	-	-
				Ignition	MSV (a)	SC (b)	End
DCT3.22		Elapsed time --->		1.3	5.0	19.3	43.6
DCT3.23		Elapsed time --->		1.4	6.2	20.8	46.3
DCT3.24		Elapsed time --->		1.2	8.4		

(a) Maximum swollen volume.
(b) Smelt coalescence.

described in the Experimental chapter.

Analysis of Filters

The measured species concentrations are given in Table 12. All values are significantly higher than detection limits; however, the average level of Na and $CO_3^=$ in the blank sample is higher than in either of the exposed filters. The assay values in Table 12 represent total material collected over discrete time intervals equal to the width of the section (Δx) divided by the linear speed of the collection medium carriage (s_l).

Although BGF filters are an attractive medium for aerosol collection, sodium

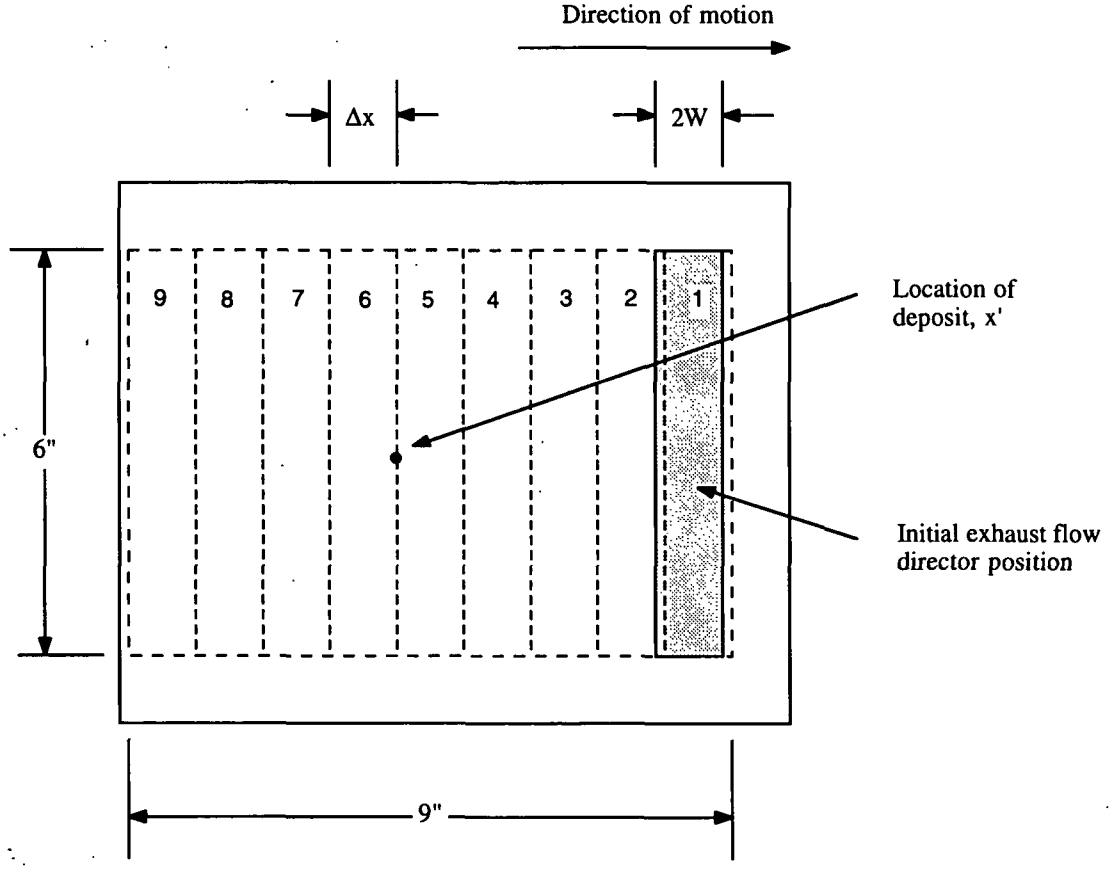

Figure 41. Schematic of BGF filter (F1) showing locations of analyzed sections.

Table 12. Analysis of BGF filters and drop residues from dynamic aerosol collection.

Drop no. >	DCT3.20			DCT3.22			DCT3.23			DCT3.24		
Sample (a)	Na, (b) mg/kg	$CO_3(2-)$, (c) mg/L	$SO_4(2-)$, (c) mg/L	Na, (b) mg/kg	$CO_3(2-)$, (c) mg/L	$SO_4(2-)$, (c) mg/L	Na, (b) mg/kg	$CO_3(2-)$, (c) mg/L	$SO_4(2-)$, (c) mg/L	Na, (b) mg/kg	$CO_3(2-)$, (c) mg/L	$SO_4(2-)$, (c) mg/L
F1-1	78	33.0	0.35	93	23.0	1.26	78	30.0	1.58	-	-	-
F1-2	76	31.0	0.21	99	20.0	2.41	71	30.0	1.44	-	-	-
F1-3	89	35.0	0.32	71	27.0	1.09	79	27.0	0.62	-	-	-
F1-4	87	39.0	0.38	88	35.0	0.55	80	33.0	0.57	-	-	-
F1-5	86	35.0	0.26	78	35.0	0.40	83	38.0	0.45	-	-	-
F1-6	85	35.0	0.25	76	37.0	0.40	81	38.0	0.49	-	-	-
F1-7	105	38.0	0.23	78	25.0	0.35	79	24.0	0.41	-	-	-
F1-8	109	27.0	0.19	82	30.0	0.36	72	29.0	0.44	-	-	-
F1-9	111	37.0	0.47	92	34.0	0.40	75	39.0	0.55	-	-	-
Av. section	92	34.4	0.30	84	29.6	0.80	78	32.0	0.73			
F2	131	78.0	0.84	133	57.0	1.38	124	49.0	1.24	-	-	-
Residue	-	-	-	26	75.0	16.60	37	80.0	17.60	10	34.0	4.80
Detection limit	0.5	0.1	0.05	0.5	0.1	0.05	0.5	0.1	0.05	0.5	0.1	0.05

(a) F1 designates 8 by 10 in. filter; F2 is 4 by 4 in. backup.
(b) Analysis by Analytical Services, Inc., Atlanta, GA.
(c) Analysis by IPST.

oxide is a significant component of borosilicate glass. Technical information from the Whatman company[88,89] indicates that, depending on extraction procedure, between 22 and 51 mg Na/g filter can be dissolved from the EPM-2000 BGF filters. An average value of 16.5 mg of extractable sodium per gram of filter was calculated from the data in Table 12 and the recorded mass of each filter. The soluble quantity of sodium in the glass fibers is both non-uniformly distributed and approximately 27 times higher in each section than the total amount expected to be captured from combustion of a 23 mg drop.* The average background level of carbonate in each filter section was approximately 7 times greater than the total amount expected to be collected during combustion.** The data in Table 12 clearly show that analytical determination of the amounts of captured sodium carbonate was impossible.

The amounts of background $SO_4^=$ in the blank filter sections were consistently lower than those of the exposed filters. There are significant quantities of barium, calcium, potassium, magnesium, and sodium in Whatman EPM-2000 filters;[89] these elements may readily react with acidic gases to form artifact products which could be mistaken for collected material. Reduced sulfur gases (TRS) released during black liquor devolatilization are readily oxidized to SO_2 and SO_3. In the presence of water vapor, SO_3 can form gaseous H_2SO_4. This conversion is greatly favored at low temperature.[61] Sulfuric acid dewpoint decreases with decreasing SO_3 and water vapor concentration in flue gases; for 1 ppm SO_3 and 5 volume percent H_2O the H_2SO_4 dewpoint would be about 110°C.[90] Mitchell and Bruffey[91]

---

* Calculated from liquor properties in Table 3 and assumption that 10% of the sodium in the drop will be collected as fume on the filter.

** Assuming that 50% of the captured sodium is Na_2CO_3.

evaluated emissions samplers that simultaneously measure particulate, H_2SO_4, and SO_2. They reported significant collection of H_2SO_4 by borosilicate glass fiber filters when sampling at 30-60°C above the acid dewpoint. This information suggests that some of the $SO_4^=$ measured on the BGF filters from this experiment was undoubtedly a result of artifact formation.

Time Resolution of Dynamic Filtration Data

Dynamic aerosol filtration data was transformed into a quasi-continuous record of sulfate collection in order to determine the time during combustion when sulfur containing species were formed. The technique was based on the approach used by Nelson et al.[92] to "time resolve" atmospheric aerosol concentrations from "filter streaker" samples.

As discussed in the Results section of the text, the time resolution* (δ) is set by the width and shape of the flow director opening:

$$\delta_R = \pm \frac{2W}{s_1} \quad , \tag{13}$$

where δ_R is the time resolution for a rectangular slot opening and W is the half-width of the flow director opening. For this experiment the time resolution was 6 seconds. Note that the width of each filter section (Δx) equalled the width of the flow director opening (2W); therefore, the time interval represented by a filter segment ($t_{\Delta x}$) also equalled 6 seconds. The temporal uncertainty of determining the origin of an instantaneous combustion event from filter analysis was $\pm$ W/s_1 or exactly half of the time resolution.

* Not to be confused with the process of time resolution.

The data were time resolved by applying a weight function, $f_R(t)$, that described the fraction of the flow director which was inside an area corresponding to t_x at any time t:

$$f_R(t) = \begin{cases} 1 - \left|\frac{t-t_x}{\delta_R}\right| & ; \ |t-t_x| \le \delta_R \\ 0 & ; \ |t-t_x| > \delta_R \end{cases} \tag{14}$$

This function is shown graphically in Fig. 42a. The average mass of sulfate collected at any time, for a specified time step (dt), was given by

$$\bar{m}_x = \frac{\int_{t_x-\delta}^{t_x+\delta} m(t)\, f_R(t)\, dt}{\int_{t_x-\delta}^{t_x+\delta} f_R(t)\, dt}, \tag{15}$$

where $\bar{m}_x$ is the average time-resolved mass and m(t) is the mass distribution function. The mass of sulfate collected on each section of the filters was calculated from the measured concentrations given in Table 12 minus the average background level from the DCT3.20

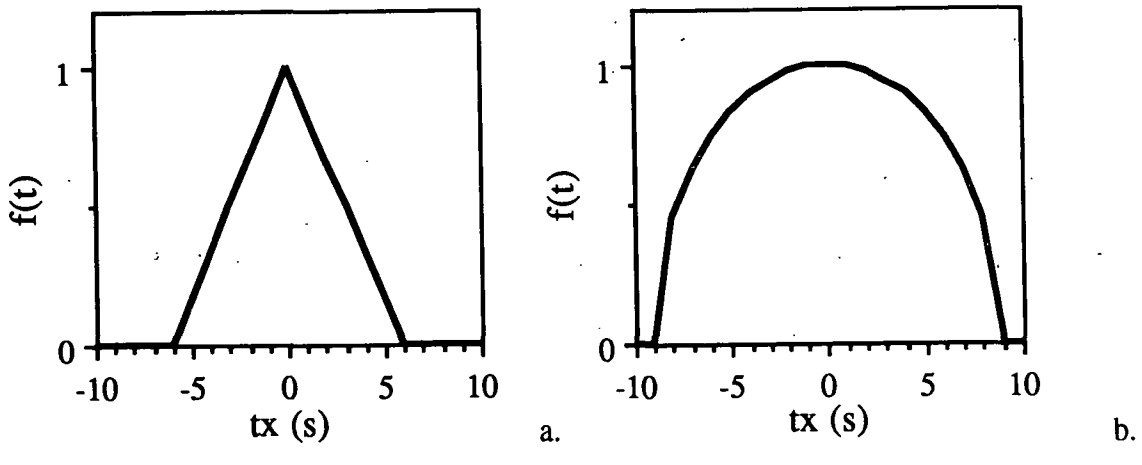

Figure 42. Weight functions for time resolution of dynamic aerosol collection experiments: a) 25-mm rectangular opening, b) 76-mm circular opening.

blank. In order to evaluate the integral in Eq. 15, the data must be treated as a discrete function:

$$m(t) = \begin{cases} 0 \ ; \ t = 0 \\ m_1 \ ; \ 0 < t \le t_{\Delta x} \\ m_2 \ ; \ t_{\Delta x} < t \le 2t_{\Delta x} \\ \vdots \\ m_n \ ; \ (n-1)t_{\Delta x} < t \le nt_{\Delta x} \end{cases} \qquad (16)$$

Residence time was calculated from the steady state heat transfer model described below. Three heat transfer resistances were considered in the exhaust flow director model: 1) The Graetz correlation for simultaneously developing laminar flow was used to estimate the contribution of forced convection inside the director.[80] 2) Laminar natural convection along a vertical flat plat was applied to the outside wall. 3) The gray outside walls were assumed to radiate to the surroundings through a transparent gas.[81] In order to approach the isothermal wall constraint of the heat transfer relations, the exhaust flow director was treated as a series of short stacked cylinders of negligible wall thickness. The diameter of each cylinder was taken as the effective diameter of the flow director at the same elevation. Once the temperature drop across each cylindrical segment j was known, an average gas velocity at the bulk temperature ($\langle v \rangle_j$) could be calculated by

$$\langle v \rangle_j = \frac{\dot{m}}{\rho(T_{b,j}) \times A_{e,j}} \ , \qquad (17)$$

where $\dot{m}$ is mass flow rate of the exhaust gas, $\rho(T)$ is ideal gas density, $T_{b,j}$ is the bulk temperature in segment j, and $A_{e,j}$ is effective cross-sectional area of segment j. Total residence time between the drop and the filter (Θ) was taken as the sum of the height of each segment divided by the average gas velocity given in Eq. 17:

$$\Theta = \sum_{j=1}^{n} \frac{\Delta y_{FD,j}}{\langle v \rangle_j} \quad , \tag{18}$$

where $\Delta y_{FD,j}$ is the height of segment j.

The time-resolved sulfate mass from Eq. 16 was plotted against elapsed drop combustion time from Eq. 12 (see text) in Figs. 43 and 44; these continuous lines may approximate the actual sulfate-containing aerosol generation that occurred during drop combustion. Equation 16 was used to calculate total $SO_4^=$ collected over the 6-second time intervals corresponding to each section of the filter; these data are plotted as vertical bars in Figs. 43 and 44. Note that the temporal uncertainty of 3 seconds was accounted for when overlaying the combustion stage times from Table 11 on Figs. 43 and 44.

Results from the first dynamic experiment exhibited a peak in the amount of $SO_4^=$ collected, corresponding to the overlapped region of the devolatilization and char burning stages. Although the form of sulfur was not directly determined, it was presumably as Na_2SO_4. Sodium sulfate fume could have been produced from the reaction of sodium metal and the gas species indicated in Fig. 27c (see text). However, the substantial amount of sulfate measured on the first filter section, shown as the discrete functions in Figs. 43 and 44, could also have resulted from artifact formation. During the first few seconds of combustion the simultaneous presence of reduced sulfur gases, oxygen, and water vapor could have resulted in H_2SO_4 formation.[91] As all of the sulfur gases should have evolved by the end of the devolatilization stage, the "shoulder" during the overlapped char burning and smelt oxidation stages in Figs. 43 and 44 may have resulted from entrainment of ejected matter. This ejecta which would have been similar in composition to oxidized smelt (65% Na_2SO_4).

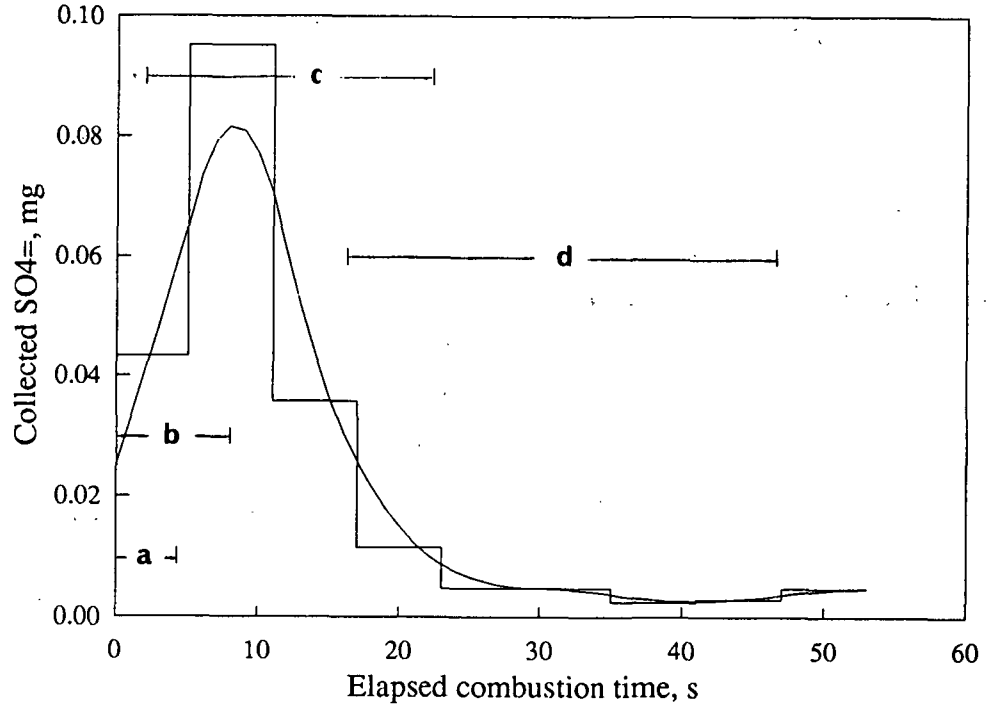

Figure 43. Time-resolved sulfate deposition history from dynamic aerosol collection experiment. Combustion of 19.0 mg drop (DCT3.22 in Table 11). a) drying, b) devolatilization, c) char burning, d) inorganic reactions.

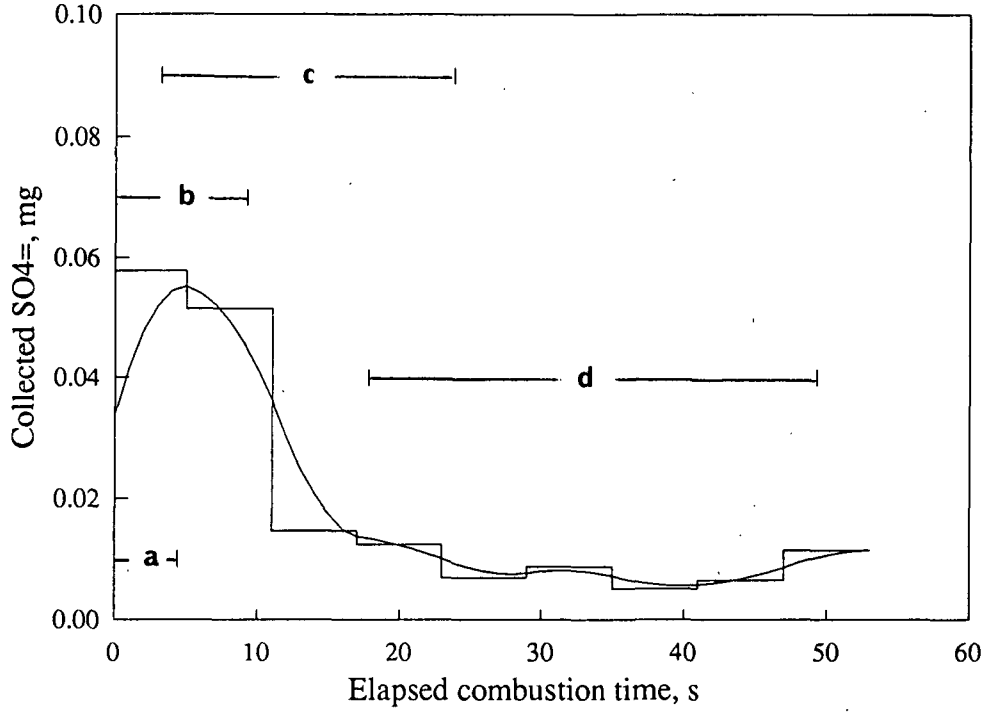

Figure 44. Time-resolved sulfate deposition history from dynamic aerosol collection experiment. Combustion of 27.6 mg drop (DCT3.23 in Table 11).

DYNAMIC AEROSOL COLLECTION ON SILVER MEMBRANES

Due to uncertainties regarding artifact formation, the time-resolved $SO_4^=$ data from the BGF filters provided more of an indication of sulfur release history than of aerosol formation. The use of silver membranes as the aerosol collection medium prevented artifact formation because acidic combustion products did not react with the inert material at the conditions of these experiments. Accurate determination of microgram quantities of sodium was possible with silver membranes because the levels of soluble contaminants in the membranes were extremely low. The measurable quantity of extractable sodium was approximately 5.3×10^{-3} mg per gram of membrane material, as compared to a value of 16.5 mg Na per gram for the EPM-2000 BGF filters.

An insert was placed in the collection medium carriage to reduce the size of the opening from 152 by 229-mm (6 by 9-in.) to 76 by 203-mm (3 by 8-in.) so that a smaller amount of the costly membranes could be used for each dynamic aerosol collection. In an attempt to lower the exit gas temperature during the evaluation of various aerosol collection media, a 76 mm (3-in.) diameter metal flue was installed in place of the exhaust flow director. The original equipment should have been replaced before conducting the experiment because the wider flue opening significantly increased the temporal uncertainty of the results.

Time Resolution of Dynamic Impaction Data

Drop combustion exhaust gas was impacted on two 89 by 229-mm (3.5 by 9-in.) moving silver membranes (AFT 3.8 and AFT3.9 in Table 13); a smaller piece of membrane was exposed to only the hot gases to provide a "blank" sample. After exposure each membrane was divided into eight 13-mm (0.5-in.) sections as indicated in Fig. 29.

Table 13. Furnace conditions and drop combustion data for dynamic aerosol collection on silver membranes.

Furnace Conditions

Furn. temp.	750 C
Av. gas vel.	0.61 m/s
Gas comp.	7.5% O_2 in N_2
Gas flow	2.50 kg/hr
Vacuum flow	-
Drive speed	1500 rpm (25.4 cm/min)

Drop Combustion Data

Drop no.	Mass drop, mg	Drop o.d. mass, mg	Loss on wire, mg	Drying time, s	Devol. time, s	Char burning time, s	Smelt oxidation time, s
AFT3.8	14.1	10.1	3.5	1.3	3.2	9.6	10.6
AFT3.9	14.3	10.2	2.2	1.0	3.6	10.8	11.1
				Ignition	MSV (a)	SC (b)	End
AFT3.8		Elapsed time --->		1.3	4.5	14.1	24.7
AFT3.9		Elapsed time --->		1.0	4.6	15.4	26.5

(a) Maximum swollen volume.
(b) Smelt coalescence.

The measured species concentrations are given in Table 14. Amounts of sulfate and chloride ion were at or below the IC detection limits. The carbonate in the two blank 13-mm sections was higher than in any of the exposed sections. If all of the collected material were Na_2SO_4 or NaCl, then the mean $SO_4^=$ concentration would have been 0.23 mg/L and Cl^- would have been 0.17 mg/L, about twice the detection limits for these anions. If 100% of the sodium was in the form of Na_2CO_3, the expected concentration of $CO_3^=$ would have been only 15% of the detection limit. Since the actual material collected was probably a mixture of these salts, sodium was the only measurable compound for this experiment.

The previously described technique of time resolution was applied to the results of the dynamic impaction experiment. A weight function was assigned that equalled 1 at the point of evaluation (x') and 0 at a distance equal to the radius:

$$f_C(t) = \begin{cases} \frac{1}{\delta_c}\sqrt{\delta_C^2 - (t-t_x)^2} \; ; & |t-t_x| \le \delta_C \\ 0 \; ; & |t-t_x| > \delta_C \end{cases} \qquad (19)$$

The weight function is shown graphically in Fig. 42b; clearly there was more spatial convolution of these results. For this experiment $\delta_C = 9$ s and $t_{\Delta x} = 3$ s. The time-resolved sodium mass was obtained by integrating Eq. 15 with the weight function given in Eq. 19.

Figures 45 and 46 show the time-resolved results. A residence time of 1.0 second was estimated for the aerosol to reach the collection plane from the burning drop. Note that the quasi-continuous sodium release history does not follow the discrete vertical bars as closely as in Figs. 43 and 44. Combustion stages were indicated as before, using a temporal uncertainty of 9 seconds. It can be concluded from this experiment that most of the

Table 14. Analysis of silver membranes and drop residues from dynamic aerosol collection.

Drop no. >	AFT3.8			AFT3.9			
Membrane section	Na, (a) mg/l	CO_3(2-), (b) mg/l	Cl-, (b) mg/l	Na, (a) mg/l	CO_3(2-), (b) mg/l	Cl-, (b) mg/l	SO_4(2-), (b) mg/l
1	0.04	1.16	0.13	<0.10	0.12	<0.10	<0.10
2	0.12	1.34	0.11	<0.10	0.08	0.10	<0.10
3	0.10	1.58	-	<0.10	0.08	<0.10	<0.10
4	0.14	1.44	-	<0.10	0.18	<0.10	<0.10
5	0.16	1.42	-	<0.10	0.30	0.10	<0.10
6	0.26	1.53	0.11	<0.10	0.26	<0.10	<0.10
7	0.18	1.72	-	<0.10	0.21	0.16	<0.10
8	0.09	1.67	-	<0.10	0.11	<0.10	<0.10
Av. section	0.14	1.48	0.04	<0.10	0.17	<0.10	<0.10
Residue	32.8	-	-	-	23.2	-	-
Detection limit	0.01	1.00	0.10	0.10	0.01	0.10	0.10
Mean background	0.04	2.13	<0.10	<0.10	0.04	<0.10	<0.10

(a) Analysis by Huffman Laboratories, Golden, CO.
(b) Analysis by IPST.

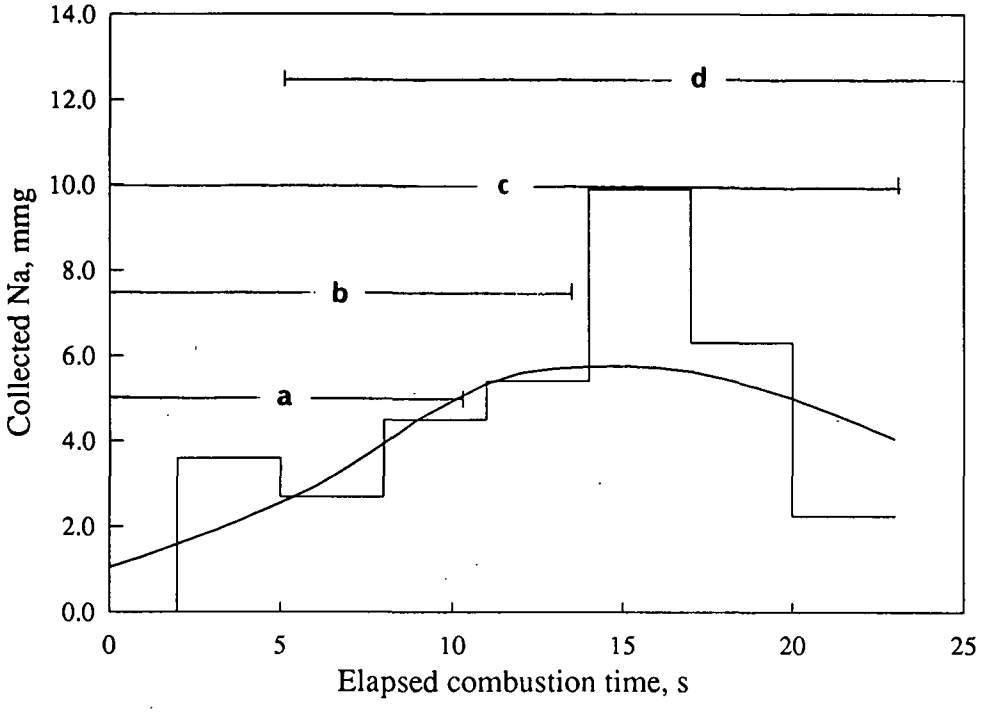

Figure 45. Time-resolved sodium deposition history from dynamic aerosol collection experiment. Combustion of 14.1 mg drop (AFT3.8 in Table 13).

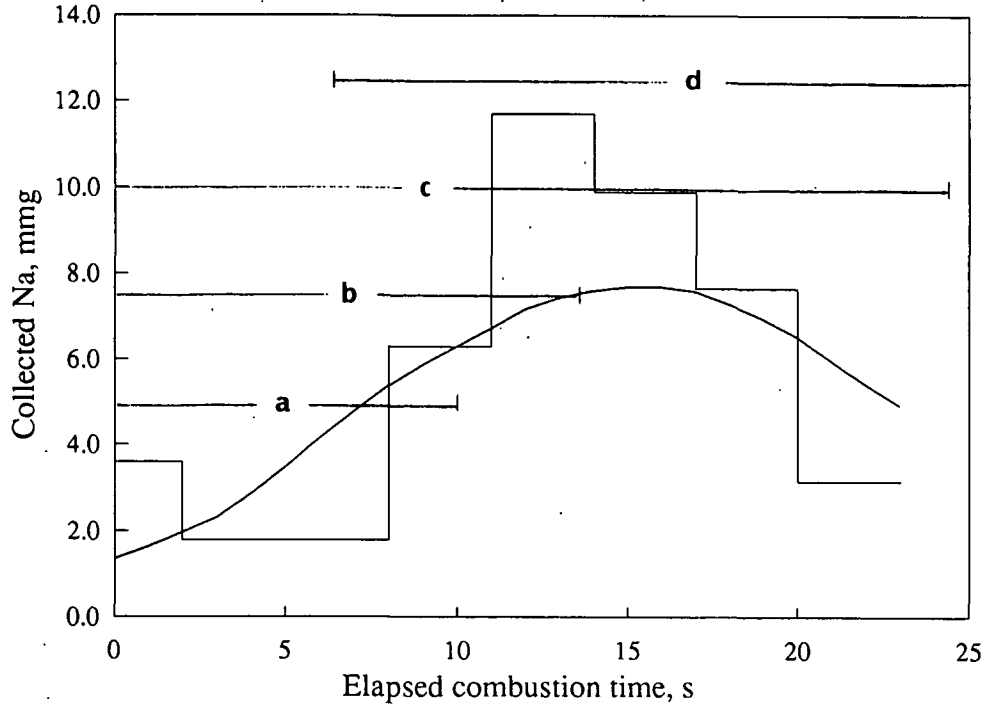

Figure 46. Time-resolved sodium deposition history from dynamic aerosol collection experiment. Combustion of 14.3 mg drop (AFT3.9 in Table 13).

sodium originated during the char burning and smelt oxidation stages of black liquor combustion. It is not expected that a significant amount of sodium deposition would have been caused by sparking during smelt coalescence since this phenomenon was not observed for black liquor combustion in 7.5% O_2.

APPENDIX VII. COLLECTION EFFICIENCY AND CLOSURE

Combustion videos revealed three types of inorganic materials that were produced during combustion: fume, ejecta, and shedded smelt. In order understand the fate of these materials in the experimental system, it was necessary to evaluate losses by limited collection efficiencies and deposition within the furnace. This appendix contains calculations of the maximum size aerosol particles reaching the collection surface. Theoretical collection efficiencies of the BGF filters and silver membranes are then evaluated. Inorganic material balances, based on measured quantities and assumed compositions, indicate the range of actual collection efficiencies for comparison with the predicted values.

AEROSOL ENTRAINMENT

Submicron-sized fume behaves as a colloidal suspension; it is easily entrained in a moving air stream and remains dispersed in still air for a very long time.[48] For particle sizes greater than 1 μm, gravitational settling cannot be neglected.[93] The largest particle that can be entrained by a gas stream is one with a settling velocity equal to the maximum upward gas velocity ($u_t = v_{max}$).[26] During the drop combustion experiments, the mass flow of gas was adjusted to produce a desired average gas velocity at the set temperature of the quartz reaction chamber. Gas velocity decreased as a result of progressive cooling with displacement past the top of the drop reactor heating elements. The expanding cross-sectional area of the exhaust flow director also decreased gas velocity. Entrained material would have fallen out of the gas stream when its settling velocity exceeded the upward gas velocity. The critical velocity necessary to determine the maximum size of the material reaching the aerosol collection plane is therefore the gas velocity at the exit of the exhaust flow director.

For low particle Reynolds number, $Re_p < 1$, and small size, $d_p \approx 10$ μm, inertial forces acting on a body are negligible compared to viscous forces. For this so called Stokes' law range, the terminal or settling velocity of spherical particles in still air (u_t) is given by

$$u_t = \frac{g}{18} \frac{d_p^2 \rho_p}{\mu} \quad , \tag{20}$$

where g is the gravitational acceleration constant, ρ_p is particle density, and μ is gas viscosity. Gas density is very much larger than ρ_p and was therefore assumed to be negligible in this formulation. Although not theoretically correct, equations of motion based on Stokes' law can be utilized with reasonable accuracy up to $Re_p = 2$.[80] Appropriate correction factors extend the valid range of particle sizes for Stoke's law calculations to $0.2 < d_p < 100$ μm.[84]

During all aerosol collection experiments there was laminar flow in the drop reactor; assuming that a fully developed laminar profile was maintained within the exhaust flow director, then $v_{max} = 2\langle v \rangle$ at any given location (y).[80] Exit velocity was predicted by the flow director heat transfer model described in Appendix VI. The majority of generated aerosol was assumed to follow the central "core" of gas flowing at between maximum and average velocity. Equation 20 was rearranged to calculate maximum entrainable particle size (d_e). For the region of interest, $\langle v \rangle \leq u_t \leq v_{max}$,

$$d_e = \sqrt{\frac{18\, u_t \mu}{g\, \rho_p\, C_c}} \quad , \tag{21}$$

where C_c, the Cunningham correction factor, accounts for the reduced resistance of viscosity

as particle size approaches the mean free path of the gas. Assuming that the maximum entrainable particle size is greater than 10 μm, C_c = 1.0 may be used with little error.[78]

Table 15 contains the values of d_e calculated for both aerosol collection experiments. ρ_p = 2.5 g/cm^3 was chosen as the density of inorganic aerosol. For all cases, Stokes' law assumption and C_c = 1.0 were valid because $Re_p < 2$ and 10 μm < d_p < 100 μm. SEM analysis of collected aerosol indicated that most particles were spherical in shape; slight irregularities in shape would not be expected to cause significant error in the Stokes' law calculations.[94]

Table 15. Calculation of maximum entrainable particle size at given locations for dynamic aerosol collection experiments.

Location	d_e @ ⟨v⟩, μm	Re_p @ ⟨v⟩	d_e @ v_{max}, μm	Re_p @ v_{max}
Exp. 1: Drop plane	136	0.68	193	1.9
Exp. 1: Exit plane	67	0.62	95	1.7
Exp. 2: Drop plane	136	0.67	193	1.9
Exp. 2: Exit plane	57	0.36	80	1.0

It can be concluded from this analysis that particles larger than 0.1-0.2 mm (smelt ejecta, shedded smelt droplets) fell to the bottom of the furnace. Particles smaller than 67-95 μm reached the filter plane in the first experiment, and particles smaller than 57-80 μm reached the silver membrane in the second experiment. The largest aerosol observed from the dynamic filtration trials was 25 μm (DCT3.24); this may imply that larger particles were not retained by the collection medium. Losses due to vibration and handling of the filters could have occurred during the dynamic collection experiments.

AEROSOL COLLECTION EFFICIENCY

Collection Efficiency by Filtration

Aerosol collection by fibrous filters is by a combination of diffusion, inertial impaction, interception, and gravitational settling. The relative importance of each of these mechanisms depends on particle size and velocity. Overall collection efficiency (η) of a fibrous filter can be correlated with mean fiber diameter (d_f), thickness (t) and porosity (α) of the fiber mat, particle size (d_p), and the velocity of the gas at the surface of the filter.[78] The latter quantity, referred to as face velocity (v_f), is calculated as

$$v_f = \frac{Q}{A} \quad , \tag{22}$$

where Q is volumetric flow rate, and A is filtration area.

For a given type of filter there is a particle size that has a minimum collection efficiency, known as the size of maximum penetration. Furthermore, there is a velocity that will result in minimum collection of a given particle size. Collection efficiency generally approaches 100% for very large and very small particles, as well as for very high and very low v_f.[84] Figure 47 shows the dependence of overall collection efficiency on particle size and face velocity for a fibrous filter.[78] The data in Fig. 47 suggest that, at a face velocity of 30 cm/s, η = 50-90% for d_p = 0.1-0.3 μm, η = 90-99% for d_p = 0.3-0.5 μm, and η > 99% for d_p > 0.5 μm. The filter described by Fig. 47 has a somewhat lower collection efficiency than the Whatman EPM-2000 BGF filter. A reasonable assumption of collection efficiency would be η = 70% for d_p = 0.1-0.5 μm, η = 100% for d_p > 0.5 μm for the EPM-2000.[95]

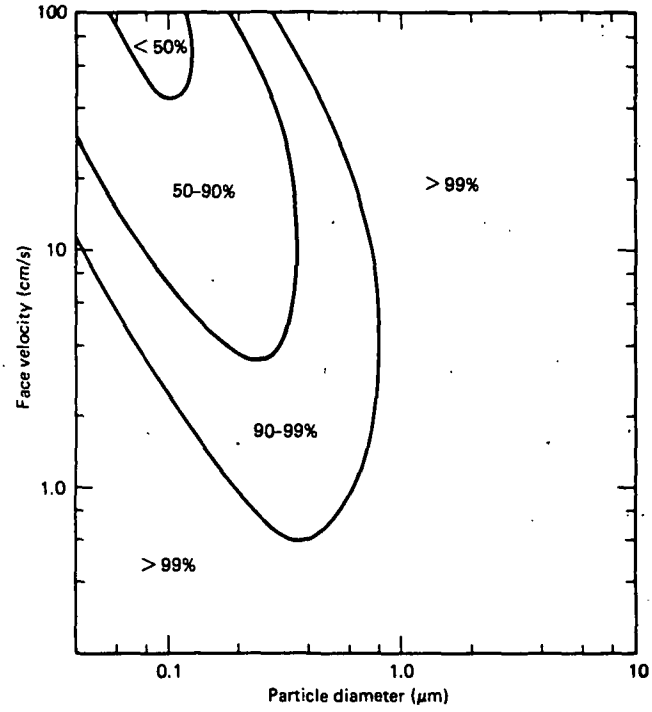

Figure 47. Overall filter efficiency isopleths for a fibrous filter; t = 1 mm, α = 0.95, and d_f = 2 μm. Reprinted from Hinds.[78]

Ramskill and Anderson[95] studied penetration (1-η) versus face velocity for a monodisperse aerosol mist having d_p = 0.3 μm. One of their curves closely approximates the characteristics of Whatman EPM-2000 BGF filters. Maximum penetration occurred at v_f = 25 cm/s (η = 65%), and maximum efficiency was achieved for v_f > 110 cm/s. Face velocity during the first dynamic aerosol collection trail was 31 cm/s at the moving filter and 12 cm/s at the backup filter. According to Ramskill and Anderson's data, the best possible collection efficiency for 0.3 μm fume by EPM-2000 filters would have been 77%.

Efficiency for large aerosol may be somewhat lower due to particle bounce; there is a 50% probability of bounce for a 10 μm solid particle striking a collection surface at 9-60 cm/s.[78] Electrostatic attraction is an important mechanism of aerosol deposition; however, in most filtration analyses electrostatic collection is neglected because it is difficult

to quantify unless the charge on the particles and fibers are known.[78] Filtration efficiency can be greatly enhanced by charging the particles and/or filter.[84]

Collection Efficiency by Impaction

When a particle-laden gas stream encounters a fixed object, submicron-sized particles will tend to follow the streamlines of the gas flowing around the object. The Brownian motion of small particles causes deviations from the streamlines and may result in some of the fine aerosol particles striking the immersed object.[78] Particles greater than 1 μm in size have sufficient inertia to prevent them from following streamlines when a flow suddenly changes direction. Depending on their size and velocity, they may collect on the immersed object by either interception or impaction. Interception occurs when the particle comes within one particle radius of the collecting surface.

Inertial impactors are devices used to measure the size distributions of atmospheric and industrial aerosols by impinging a high velocity stream of air against a flat collection surface. A commonly used dimensionless group to characterize impactor performance is Stokes number:

$$\mathrm{Stk} = \frac{\langle v \rangle \tau}{W} \quad , \tag{23}$$

where $\langle v \rangle$ is average nozzle exit velocity, τ is relaxation time, and W is the half-width of opening. Relaxation time characterizes the time required for a particle to adjust its velocity to a new condition of external forces.[78] For particle motion in the Stokes' law range

$$\tau = \frac{1}{18} \frac{d_p^2 \rho_p C_c}{\mu} \quad , \tag{24}$$

where the quantities and assumptions are given in Eqs. 20 and 21.

For a given geometry, there is a theoretical Stokes number below which inertial impaction will not occur. The critical Stokes number, Stk_{cr}, equals $2/\pi$ for potential flow of a flat jet impinging on a perpendicular plate with $S/2W = \infty$.[84] In the second dynamic aerosol collection experiment, described in Appendix VI, a cylindrical flue directed the exhaust flow to the silver membrane surface. This geometry ($S/2W = 0.08$) does not satisfy the dimensional restraint of the model; nevertheless, the model was used as an approximation of the dynamic aerosol collection system. Substitution of Eq. 24 into Eq. 23 and rearranging yields a formula for determining the minimum particle size with sufficient inertia to be collected by impaction (d_t):

$$d_t = \sqrt{\frac{18\, Stk_{cr}\, W\, \mu}{\langle v \rangle\, \rho_p\, C_c}} \quad . \tag{25}$$

As it is expected that the collection efficiency is less for viscous flow than for potential flow,[84] $Stk_{cr} > 0.637$ was used for evaluating Eq. 25. An average gas velocity at the exit plane of 0.19 m/s was calculated by the flow expander heat transfer model. Eq. 23 indicates that $d_t > 150$ μm for the second dynamic aerosol collection experiment.

In Table 15, d_e was calculated to be less than 80 μm at the exit plane for the second experiment; clearly there would have been no aerosol collection by impaction on the silver membranes. Theoretical collection efficiency, however, does not necessarily accurately represent the true efficiency of aerosol capture.[96] In the above analysis only the mechanism of impaction was considered. As the impinging jet spread out across the surface of the silver

membrane there may have been submicron-sized aerosol collection by electrostatic attraction and diffusion. Loss of aerosol after contact by reentrainment is unlikely for particles smaller than 10 μm because the adhesive forces that act on the particle are two orders of magnitude greater than the removal force of a 10 m/s air current.[78]

INORGANIC MATERIAL BALANCES

Accurate gravimetric determination of total accumulation on BGF filters was impossible because the fiber loss that occurred during handling was greater than the small mass of captured particulate. Conditioning in a constant humidity environment minimized the variation in BGF filter moisture content; however, the 203 by 254-mm filters typically lost 8-11 mg during a dynamic aerosol collection trial and the backup filters gained 1-4 mg. SEM analysis substantiated the assumption that the mass gain on the backup filters was caused by accumulation of filter fragments scraped off the large filters by the vacuum flow director.

Due to high background levels of sodium and carbonate ions in the BGF filters, sulfate ion was the only component available to evaluate material balance closure in the first experiment. The following estimations of drop residue and captured material composition allowed a sulfur material balance to be made. Accurate measurement of very small quantities of collected sodium were possible with the silver membranes. Amounts of the expected anions were below instrument detection limits; therefore, sodium was the only component with which to check closure in the second experiment.

Table 16 contains literature values of the composition of highly oxidized smelt and inorganic aerosols captured close to their points of origin. A smelt composition of

Table 16. Typical composition of oxidized smelt and inorganic aerosols (values reported as % of o.d. solids).

Species	Drop residue[11,a]	Collected aerosol[11,b]	Probe deposit[55,c]	Impactor sample[4,d]
Na_2CO_3	53.0	12.7	16.7	6
NaOH	2.0[e]	25.0[e]	0.0	-
Na_2SO_4	43.0	61.6	68.5	64[f]
$Na_2S_2O_3$ Na_2SO_3	-	-	-	18[f]
Na_2S	2.0	0.7	-	11[f]
NaCl	-	-	15.4[g]	-
Total	100.0	100.0	100.6	99

[a] Residue from combustion of single 3 mm drops in air at 900°C, unspecified exposure time and sample size.
[b] Aerosol collected from combustion of single 3 mm drops in air at 900°C, unspecified exposure time and sample size.
[c] Fine particulate from downstream side of cooled probe located 3.2 m above bottom of superheater; exposure time 4 hours.
[d] Material from tertiary air level of furnace; collected on BGF filter, unspecified analysis.
[e] Values may be high due to moisture in combustion air.
[f] Total amount of sodium-sulfur compounds may be high due to artifact formation.
[g] Mill had unusually high chlorine content in liquor.

80% Na_2CO_3, 15% Na_2SO_4, 3% Na_2S, and 2% NaOH was estimated from the following analysis. The average sodium content of the five measured drop residues was 45.7%; this value was calculated from data in Tables 12 and 14. The ratio of Na_2CO_3 to Na_2SO_4 in the residue from the first experiment was 5.4 to 1. Three assayed species (Na, $CO_3^=$, $SO_4^=$) accounted for 95% of the residue mass. The remainder was assumed to be split between hydroxide and sulfide, as suggested by the data of Volkov et al.[11] in Table 16. A slightly

higher Na_2S content was chosen because the lower temperature and oxygen content used during the aerosol collection experiments should have resulted in less sulfide oxidation.

There was not enough aerosol captured during the experiments to determine composition; however, its analysis should have been similar to the literature values given in Table 16. An assumed composition of 65% Na_2SO_4, 15% Na_2CO_3, 5% Na_2S, 5% NaOH, 5% NaCl, and 5% other was used in the sodium and sulfur balances for the aerosol collection experiments; these results are presented in Table 17. Amounts of sodium and sulfur in each drop were calculated from the elemental analysis of liquor no. 2B (19.2% Na, 4.1% S). The mass of material collected by the filter or membrane was the sum of all sections plus backup filter (for the first experiment) minus the background from appropriate blanks. The value of "capture" is the percentage of the lost material that was collected; this can be thought of as a minimum collection efficiency.

Minimum Collection Efficiency

Sodium loss for the first two drops given in Table 17 was much less than for the other three. Stage times were somewhat shorter due to smaller initial drop sizes in the second experiment, otherwise drop combustion was nearly identical. A review of the video images revealed that there were significant differences in the extent of smelt shedding during the final seconds of char burning. Drops DCT3.22 and DCT3.23 shed only a few droplets of smelt, amounting to less than 10% of the molten material. For DCT3.24 almost all of the char fell off the nichrome wire before the end of char burning. During the second experiment one drop (AFT3.8) shed approximately 10% of its smelt while the other (AFT3.9) lost about 40% of its smelt at the moment of coalescence.

Table 17. Sulfur and sodium balances for dynamic aerosol collection experiments.

Drop no.	Species	Drop o.d. mass, mg	Residue mass, mg	Species assay, % res. (b)	"Lost" mass, mg	Relative loss, %	Collected mass, mg	Minimum capture, %
DCT3.22	Solids	13.6	5.3		8.3	61.1		
	Sulfur	0.56	0.34 a	6.4	0.22	39.0	0.087 a	40.1
	Sodium	2.62	2.43	45.8	0.19	7.1		
DCT3.23	Solids	19.8	7.9		11.9	60.1		
	Sulfur	0.81	0.36 a	4.6	0.45	55.5	0.074 a	16.3
	Sodium	3.80	3.46	43.8	0.34	9.0		
DCT3.24	Solids	38.9	1.9		37.0	95.1		
	Sulfur	1.60	0.10 a	5.2	1.50	93.8	-	-
	Sodium	7.48	0.93	49.2	6.54	87.5		
AFT3.8	Solids	10.1	3.5		6.6	65.2		
	Sodium	1.96	1.48	42.2	0.49	24.8	0.0347	7.1
AFT3.9	Solids	10.2	2.2		8.0	78.5		
	Sodium	1.99	1.04	47.5	0.95	47.6	0.0459	4.8

(a) Determined from assumed compositions of material and sulfate ion assay.
(b) Mass percent of given element.

The following prediction, based on literature information, indicates that the calculated 39-56% sulfur loss presented in Table 17 was reasonable for the combustion conditions of the first experiment. The density of liquor no. 2B was 1.79 g/cm^3; this value was calculated from the initial drop diameter and mass. Using this density the size of the first two drops in Table 17 were estimated to be 2.7 and 3.1 mm. Cantrell et al.[97] reported a total sulfur loss of 27.1% during combustion of 2.8-3.0 mm drops of 71.9% solids liquor in air at 1090°C. For 2 mm diameter drops of 63.3% solids liquor, sulfur loss increased approximately 34% for a corresponding decrease in oxygen content from 21% to about 7.5%.[97] Clay et al.[24] plotted sulfur release as a function of furnace temperature for pyrolysis of 15 mg (2.7 mm) drops of 67.4% solids liquor in nitrogen. These data indicated that sulfur release was 88% higher at 750°C than at 1100°C. Applying these adjustments to Cantrell's data predicts the sulfur loss for 3.0 mm drop of liquor burned at 750°C in 7.5% O_2 to be 68%.

This approach may have overpredicted sulfur loss by underestimating the extent of competing sulfur recapture mechanisms. The assumed smelt composition could also account for the difference. If the residue were fully oxidized (i.e., no Na_2S remaining) then the calculated sulfur loss would have been 55-67% and the minimum capture efficiency would have been 13.5-28.3%.

Maximum Collection Efficiency

The first two drops identified in Table 17 lost between 7 and 9% of their sodium. This agrees remarkably well with field data of Borg et al.[5] that indicate total sodium loss from the lower furnace is 9% of that fired with the liquor. Assuming the measured 7-9%

sodium loss resulted entirely from vaporization, the amount of sulfur or sodium collected as aerosol was predicted for each experiment. The results of this analysis, presented in Table 18, indicate maximum efficiency of the aerosol collection systems.

In the first experiment the losses of sulfur and sodium were measured, and the amount of sulfur collected was determined. Because sulfur was in excess, that which did not react with fume species would have been present as SO_2 gas.[5] Assuming that all of the sodium lost from the first two drops became aerosol with a composition based on the data in Table 16, then the amount of lost sulfur as fume could be determined. The collection efficiency, from this material balance, was 45-99%.

The average maximum collection efficiency of DCT3.22 and DCT3.23 in Table 18 (72%) agrees very well with the predicted value of $\eta = 70\%$ for 0.1-0.5 μm diameter particles. If sulfur gas reactions with the filter material was responsible for a large amount of "artifact" production this value would have been much greater. Considering the uncertainties of the technique, this result indicates that a substantial part of the $SO_4^=$ containing material was aerosol; however, it does not rule out the possibility of artifact production.

Assuming sodium vaporization occurred independently of drop size, the total sodium loss for AFT3.8 and AFT3.9 was partitioned into vaporized and shed fractions. Table 18 indicates that between 5 and 7% of the sodium "lost" during drop combustion could be accounted for on the silver membranes. If 8% of the sodium present in the liquor became fume, then the collection efficiency would have been 22-29%. It is not certain how much of the sodium loss was in the form of fume and how much was shed smelt droplets; however, it is expected that only a fraction of the airborne material was collected on the silver membrane.

Table 18. Estimated amount of fume formation and maximum collection efficiency during dynamic aerosol collection experiments.

Drop no.	Species	Drop o.d. mass, mg	"Lost" mass, mg	Collected mass, mg	"Fume" mass, mg	Non-"fume" mass, mg	Maximum capture, %
DCT3.22	Solids	13.6	8.3		0.53 a		
	Sulfur	0.56	0.22	0.087 a	0.09 a	0.13 d	99.3
	Sodium	2.62	0.19		0.19 b		
DCT3.23	Solids	19.8	11.9		0.97 a		
	Sulfur	0.81	0.45	0.074 a	0.16 a	0.29 d	45.4
	Sodium	3.80	0.34		0.34 b		
AFT3.8	Solids	10.1	6.57		0.44 a		
	Sodium	1.96	0.49	0.0347	0.16 c	0.33 e	22.1
AFT3.9	Solids	10.2	8.01		0.45 a		
	Sodium	1.99	0.95	0.0459	0.16 c	0.79 e	28.8

(a) Determined from assumed compositions of material and sulfate ion assay.
(b) Taken as 100% of lost Na mass.
(c) Taken as 8% of drop Na mass.
(d) Assumed to be sulfur gases.
(e) Assumed to be shed smelt droplets.

ADDITIONAL CITATIONS

88. Whatman publication no. 824 GMF A. Whatman Inc., Clifton, NJ.

89. Data from Internal Whatman Communications. Whatman Inc., Clifton, NJ.

90. Balasic, P.J., Basic corrosion control techniques for electrostatic precipitators. Pulp Paper 53(10):154-156 (1979).

91. Mitchell, W.J.; Bruffey, C.L., Effect of sampling temperature, filter material, and sample treatment on combustion source emission test results. Environ. Sci. Technol. 18(10):803-808 (1984).

92. Nelson, J.W.; Jensen, B.; Desaedeleer, G.G.; Akelsson, K.R.; Winchester, J.W., Automatic time sequence filter sampling of aerosols for rapid multi-element analysis by proton-induced X-ray emission. Advances in X-ray Analysis, Vol. 19:403-413 (1975).

93. Dorman, R.G., Filtration. Aerosol Science, Davis, C.N., ed. Academic Press, New York, NY, p. 195-222 (1966).

94. Reist, P.C., Introduction to Aerosol Science. Macmillan Publishing Co., New York, NY (1984).

95. Ramskill, E.A.; Anderson, W.L., The inertial mechanism in the mechanical filtration of aerosols. J. Colloid Sci. 6(5):416-428 (1951).

96. Davies, C.N., Deposition from moving aerosols. Aerosol Science. Davies, C.N., ed. Academic Press, New York, NY, p. 393-446 (1966).

97. Cantrell, J.G.; Clay, D.T.; Hsieh, J.S., Sulfur release and retention during combustion of kraft black liquor. Chemical Engineering Technology in Forest Products Processing, Volume 2. Crowell, B., ed. AIChE Forest Products Division, p. 31-39 (1988).